The femtosecond dynamics of electrons in metals

2009 Phys.-Usp. 52 105

(http://iopscience.iop.org/1063-7869/52/2/R01)

Physics – Uspekhi **52** (2) 105 – 136 (2009)

REVIEWS OF TOPICAL PROBLEMS PACS numbers: **71.15. – m**, **78.47. – p**, **79.60. – i**

The femtosecond dynamics of electrons in metals

V P Zhukov, E V Chulkov

DOI: 10.3367/UFNe.0179.200902a.0113

Contents

Abstract. The current state of research in the femtosecond dynamics of low-energy excited electronic states in metals is reviewed. Some of the major approaches to the experimental study of the decay of excited states are discussed, including time-resolved two-photon photoemission spectroscopy, angle-resolved photoemission spectroscopy, and spintronic techniques. Semiempirical and first-principle theoretical approaches to electron dynamics are presented. Results of studies on the dynamics of electron excitations in some simple, noble, paramagnetic, and ferromagnetic metals are analyzed.

1. Introduction

The dynamics of low-energy electron excitations (the lifetime and the mean free path of an excited electron, screening effects, and the mechanisms of damping of excitations) are important for understanding many physical and chemical phenomena both in the bulk and on the surface of solids. These excitations are the key mechanism of energy transfer in reactions on the surface of a solid, in particular, in oxidation processes and in desorption [1], photodissociation, and photodesorption [2, 3], as well as in catalytic reactions [4, 5]. For simulating such reactions, numerous theoretical approaches have been developed, in which the transfer of energy into the bulk of a crystal and to molecules on the surface is considered [6]. The basic quantities in such models are the relaxation times of the excited states of the molecule and the crystal. Low-energy electron excitations play an important role in the processes of electron localization and in the charge and spin transport in bulk metals and on the internal and external interfaces [7]. The relaxation time and relaxation length of an excited electron are valuable characteristics of electron transport in the bulk of solids and through interfaces [7]; therefore, they are widely used in the analysis of processes in spintronic devices [11 – 13]. The characteristics of the dynamics of excited states in a crystal such as the attenuation length or the inelastic mean free path are very important in the theory of photoelectron and Auger spectroscopy [8 – 10].

In the last decade, the femtosecond dynamics of electrons in metals has been given much attention. A number of experimental methods have been developed that allow determining the relaxation time and relaxation length of an excited electron. In particular, the high-precision methods of measuring spectral-line width, i.e., the inverse of the relaxation time, have been used, based on angle-resolved photoemission spectroscopy (ARPES) [8, 14, 15]. A very important point was the invention of methods that allow directly investigating the time characteristics of the dynamics of excited states and, first and foremost, the method of time-resolved two-photon photoemission spectroscopy (TR-2PPE) [16, 17]. In this method, the first (pumping) photon excites an electron into an intermediate state, and the second photon (probing photon), which comes after a certain time delay, transfers the electron from the intermediate state to the

V P Zhukov Institute of Solid State Chemistry,
Ural Branch of the Russian Academy of Sciences,
ul. Pervomaiskaya 91, 620219 Ekaterinburg, Russian Federation
Tel. (7-343) 362 35 27. Fax (7-343) 374 44 95
E-mail: zhukov@ihim.uran.ru
E V Chulkov Departamento de Fisica de Materiales,
Facultad de Ciencias Quimicas,
UPV/EHU, Apdo 1072, 20080 San Sebastian, Basque Country, Spain
Tel. (1034) 943-018216. E-mail: waptctce@ehu.es

Received 28 May 2008, revised 18 August 2008
Uspekhi Fizicheskikh Nauk **179** (2) 113 – 146 (2009)
DOI: 10.3367/UFNr.0179.200902a.0113
Translated by S N Gorin; edited by A M Semikhatov

vacuum. Such experiments can be carried out at a low intensity of laser radiation, when investigating the dynamics of excitations of a single electron, or at a high intensity, when studying collective excitations. The TR-2PPE experiment at a low intensity of radiation does not directly yield the value of the lifetime of an electron in the intermediate state; therefore, to extract this lifetime from the experimental TR-2PPE data — the so-called cross-correlation traces — simple and, as follows from a comparison with the results of first-principle calculations, sufficiently correct computational procedures have been developed [18 – 20].

Among the methods of determining the relaxation length, the most successful are those based on measurements of the collector current in spintronic devices, namely, in the spin-valve transistor (SVT) and in the magnetic tunnel transistor (MTT), depending on the thickness of the layers that form their base. The main difference between the SVT and MTT consists in the method of injecting excited electrons; in the SVT, the excited electrons are generated due to the application of a Schottky barrier, whereas in the MTT, they are obtained upon passage through the tunnel barrier between the probe and the base of the device. With increasing the thickness of the base layers, an exponential reduction is usually observed in the collector current, which allows determining the relaxation length [12].

This review is aimed mainly at the consideration of investigations into the dynamics of the relaxation of excited states in bulk metals (carried out by the ARPES, TR-2PPE, SVT, and MTT methods), as well as of related theoretical studies. We note that the relaxation of excited states studied by these methods includes, as the basic process, the inelastic scattering of electrons accompanied by the excitation of electron–hole pairs, as well as some 'additional' processes, which depend on the type of the experiment. In the case of TR-2PPE experiments, the additional processes are cascade electronic processes, which are discussed in this review, transport processes, and processes for the generation of Auger electrons. An essential achievement of experimental works is that the basic qualitative features of these processes (their dependence on the excitation energy, the type of electronic structure, the presence of defects, etc.) have been revealed and methods of controlling these processes (i.e., controlling the relaxation rate) have been suggested. For studying inelastic scattering and additional processes, a number of semiempirical models based on the scattering theory and the Boltzmann theory [21 – 24] have been developed. Their brief description and an analysis of the degree of their correctness are also given in this review.

The most complete theoretical studies were performed for the processes of inelastic scattering using first-principle approaches based on the formalism of the self-energy operator of the many-body solid-state theory. The self-energy formalism was first developed by Quinn and Ferrell for describing the relaxation of excited states in a homogeneous interacting electron gas [25, 77]. For a number of years, the Quinn–Ferrell theory was used for a qualitative interpretation of the results of measuring spectral linewidths and the lifetimes of excited states [26 – 29]. However, noticeable contradictions were gradually discovered between the predictions of the Quinn–Ferrell theory and the experimental spectral linewidths and lifetimes of excited states in noble metals [30 – 34]. It was shown that to correctly calculate the lifetime, it is necessary to include the real energy-band structure in the theory.

Therefore, subsequent calculations of the lifetimes were performed on the basis of the many-body theory [35], mainly using the first-principle GW method proposed by Hedin [36 – 39], in which the band structure obtained by the methods of the electron-density functional theory (see reviews [40 – 44]) is used as the starting information. In the GW method, when considering the self-energy of a quasiparticle, i.e., an excited electron or hole, only the first term of the exact series expansion of the self-energy with respect to the screened potential W is taken into account. Therefore, the GW approximation is insufficient, for example, for describing low-energy excitations in ferromagnets, where the interacting electrons and holes form Stoner pairs and (or) spin waves. The interaction between particles is taken into account in the T-matrix generalization of the GW method, the so-called GW+T method [39, 45 – 47]. In combination with TR-2PPE experiments, this method was used to investigate the lifetimes and mean free paths of electrons in simple, noble, transition, and rare-earth metals [47 – 50].

Both experimental and theoretical studies of the femtosecond dynamics of electrons in metals were marked by a number of achievements. On the whole, the femtosecond dynamics of electron excitations is a rapidly developing part of contemporary solid-state physics. Recently, such studies were carried out for some chemical compounds of simple and transition metals [51 – 56], compounds with heavy fermions [57, 58], superconductors [17, 59 – 64], and nanotubes [65]. Studies were conducted for image states above the surface of metals, for surface and bulk states of metals, and for adsorbate states on metal surfaces [41, 42]. The experimental aspects of these studies, predominantly for the image states and surface and adsorbate states, were considered in reviews [12, 15, 16], and the theoretical aspects, in reviews [17, 34, 41–44].

Investigations of the dynamics of bulk excited states in metals are a good basis for the understanding of dynamics in more complex cases, in particular, in the practically important research on the dynamics of chemical reactions on a catalyst surface or of electron and spin transport in spintronic devices. Therefore, our goal in writing this review was to give a consistent description of the physical foundations of all the main stages of the research on the dynamics. Following the Introduction, we give a brief description of the main experimental approaches, i.e., the TR-2PPE, ARPES, SVT, and MTT techniques. This description is accompanied by a consideration of the possible mechanisms of relaxation of excited states and of the problems related to the complexity of these processes. We discuss the basic models used for the extraction of characteristics of relaxation processes from experimental data. In Section 3, we give a brief description of the theoretical approaches to femtosecond relaxation processes. It includes a consideration of both semiempirical models based on the scattering theory and Boltzmann theory, and the first-principle approaches to the electronic characteristics of relaxation based on the Quinn–Ferrell theory and on the GW and GW+T methods. In Section 4, the concrete results of experimental and theoretical studies of the dynamics of relaxation processes in a number of simple, noble, nonmagnetic, and magnetic transition metals are discussed. Emphasis is placed on the reliability of the results obtained and on the existing contradictions between different experimental studies and between theory and experiment. In the last section, conclusions are drawn about the degree of success of experimental and theoretical approaches in

research on the dynamics of the relaxation of excited states, and the problems to be solved are discussed.

2. Experimental methods for investigating the femtosecond dynamics of electrons

Introductory remarks. Some uncertainties exist in the terminology related to the dynamics of relaxation processes. For example, the relaxation time is considered by some researchers to be equivalent to the lifetime. In this review, by relaxation characteristics, we mean the characteristics that are obtained from the experimental data via the procedures for processing these data described in Sections 2.1.2, 2.2, and 2.3. These quantities are usually determined by the contributions from several relaxation processes. By the lifetime and mean free path of electrons, we mean the quantities introduced in the theory of electron dynamics. They describe the rates of concrete processes of scattering of excited electrons, for example, elastic or inelastic, electron–phonon, or electron–magnon scattering.

Additional information concerning the methods for investigating femtosecond dynamics, which are used predominantly for studying surface states, image states, and the states of adsorbates, can be found in reviews [15 – 17, 34, 41 – 43] and in Refs [50, 66].

2.1 Time-resolved two-photon photoemission spectroscopy

2.1.1 Description of experiment. The method of time-resolved two-photon photoemission spectroscopy (TR-2PPE) is based on a two-step excitation of a crystal, schematically shown in Fig. 1. First, an electron is excited by a pumping pulse photon ($h\nu_1$) from one of the populated states into an unoccupied intermediate state (E_i) with an energy below the vacuum level. Then, the probing photon ($h\nu_2$), which comes with a certain delay, excites the electron from this temporarily populated level E_i into a certain final level above the vacuum level E_{vac}, and the kinetic energy of this electron E_{kin} is measured using an analyzer. (There also exists a small probability of excitation of the electron into a level above E_{vac} via the absorption a second photon from the pumping pulse; see Section 2.1.2.) Because $E_i = E_{kin} + \Phi - h\nu_2$, where Φ is the electron work function, the energy of the intermediate state is known. The pumping and probing photons can have the same or different energies in the visible or near-ultraviolet ranges. The pulse duration is several tens of femtoseconds; the delay between the pulses can vary from zero to ~ 200 fs. In the time between the pulses, the population of the intermediate state decreases under the effect of various scattering processes (electron–electron, electron–phonon, etc.). The electron lifetime in the intermediate state is estimated by measuring the number of emitted electrons.

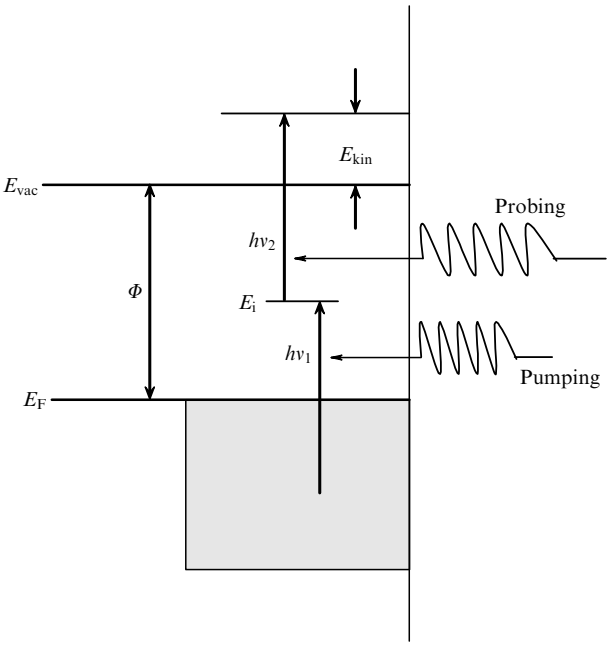

Figure 1. Schematic of a TR-2PPE experiment. The shaded region is the density of occupied states; E_F is the Fermi level; $h\nu_{1,2}$ are the energies of the pumping and probing photons; E_{kin} is the energy of the probed photoexcited electron; E_i is the intermediate state; Φ is the work function; and E_{vac} is the vacuum level.

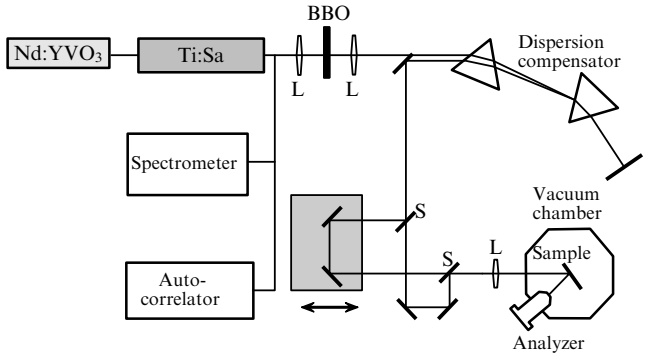

Figure 2. Setup for two-photon femtosecond laser spectroscopy (schematic).

As a concrete example, Fig. 2 displays a simplified scheme of the two-photon spectroscopy setup used in Ref. [67]. A more detailed description of experiments can be found in Refs [16, 26, 32]. The experiment is conducted using a pulsed titanium–sapphire laser (Ti:Sa) with the frequency about 80 MHz, a variable wavelength about 800 nm, and the pulse duration from 20 to 40 fs. The pumping is effected using an Nd:YVO_3 laser. The titanium–sapphire laser yields linearly polarized light with the photon energy 1.5 – 1.7 eV; the shape of the pulse is close to the sech^2 function. Its frequency is doubled using a β barium borate (BBO) crystal. The light is passed through a dispersion compensator on the basis of two prisms of quartz glass, which carries out a preliminary compensation of the pulse broadening that arises while the beam passes through the beam splitters (S), lenses (L), and windows of the vacuum chamber. Then, the beam is split into two beams of equal intensity for the pumping and probing channels. The pulse in the probing channel is delayed relative to the pulse in the pumping channel by passing it through a delay line controlled by a computer. The pulses are made collinear by passing them through a second splitter. Two types of polarization of the pumping and probing pulses can be used: with an electric field parallel to the plane of the incident and reflected beam (p polarization) or with the field perpendicular to this plane (s polarization). The analyzer (in this work, cylindrical sector analyzer Focus CSA300) measures the number and the kinetic energy of photoelectrons emitted with the maximum deviation $\pm 3^\circ$ from the normal to the surface of the sample.

In these experiments, two types of primary data are usually obtained. The first is a two-photon photoemission spectrum, i.e., the dependence of the number of photoelec-

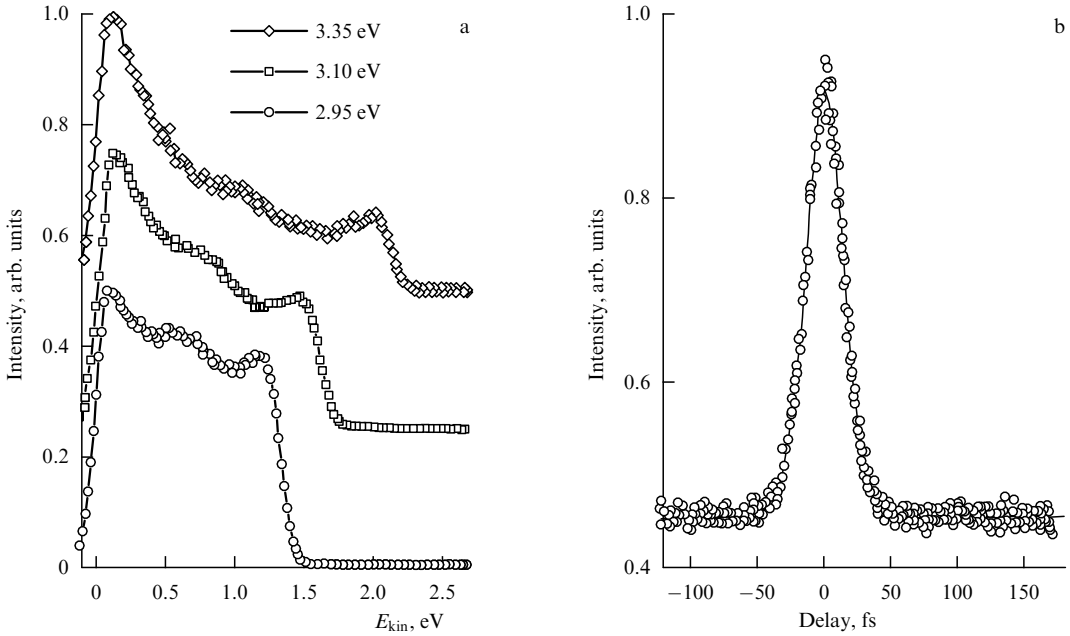

Figure 3. (a) Two-photon photoemission spectrum recorded at three different photon energies and (b) cross-correlation trace of molybdenum [68]. Both types of data are normalized to unity at the maximum.

trons on the kinetic energy at a fixed time interval Δ between the pulses. The second type is the correlation trace $I^{2PPE}(\Delta)$, i.e., the dependence of the integrated number of photoelectrons on the delay Δ at a fixed kinetic energy. Usually, it is normalized to unity with respect to the maximum at $\Delta = 0$. For studying the dynamics of single-particle excited states, experiments are conducted at a small radiation intensity, about 1 nJ per pulse. With the size of the laser spot being of the order of 1 μm and the depth of light penetration approximately 150 Å, only $\sim 10^6$ of 10^{23} atoms are excited in one pulse, and heating of the sample is virtually absent. As an example, Fig. 3 demonstrates the shape of a two-photon photoemission spectrum of Mo (at three different photon energies) and the cross-correlation trace (for the perpendicular polarization of the pumping and probing pulses) for Mo [68] normalized by the authors of this review. The interpretation of changes in the photoelectron spectrum with a change in the energy of the photons is given in Ref. [68].

2.1.2 Models for the extraction of dynamic characteristics from the experimental data. In two-photon photoemission spectroscopy, measurements are conducted with laser pulses that strongly overlap in time. The quantum mechanical analysis of this emission process is an extremely complicated problem, which must be solved based on the many-body theory. A complete solution of this problem is presently impossible, although attempts were recently undertaken to approach it [69, 70]. Instead, a number of comparatively simple semiempirical models were developed, which allow obtaining the dynamic characteristics of the relaxation of excited states from correlation traces. The degree of the success of these models is characterized by the data given in Sections 4.1, 4.2, and 4.4.

Historically, the first model of this type, based on the Fermi golden rule, was proposed in [18]. The authors examined the dynamics, in a laser field, of only two quantum levels, the ground and an intermediate excited levels, in the approximation of the instantaneous reaction of the population of the intermediate level to a change in the laser field, inherent in the Fermi golden rule. Although the model gave qualitatively accurate results for the lifetime of the intermediate level, the applicability of the approximation of the instantaneous reaction has not been confirmed [19]; therefore, a more common model for the two-level system was developed [19], based on the so-called optical Bloch equations [71]. The model in [19] is a special case of the three-level model, which was later developed in [20] and has found wide application.

The three-level model in [20] is based on the density matrix formalism [71, 72]. In the general case, the density matrix satisfies the Liouville–von Neumann equation

$$\frac{\partial \rho}{\partial t} = \frac{\mathrm{i}}{\hbar}\,[\rho, H] + \left(\frac{\partial \rho}{\partial t}\right)^{\mathrm{diss}}, \qquad (1)$$

where $H = H_0 + H_\mathrm{I}$ is the total Hamiltonian, in which H_0 is the main part corresponding to the electron system in the absence of a laser field and H_I describes the interaction of the system with the laser field. Because the wavelength of the laser radiation is much larger than the lattice parameter of metals, we can disregard the spatial variation of the field amplitude and assume that the electric field of the laser pulse has the form $\mathbf{E}(t) = \mathbf{E}_0(t)\cos(\omega t)$, where ω is the angular frequency and $\mathbf{E}_0$ is the time-dependent envelope of the field (a vector quantity). The perturbation H_I can then be described as an interaction between the field and the atom dipole moment $\mathbf{d}$:

$$H_\mathrm{I} = e\,\mathbf{d}\mathbf{E}_0(t)\cos(\omega t), \qquad (2)$$

where

$$\mathbf{d} = \sum_{j=1}^{Z} \mathbf{r}_i \qquad (3)$$

is the dipole moment of an atom with Z electrons. The dissipative term $(\partial\rho/\partial t)^{\mathrm{diss}}$ describes the change in the

density matrix of the system caused by the interaction with the environment. For a model three-level system, the following dynamic equations can be obtained [71]:

$$\begin{aligned}
\frac{\partial\rho_{11}}{\partial t} &= -\mathrm{i}\phi_{12}(\rho_{21}-\rho_{12}) + D_{11}\,,\\
\frac{\partial\rho_{22}}{\partial t} &= -\mathrm{i}\phi_{12}(\rho_{12}-\rho_{21}) + \phi_{23}(\rho_{32}-\rho_{23}) + D_{22}\,,\\
\frac{\partial\rho_{33}}{\partial t} &= -\mathrm{i}\phi_{23}(\rho_{23}-\rho_{32}) + D_{33}\,,\\
\frac{\partial\rho_{13}}{\partial t} &= -\mathrm{i}(\phi_{12}\rho_{23}-\phi_{23}\rho_{12}) + \mathrm{i}(\omega_1-\omega_3)\rho_{13} + D_{13}\,,\\
\frac{\partial\rho_{12}}{\partial t} &= -\mathrm{i}\phi_{12}(\rho_{22}-\rho_{11}) + \mathrm{i}\phi_{23}\rho_{13} + \mathrm{i}(\omega_1-\omega_2)\rho_{12} + D_{12}\,,\\
\frac{\partial\rho_{23}}{\partial t} &= -\mathrm{i}\phi_{23}(\rho_{33}-\rho_{22}) + \mathrm{i}\phi_{12}\rho_{13} + \mathrm{i}(\omega_2-\omega_3)\rho_{23} + D_{23}\,.
\end{aligned} \tag{4}$$

Diagonal elements of the density matrix represent time-dependent populations of the levels E_s ($s=1$, the ground level; $s=2$, the intermediate level populated due to the first pulse; $s=3$, the upper (vacuum) level, which is populated as a result of the excitation of an electron from the intermediate level by the second pulse). The quantities $D_{ij} = (\partial\rho_{ij}/\partial t)^{\mathrm{diss}}$ characterize a change in the density matrix caused by interaction with the environment. The quantities $\omega_s - \omega_t = (E_s - E_t)/\hbar$ are the excitation energies. The quantities

$$\phi_{st} = \frac{e}{\hbar}\int \psi_s^*\mathbf{E}_0\mathbf{d}\psi_t\,\mathrm{d}V \tag{5}$$

are matrix elements of the dipole moment between the wave functions of states; they determine the probability amplitudes of transitions between these states. The probability ϕ_{13} of the direct excitation from the ground state E_1 into the upper vacuum state E_3 is neglected.

At a small intensity of the laser field, the population of the ground state is close to saturation, i.e., $\rho_{11}(t) \approx 1$ and $(\partial\rho_{11}/\partial t)^{\mathrm{diss}} \approx 0$. Because the third level is a vacuum level (the electron left the crystal!), it can also be assumed that $(\partial\rho_{33}/\partial t)^{\mathrm{diss}} \approx 0$. The finite time of electron residence in the intermediate state is introduced by defining the dissipative term as

$$\left(\frac{\partial\rho_{22}}{\partial t}\right)^{\mathrm{diss}} = -\frac{1}{\tau_2}\,\rho_{22}\,. \tag{6}$$

In the absence of a laser field, the solution of dynamic equation (4) with this definition of the dissipative term has the form

$$\rho_{22}(t) = \rho_{22}(0)\exp\left(-\frac{t}{\tau_2}\right), \tag{7}$$

and therefore the quantity τ_2 introduced here is the lifetime of electrons being sought at the intermediate level in a weak laser field (relaxation time), and the quantity $\gamma_2 = 1/\tau_2$ is the rate of decrease in the population of the level.

The time dependence of the wave function of an electron in the three-level system can be represented as [71]

$$\Psi(t) = C_1(t)\Psi_1(t) + C_2(t)\Psi_2(t) + C_3(t)\Psi_3(t)\,, \tag{8}$$

where

$$\Psi_s(t) = \exp\left(-\frac{\mathrm{i}E_s t}{\hbar}\right)\psi_s \tag{9}$$

are the states of the system in the absence of a perturbation and ψ_s are solutions of the equation $H_0\psi_s = E_s\psi_s$. Therefore, the elements of the density matrices are expressed as $\rho_{ss} = |C_s|^2$, $\rho_{st} = C_sC_t^*$, and $\rho_{ts} = \rho_{st}^*$. Hence, it follows that in a weak laser field, the intermediate state relaxes in accordance with the law

$$C_2(t) = C_2(0)\exp(-\Gamma_2 t)\,, \tag{10}$$

where the relaxation rate of the state is $\Gamma_2 = \gamma_2/2 = 1/(2\tau_2)$, and the corresponding characteristic time, called the *electron dephasing time*, is equal to $1/\Gamma_2 = 2\tau_2$. It is then natural to introduce the following approximation for the off-diagonal elements of the density matrix:

$$\begin{aligned}
&\left(\frac{\partial\rho_{st}}{\partial t}\right)^{\mathrm{diss}} = -\Gamma_{st}\rho_{st}\,,\\
&\Gamma_{st} = \Gamma_s + \Gamma_t\,,
\end{aligned} \tag{11}$$

with $s, t = 1, 2, 3$. The physical meaning of the quantities Γ_{st} becomes obvious from the consideration of the dipole moment. It can be easily shown that because the operator of dipole moment (3) is antisymmetric under inversion, the average value of the dipole moment is equal to

$$\langle\mathbf{d}\rangle = \sum_{s>t}^{3} 2\,\mathrm{Re}\,\rho_{st}\int\psi_s^*\mathbf{d}\psi_t\,\mathrm{d}V. \tag{12}$$

Hence, it follows that the Γ_{st} characterize the relaxation rate of the dipole moment that was induced during the excitation by the pumping pulse. However, in contrast to the relaxation of the level populations, which is mainly determined by inelastic scattering, the relaxation of the dipole moment can also occur due to the processes of misorientation of the moment, which are related to elastic scattering. Therefore, it makes sense to introduce a correction for elastic scattering into the quantities Γ_s, i.e., to redefine Γ_s by writing it as $\Gamma_s = 1/(2\tau_s) + \Gamma_s^*$. These processes can be especially important for the low-energy (i.e., first) state because of the interaction with the phonons and impurities. If we neglect the dephasing of the third (vacuum) state and the elastic dephasing of the second state, then $\Gamma_{23} = \Gamma_2 + \Gamma_3 \approx \Gamma_2 \approx 1/2\tau_2$. Because $\Gamma_{12} = \Gamma_1 + \Gamma_2$ and $\Gamma_{13} = \Gamma_1 + \Gamma_3$, then, for the strong elastic scattering of the first state, the approximation of 'rapid dephasing' is introduced for these quantities by setting $\Gamma_{12} = \Gamma_{13} \approx 1\ \mathrm{fs}^{-1}$. The electric field in the TR-2PPE experiment is written as

$$\begin{aligned}
\mathbf{E}(t) = {}& \mathbf{E}_1(t)g_1(t)\cos(\omega_1 t)\\
&+ \mathbf{E}_2(t)g_2(t+\Delta)\cos\left[\omega_2(t+\Delta)\right],
\end{aligned} \tag{13}$$

where $g_1(t)$ and $g_2(t+\Delta)$ (where Δ is the delay time of the second pulse) are the envelope functions of the pulses, which are determined from special measurements [73].

In a weak field, the matrix elements ϕ_{st} can be given arbitrary sufficiently low values because they are proportional to the electric field strength. Both the experimental and calculated correlation traces are normalized to unity at $\Delta = 0$; therefore, it barely depends on the concrete choice of $\phi_{12,23}$.

In the final analysis, only one unknown parameter, the relaxation time τ_2, remains in dynamic equations (4). Neglecting the dependence of ρ_{22} on the distance to the surface, we can write the correlation trace for electrons excited by a pumping photon $\hbar\omega$ into the intermediate level E_2 as

$$I^{2\mathrm{PPE}}(\hbar\omega + E_\mathrm{i}, \Delta) = \int_{-\infty}^{\infty} \mathrm{d}t\, P(t)\, \rho_{22}(t)\,, \qquad (14)$$

where $P(t) = |\mathbf{E}(t)|^2$ is the intensity of the laser field. For experiments with cross correlation, the trace can be written in the form [73]

$$\begin{aligned} I^{2\mathrm{PPE}}&(\hbar\omega + E_\mathrm{i}, \Delta) \\ &\sim \int_{-\infty}^{\infty} P(t) \int_{-\infty}^{t} P(t') \exp\left(-\frac{t-t'}{\tau_2}\right) \mathrm{d}t\, \mathrm{d}t' \\ &+ \int_{-\infty}^{\infty} P(t+\Delta) \int_{-\infty}^{t} P(t'+\Delta) \exp\left(-\frac{t-t'}{\tau_2}\right) \mathrm{d}t\, \mathrm{d}t' \\ &+ \int_{-\infty}^{\infty} P(t) \int_{-\infty}^{t} P(t'+\Delta) \exp\left(-\frac{t-t'}{\tau_2}\right) \mathrm{d}t\, \mathrm{d}t' \\ &+ \int_{-\infty}^{\infty} P(t+\Delta) \int_{-\infty}^{t} P(t') \exp\left(-\frac{t-t'}{\tau_2}\right) \mathrm{d}t\, \mathrm{d}t'\,, \qquad (15) \end{aligned}$$

where the first two terms are independent of the delay and form the 'background' of the trace (see Fig. 3); the two following terms form the 'bell' of the trace. By fitting the calculated trace to the experimental trace, we can find the relaxation time τ_2. With a parallel orientation of the fields in the first and second pulses, their sum contains a second harmonic; therefore, there appears a probability of coherent excitation, i.e., of the direct transition of an electron from the ground to the vacuum state. The more complete version of the three-level model including the possibility of coherent excitations was developed in [16, 33, 74]. In the experimental correlation trace, coherent excitations manifest themselves in the form of an additional peak near $\Delta = 0$, which is narrower than the basic bell. Because the narrow peak does not bear information on the lifetime of the intermediate state, the measurements are most frequently carried out using orthogonal pumping and probing pulses.

In Refs [32, 33, 75], special versions of the three-level model were developed, which allowed evaluating the lifetime of hole excited states. But the cross-correlation TR-2PPE methods were most widely used in combination with the three-level model in studies of electron excitations on the surface [32, 67, 75, 76] and in the bulk of crystals [19, 67, 75] and of adsorbate states on the surface of metals [20]. In combination with the first-principle approaches, the above methods were also used for studying the dynamics of electrons in Ta [49], Yb [50], and Rh and Mo [68]. In the absence of additional processes, which are discussed in Section 2.1.3, the relaxation times obtained from the experiment agree quite well with the lifetimes calculated from first principles (see Section 4.4). The statistical error in the determination of relaxation times is estimated as $\pm(2-3)$ fs.

2.1.3 Inelastic scattering of electrons and 'additional' processes. Figure 4 schematically presents processes that can affect the relaxation time of an electron excited by a pumping pulse onto an intermediate level E_i (the second level in a three-level model) located above the Fermi energy. The main process is the inelastic scattering of the primary excited electron (e_1)

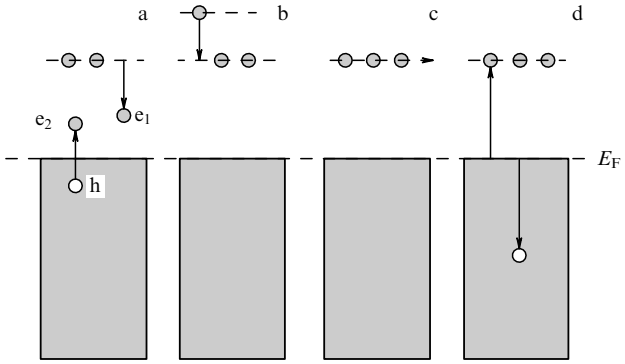

Figure 4. Processes that determine the lifetime of electrons in the excited state (schematic): (a) inelastic scattering of a primary electron (e_1) with the excitation of an electron–hole pair ($\mathrm{e}_2-\mathrm{h}$); (b) cascade process; (c) transport process; and (d) the excitation of Auger electrons.

with the excitation of an electron–hole pair ($\mathrm{e}_2-\mathrm{h}$) due to the energy lost by the primary electron. This was first shown by measurement of the relaxation times of electrons in simple and noble metals and by comparison with the lifetimes obtained from the theory of the interacting free electron gas [16, 19, 26–28, 76]. Later, the principal role of this process was confirmed by a comparison of experimental data with the lifetimes obtained from the first-principle calculations based on the many-body theory. Such calculations, mainly performed using the GW method, which considers processes of only this type, are discussed in Section 4. The processes b, c, and d in Fig. 4 are additional; they can manifest themselves for a number of objects under some specific experimental conditions.

Cascade processes. If the pumping pulse has an energy $\hbar\omega$, then electrons with energies in the range from $E_\mathrm{F} - \hbar\omega$ to E_F can be excited, i.e., the energy of the excited electron E_i can be from E_F to $E_\mathrm{F} + \hbar\omega$. Therefore, if $E_\mathrm{i} < E_\mathrm{F} + \hbar\omega$, then in the time between the pumping and probing pulses, the population of the intermediate level can increase due to electrons that fall from the higher populated levels; this is the heart of so-called cascade processes, which can lead to an increase in the relaxation time. More precise estimates can be obtained from the many-body theory. According to the classic work by Quinn and Ritchie performed in the framework of the Fermi liquid theory [77, 78], the electron loses from 1/2 to 2/3 of the excess energy $E_\mathrm{i} - E_\mathrm{F}$ in a single scattering; therefore, due to the cascade processes, the population of the levels from E_F to $E_\mathrm{F} + \hbar\omega/2$ can increase. The effect of cascade processes was first noted in paper [19] devoted to relaxation times of excited electrons in copper. In Ref. [22], a semiempirical method for the evaluation of the effect of cascade processes on the relaxation time was developed based on the Boltzmann equation. A brief description of this theory is given in Section 3.1, and the applications of the theory are compared with experimental results in Section 4.2. In particular, it was shown that the increase in the relaxation time connected with the cascade processes can be partially compensated due to transport processes (see below), and the total effect can be insignificant. No first-principle theory of cascade processes exists yet, but there are at least two experimental methods for probing their presence. If the photoemission spectrum is independent of the delay time of the second pulse, this means that the cascade processes do not influence the

population of the intermediate level. On the other hand, the effect of cascade electrons on the relaxation time for a certain level E_i depends on the energy of the pumping photon, and if this dependence is absent, then the contribution of cascade processes during relaxation for the E_i level is also insignificant.

Transport processes. A second type of additional processes is the transport of electrons from the laser-irradiated region. It can diminish the time-dependent electron population of the intermediate state, i.e., decrease its relaxation time. The basic features of transport processes were first considered for the noble metals in Refs [26, 27]. In particular, it was shown that the transport of electrons in single-crystal films occurs with a velocity comparable with the electron velocity at the Fermi level, $\sim 10^8$ cm s^{-1}, i.e., it is predominantly ballistic. Because the size of the irradiation spot is a macroscopic quantity (approximately 100 μm) and because the depth of light penetration is approximately 100 Å, transport occurs mainly perpendicular to the surface, since the transport in any direction parallel to the surface is compensated by transport in the opposite direction. With these factors taken into account, it was concluded in [27] that for 20–30 fs after the maximum of the first pulse, the transport effects in noble metals noticeably reduce the relaxation time.

According to Matthiessen's rule [79], if the relaxation of a state is controlled by several independent processes, the relaxation rates that correspond to these processes are summed. In particular, if the decay of an excited state is defined by inelastic electron–electron scattering and transport processes, then the total relaxation time is given by

$$\frac{1}{\tau} = \frac{1}{\tau_{\text{inel}}} + \frac{1}{\tau_{\text{trans}}}\,, \tag{16}$$

where τ_{inel} characterizes the effect of inelastic scattering and τ_{trans} corresponds to the contribution of transport processes. In the framework of this approximation, the dependence of transport effects on the electron energy at the intermediate level E_i was estimated in [32] based on first-principle band energies and electron velocities in copper. It was shown that τ_{trans} only weakly depends on E_i. According to the Fermi liquid theory, τ_{inel} decreases with increasing the energy according to a law that is qualitatively similar to $(E_i - E_F)^{-2}$ [25, 77], and therefore the role of transport effects in comparison with inelastic scattering increases with decreasing E_i. In the same work, it was shown that the transport effects depend substantially on the Miller indices of the surface.

It is obvious that for transition metals, the transport effects are much less essential than for noble metals, because the velocity of d electrons in the latter is several times lower than that of the nearly free electrons (see Section 4.6). For the simple and noble metals, if only the inelastic lifetime τ_{inel} is to be estimated, some measures can be undertaken that decrease the transport effects. Transport effects can be reduced due to the elastic scattering at grain boundaries, i.e., by using polycrystalline films instead of single-crystal ones. During elastic scattering, the directions of the wave vectors of excited electrons are randomized, which can lead to a decrease in the rate of escape of electrons from the irradiated region. A similar effect is provided by the elastic scattering of the excited electrons on phonons and defects. If experiments are conducted on thin single-crystal films, the transport can be decreased by using insulators as the substrates, which impede the draining of the excited electrons from the film [80].

Auger electrons and the role of d bands. A very interesting additional process that can increase the relaxation time of excited electrons in noble metals is the process of the generation of Auger electrons, which was first observed in copper [32, 74] and was emotionally named a 'd-band catastrophe.' It is connected with the existence of two types of holes generated by the pumping pulse along with excited electrons. If the energy of a pumping photon is less than the threshold energy of the d bands (~ 2 eV for copper), then both electrons and holes appear in the s and p bands. They have a relatively short lifetime, which qualitatively corresponds to the Fermi liquid theory. If the energy of the pumping photon exceeds the threshold energy of the d bands, the electrons appear in the s and p bands, which are similar to the bands of free electrons, but the holes are generated partially in d bands, and they have considerably longer lifetimes (see the results of first-principle calculations in Section 4.2). In this case, a process of generation of Auger electrons occurs (Fig. 4d); the electrons from levels lying above the d states fill holes existing in d bands, and the liberated energy quantum is then spent on a new electron excitation. If the energy of the level E_i is less than the threshold energy of the d bands, the population of this level increases, which is equivalent to an increase in the relaxation time. In Ref. [81], an analogous process was described for gold. If the aim of a study is the lifetime and there is a need to avoid the influence of Auger electrons, then the experiment should be conducted at photon energies less than the threshold energy of the d band, i.e., using a red laser. Such measurements were made for copper in [28]; the data obtained there correspond much better to the results of first-principle calculations than the data of measurements obtained at the photon energy of 3 eV (see Section 4.2).

Electron–phonon scattering. In principle, electron–phonon scattering can also affect the relaxation time of an electron in the intermediate excited state. But in contrast to the inelastic electron–electron scattering, the energy losses of the excited electron upon the generation of phonons are limited by the low energy of phonons. In TR-2PPE experiments, the excess energy $E_i - E_F$ of an electron is usually much greater than the energy of phonons; therefore, electron–phonon scattering can be considered a quasielastic process, i.e., can be referred to dephasing processes.

The contribution of the electron–phonon scattering can be controlled by conducting TR-2PPE experiments at an ambient temperature sufficiently low to suppress the formation of phonons. Such experiments were carried out, for example, in [82] for copper. At excess energies $E_i - E_F > 1$ eV, the relaxation time is virtually independent of temperature, but at lower energies, a certain insignificant effect is observed. Measurements at different temperatures were carried out for ytterbium [50]; they also showed that the relaxation time was independent of the temperature. In Refs [83, 84], the contribution of the electron–phonon interaction to the magnitude of the lifetime of electrons in beryllium and palladium was studied theoretically.

2.2 Angle-resolved photoemission spectroscopy

The possibility of estimating the lifetime of excited electrons and holes using ARPES follows from the uncertainty principle [72], according to which the uncertainty ΔE in the energy of a state is related to its lifetime Δt as

$$\Delta t\, \Delta E \geqslant \hbar\,. \tag{17}$$

It follows from Eqn (17) that to obtain the error in determining a lifetime equal to ± 3 fs, as in the TR-2PPE method, the resolution in the case of ARPES spectroscopy should be not worse than 10 meV. Many commercial spectrometers (see, e.g., Ref. [8]) have a similar resolution. However, many problems exist in studies of the dynamics of electrons by the ARPES method, and work in this field is quite scarce.

Because a nearly free electron, which is detected by an analyzer, and a hole in the crystal are simultaneously generated in the photoemission by one photon, it follows that the linewidth in the ARPES method is determined by the lifetimes of both the electron and the hole. Here, an essential complication arises because of the influence of the surface on the spectral line shape. This influence originates from the nonconservation of the wave vector component perpendicular to the surface, which leads to a broadening of the line. The magnitude of this effect depends strongly on the emission angle, which was analyzed in Refs [8, 14, 15, 85]. The photoemission spectrum is usually recorded in the form of the dependence of the number of photoelectrons on the kinetic energy at a fixed emission angle θ and the photon energy $\hbar\omega$. It was shown in Ref. [85] that under the assumption of a Lorentz shape of the undisturbed spectral line and linear dispersion of the electron and hole bands with the influence of the surface taken into account, the full width of the line at the half-maximum (FWHM) becomes equal to

$$\Gamma = \frac{\Gamma_\mathrm{h}/|v_{\mathrm{h}\perp}| + \Gamma_\mathrm{e}/|v_{\mathrm{e}\perp}|}{\left|1/v_{\mathrm{h}\perp}(1 - m v_{\mathrm{h}\parallel} \sin^2\theta/\hbar k_\parallel) - 1/v_{\mathrm{e}\perp}(1 - m v_{\mathrm{e}\parallel} \sin^2\theta/\hbar k_\parallel)\right|} . \tag{18}$$

(We note that in the many-body theory and in a number of experimental works, the FWHM is denoted as 2Γ!) Here, Γ_e and Γ_h are the inverse relaxation times (relaxation rates) of the electron and hole:

$$\Gamma = \frac{\hbar}{\tau} , \tag{19}$$

$v_\perp = \hbar^{-1}\,\partial E/\partial k_\perp$ is the component of the group velocity that is perpendicular to the surface, and $k_\parallel$ is the component of the wave vector that is parallel to the surface. Therefore, Γ is not the inverse relaxation time of the electron or hole, but their combination, which depends on the conditions of the experiment. Usually, the excess energy of the emitted electron, i.e., its energy with respect to the Fermi level, reaches several tens of electron volts. It is much greater than the excess energy of a hole, and therefore $\Gamma_\mathrm{e} \gg \Gamma_\mathrm{h}$, i.e., the FWHM is mainly determined by the electron lifetime. The inverse relaxation times of high-energy electrons with energies up to 100 eV satisfy the empirical relation

$$\Gamma_\mathrm{e} = a(E - E_\mathrm{F}) , \tag{20}$$

where $a = 0.13 \pm 0.1$ [86], i.e., they strongly deviate from the quadratic law $\Gamma \sim (E - E_\mathrm{F})^2$ that follows from the Fermi liquid theory; this appears to be due to the participation of plasmons in the electron relaxation [87]. Nevertheless, under some specific conditions, it is possible to determine the lifetime of holes as well. For normal emission, i.e., when $\theta = 0$ and $v_\parallel = 0$, we have

$$\Gamma = \left(\Gamma_\mathrm{h} + \frac{v_{\mathrm{h}\perp}}{v_{\mathrm{e}\perp}}\,\Gamma_\mathrm{e}\right)\left(\left|1 - \frac{v_{\mathrm{h}\perp}}{v_{\mathrm{e}\perp}}\right|\right)^{-1} . \tag{21}$$

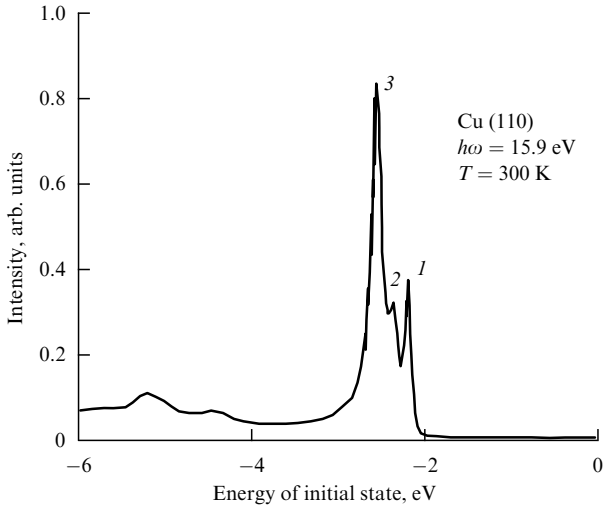

Figure 5. Photoemission spectrum of copper recorded from a Cu(110) sample at the photon energy $\hbar\omega = 15.9$ eV [88]. The energy of the initial (hole) state is given relative to the Fermi energy E_F.

If $v_{\mathrm{h}\perp} = 0$, then $\Gamma = \Gamma_\mathrm{h}$. For example, this means that in the case of an fcc structure, measurements of the relaxation time of holes are possible for states with the wave vector oriented along the azimuth $\Gamma - \mathrm{K} - \mathrm{X}$. Such studies were carried out for copper [88] and silver [89]. Figure 5 shows, as an example, the shape of the photoemission spectrum obtained from a Cu(110) thin film at $\hbar\omega = 15.9$ eV. Below 2 eV, i.e., below the d-band threshold, the spectrum contains three narrow lines, which relate to the emission from the states X_{7+} (1), X_{6+} (2), and X_{7+} (3); by resolving the spectrum into Lorentz components, it is possible to determine their FWHMs and, correspondingly, the relaxation times. But the measurements of the relaxation times of states at energies from 2 eV to E_F are impossible because of the strong broadening of the bands in view of the nonconservation of the vector $k_\perp$. We note that the surface states are free of the effect of broadening in $k_\perp$; therefore, measurements of the lifetimes for them can be carried out relatively easily [90].

The linewidth Γ also includes broadening due to surface defects, Γ_def, and due to electron–phonon interaction, $\Gamma_{\mathrm{e-ph}}$. The broadening Γ_def can be eliminated by recording ARPES spectra at different concentrations of surface defects and extrapolating the results to the zero concentration of defects [88, 91]. The concentration of defects can be changed by varying the regimes of annealing of the samples after ion bombardment [88]. In a similar way, by conducting measurements at different temperatures and extrapolating the results to the zero temperature, it is possible to estimate the contribution $\Gamma_{\mathrm{e-ph}}$. According to the many-body theory of the electron–phonon interaction [92], this quantity is expressed as

$$\Gamma_{\mathrm{e-ph}}(T) = 2\pi\hbar\lambda \int_0^{\omega_\mathrm{D}} \mathrm{d}\omega' \left(\frac{\omega'}{\omega_\mathrm{D}}\right)^2 \left[1 - f(\omega - \omega') + 2n(\omega') + f(\omega + \omega')\right] , \tag{22}$$

where $f(\omega)$ is the Fermi distribution for electrons, $n(\omega)$ is the Bose distribution for phonons, and $\hbar\omega_\mathrm{D}$ is the maximum energy of phonons in the Debye approximation. Given the experimental temperature dependence of $\Gamma_{\mathrm{e-ph}}$, it is possible to determine the electron–phonon coupling constant λ.

We note that the TR-2PPE and ARPES methods of studying the relaxation of excited states are complementary. The TR-2PPE method allows extracting the relaxation times of electrons with an excess energy from zero to the energy of pumping photons, but the relaxation times cannot be resolved in the wave vector. On the contrary, the ARPES method allows obtaining the lifetimes of states with an accurately determined wave vector, but only if there is no dispersion of the state in the vector $k_{\perp}$.

2.3 Spintronic devices: spin-valve transistor and magnetic tunnel transistor

The spin-valve transistor (SVT) and the magnetic tunnel transistor (MTT) are devices with a giant response of electron transport properties to an applied magnetic field and are the prototypes of many industrial nanoelectronic devices (magnetic sensors, storage cells, etc.). Studies on the physics of SVTs and MTTs were described in detail in Refs [11 – 13]; in this section, we therefore limit ourselves to the consideration of the role of electron relaxation in the functioning of SVTs and MTTs and of the methods of extracting data on the relaxation of excited electrons from experiments with SVTs and MTTs.

The giant response of electron transport effects to an applied magnetic field is a consequence of the difference in the relaxation lengths of electrons with spin 'up,' i.e., with the magnetization parallel to the applied field, and electrons with spin 'down,' i.e., with the magnetization antiparallel to the field. Figure 6 shows a simplified diagram of an SVT and the energy diagrams that elucidate the reaction of the device to the applied field. The electron conduction of the device is mainly ballistic, and the charge carriers are electrons with an energy exceeding the height of the Schottky barrier at the boundary between the semiconductor emitter of the n type (Si) and the first nonmagnetic layer of the base (NM1). The base has three nonmagnetic layers (Pt, or Pd, or Au) and two magnetic layers with a different coercivity (Fe, or Co, or permalloy). The electrons, after they overcome the Schottky barrier, move in the base, losing their energy. Electrons with a residual energy exceeding that of the second Schottky barrier between the last layer of the base (NM3) and the collector penetrate the collector and form the collector current I_c. Because the coercivity of the ferromagnetic (FM) layers is different, they can have parallel or antiparallel magnetizations. With properly chosen heights of the Schottky barriers and thicknesses of the FM layers, the collector currents for the parallel and antiparallel magnetizations, I_c^P and I_c^{AP}, can be very different. Figure 6b schematically also shows changes in the energy that are due to the electron motion. In a ferromagnet, electrons with spins up have a relaxation time and a relaxation length much larger than the electrons with spins down. The reasons for this are discussed in Sections 4.5 and 4.6. In the case of FM layers with parallel magnetizations, it is possible to choose their thicknesses such that spin-up electrons penetrate the collector, while spin-down electrons are reflected by the second Schottky barrier. If the magnetizations of the layers are antiparallel, the electrons that had the spin up in the FM1 layer become electrons with spins down when they pass into the FM2 layer. Their relaxation rate increases, and at a suitable thickness of the FM2 layer, they are also reflected from the second barrier. The field of magnetization reversal is equal to 22 Oe in Co and 5 Oe in Ni. Therefore, in the fields $22 > H > 5$ Oe, the magnetizations in the layers are antiparallel, and in the fields exceeding

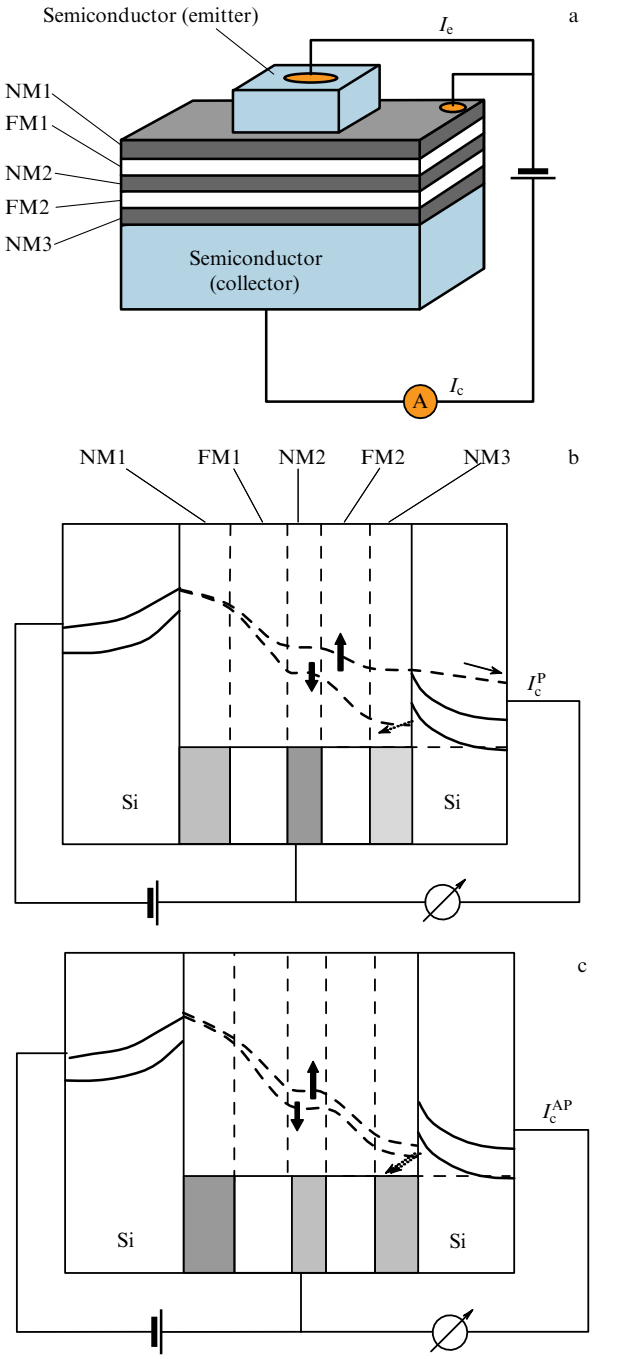

Figure 6. (a) Schematic of a spin-valve transistor and (b, c) energy diagrams of a transistor at the parallel orientation of the magnetizations in the ferromagnetic layers FM1 and FM2 (b) and at the antiparallel orientation of magnetizations FM1 and FM2 (c). NM1, NM2, and NM3 are the nonmagnetic layers of the transistor.

22 Oe, they are parallel. A practically interesting characteristic of an SVT is the so-called magnetocurrent, defined as

$$I_{MC} = \frac{I_c^P - I_c^{AP}}{I_c^{AP}}\,; \tag{23}$$

its value can reach 500% [12, 93].

It is obvious that the existence of a difference in the relaxation lengths for spin-up and spin-down electrons is very important for switching the collector current. The experimental determination of the relaxation length of an

electron is based on measuring the dependence of the collector current on the thicknesses of the ferromagnetic layers. The collector current for the parallel and antiparallel orientations of magnetizations in the FM layers can be written as [12]

$$I_c^{\mathrm{P}} \propto T_{\mathrm{FM1}}^{M} T_{\mathrm{FM2}}^{M} + T_{FM1}^{m} T_{\mathrm{FM2}}^{m}\,,$$
$$I_c^{\mathrm{AP}} \propto T_{\mathrm{FM1}}^{M} T_{\mathrm{FM2}}^{m} + T_{\mathrm{FM1}}^{m} T_{\mathrm{FM2}}^{M}\,, \tag{24}$$

where the coefficients of electron transmission in the FM1 and FM2 layers for spin up (M) and spin down (m) are introduced. It is assumed that they depend on the thicknesses of the layers d and the structure of the interfaces as

$$T_{\mathrm{FM}i}^{\mu} = \Gamma_{\mathrm{in}}^{\mu} \exp\left(-\frac{d}{\lambda_{\mathrm{FM}i}^{\mu}}\right)\Gamma_{\mathrm{out}}^{\mu}\,, \tag{25}$$

where $\mu = M$ or m, Γ_{in} is the transmission coefficient of the interface for the electrons entering the layer, and Γ_{out} is the transmission coefficient of the interface for the electrons that leave the layer. The magnitudes of Γ depend on a mismatch of the band structure on the opposite sides of the interface, on the degree of disordering of the interface, on the presence of impurities, etc. For the layer thicknesses $d > 40$ Å, the exponential dependence on d is confirmed by experiments [94]. The magnitudes of λ, the relaxation lengths, are determined by the inelastic and elastic scattering of electrons and by the electron–phonon and electron–magnon interactions (see below). Experiments show the existence of a very weak dependence of Γ_{in} and Γ_{out} on the orientation of spins. These quantities, together with the relaxation lengths, can be found by fitting the calculated collector currents to the experimental ones, using Eqn (24).

The MTT differs from the SVT mainly in that in the MTT, the injection of the excited electrons into the base occurs not through a Schottky barrier but through a tunnel barrier between the probe and the surface of the base. The physics of electron conduction in the MTT is similar to that in the SVT, and the relaxation length of the excited electrons in MTTs is measured analogously.

Similarly to the relaxation time, the relaxation length is mainly determined by inelastic scattering, but is also affected by some additional processes. According to Matthiessen's rule, the quantity $1/\lambda^{\mu}$ can be represented as the sum of contributions of different scattering processes:

$$\frac{1}{\lambda^{\mu}} = \frac{1}{\lambda_{\mathrm{inel}}^{\mu}} + \frac{1}{\lambda_{\mathrm{el}}^{\mu}} + \frac{1}{\lambda_{\mathrm{phon}}^{\mu}} + \frac{1}{\lambda_{\mathrm{swa}}^{\mu}} + \frac{1}{\lambda_{\mathrm{swe}}^{\mu}}\,, \tag{26}$$

where $\lambda_{\mathrm{inel}}^{\mu}$ is the inelastic relaxation length, $\lambda_{\mathrm{el}}^{\mu}$ corresponds to elastic relaxation, and $\lambda_{\mathrm{phon}}^{\mu}$ is the relaxation due to electron–phonon scattering. The last two terms are nonzero only for ferromagnets; λ_{swa} is connected with the spin-wave absorption, and λ_{swe}, with the spin-wave emission.

The most important contribution to the total relaxation length λ^{μ} comes from the inelastic relaxation length $\lambda_{\mathrm{inel}}^{\mu}$, but processes of elastic relaxation can also give a comparable contribution. This is confirmed by both experimental and theoretical data. If the inelastic relaxation is predominant, we can expect a monotonic decrease in λ^{μ} with increasing the energy because of a decrease in the inelastic lifetime, which is observed, for example, for the $Ni_{80}Fe_{20}$ layer in a $CoFe/Al_2O_3/NiFe$ SVT [95]. But this tendency is absent, for example, for the platinum layer in the Si/Pt/NiFe/Au/Co/Au/Si SVT [96] or for the iron layer in the NiFe/Au/Fe structure [93]. An attempt to include the elastic and inelastic scattering into the phenomenological model of the collector current in the SVT was made in [97]; however, the authors ignored the dependence of scattering on the electron energy. A series of first-principle calculations for $\lambda_{\mathrm{inel}}^{\mu}$ is discussed in Section 4.6. A comparison of the computed values of $\lambda_{\mathrm{inel}}^{\mu}$ with the experimental values of λ^{μ} confirms the significant role of elastic scattering processes.

Two terms in Eqn (26), $\lambda_{\mathrm{phon}}^{\mu}$ and $\lambda_{\mathrm{swa}}^{\mu}$, are temperature dependent. They correspond to the absorption of thermal phonons and magnons by the excited electron; therefore, they must tend to infinity as $T \to 0$. The temperature dependence of λ^{μ} was studied experimentally for $Ni_{80}Fe_{20}$ and Co layers in Ref. [94]. A substantial increase in $\lambda_{\mathrm{swa}}^{\mu}$ was revealed as the temperature decreased to 100 K. However, even at room temperature, this quantity is greater than λ^{μ} or $\lambda_{\mathrm{inel}}^{\mu}$, i.e., the absorption of magnons is an insignificant process compared to inelastic scattering.

In contrast to $\lambda_{\mathrm{phon}}^{\mu}$ and $\lambda_{\mathrm{swa}}^{\mu}$, the term $\lambda_{\mathrm{swe}}^{\mu}$, which corresponds to the emission of spin waves, does not tend to infinity as $T \to 0$, because the electrons in ferromagnets can lose energy via emission of spin waves at any temperature. (The emission of phonons, which can occur even at 0 K, is referred to as quasielastic scattering; see Section 2.1.2.) The energy loss of excited electrons by the generation of spin waves was studied based on the many-body theory in Refs [46, 48, 98] (see Sections 4.5, 4.6). Because of the conservation of the total spin angular momentum, only spin-down electrons can lose energy, generating spin waves. For Fe and Ni, first-principle calculations were carried out. They showed that the generation of spin waves was only important in iron for spin-down electrons with an excess energy up to 1 eV [46, 48].

3. Theoretical approaches to femtosecond dynamics

Note: In this section, which is mainly devoted to the many-body relaxation theory of an excited electron, we predominantly use the Hartree system of atomic units, which is usual for this theory, i.e., we assume that $\hbar = m_e = e = 1$, the unit of length is the Bohr radius $a_0 = 0.529$ Å, the energy unit (frequently called hartree) is $e^2/a_0 = 27.2116$ eV, and the velocity unit is the electron velocity on the first Bohr orbit $v_0 = \alpha c = 2.19 \times 10^8$ cm s^{-1}.

3.1 Perturbation theory and the Boltzmann equation

A series of semiempirical studies of the dynamics of electrons in the bulk of solids were carried out using a combination of the Boltzmann theory and perturbation theory (see Refs [21 – 24, 97, 99 – 103]). The Boltzmann theory in this case is used to describe the electron distribution function $g_{\sigma}(\mathbf{r}, \mathbf{k}, t)$, which depends on the spin σ, coordinate $\mathbf{r}$, momentum $\mathbf{k}$ (which is equal to the wave vector in the Hartree system), and time t. The time evolution of the distribution function for an electron in an external electromagnetic field is described by the equation

$$\frac{\mathrm{d}g_{\sigma}}{\mathrm{d}t} = \frac{\partial g_{\sigma}}{\partial t} + \mathbf{v}\,\nabla_{\mathbf{r}} g_{\sigma} + \frac{\partial \mathbf{k}}{\partial t}\,\nabla_{\mathbf{k}}\, g_{\sigma} = S_{\sigma}(\mathbf{r}, \mathbf{k}, t) + \left(\frac{\mathrm{d}g_{\sigma}}{\mathrm{d}t}\right)^{\mathrm{coll}}\,, \tag{27}$$

where $\partial \mathbf{k}/\partial t = \mathbf{F} = -e(\mathbf{E} + (1/c)\mathbf{v} \times \mathbf{H})$ is the Lorentz force, S_{σ} is the source function, and the term $(\mathrm{d}g_{\sigma}/\mathrm{d}t)^{\mathrm{coll}}$ describes the change in g_{σ} caused by 'collisions' with other electrons,

impurities, and phonons [79, 104, 105]. For the last term, a relaxation-time approximation is typically used, in which it is assumed that the collisions tend to take the system to an equilibrium with the distribution function g_0 of the system in a zero external field. For a macroscopically homogeneous system in a weak laser field with a low photon energy, we can assume that $\nabla_{\mathbf{r}} g = 0$ and neglect the term $\partial\mathbf{k}/\partial t\,\nabla_{\mathbf{k}} g$ and the source strength. Then, in the relaxation-time approximation, the following expression is valid for this system:

$$\left(\frac{\mathrm{d}g_\sigma}{\mathrm{d}t}\right)^{\mathrm{coll}} = \frac{g_{\sigma 0}(\mathbf{k}) - g_\sigma(\mathbf{k})}{\tau(\mathbf{k})}\,, \tag{28}$$

where $\tau(\mathbf{k})$ is the relaxation time. At a small source strength, the distribution function $g_{\sigma 0}$ for a homogeneous system is the usual Fermi–Dirac distribution.

We can begin with assuming that the energy loss of a primary excited electron occurs through the excitation of a secondary electron, which interacts with the primary electron via a dynamically screened potential $W(\omega)$, which depends on the transferred energy ω. Then, to compute the relaxation time we can use the perturbation theory [72]. In this theory, according to the Fermi golden rule, the probability of transition of primary electrons per unit time from the state i into a state f with a smaller energy upon excitation of the secondary electron from the state i' into a higher state f' is equal to

$$p_{f,f'}^{i,i'} = 2\pi \left|W_{f,f'}^{i,i'}(\omega)\right|^2 \delta(\epsilon_i + \epsilon_{i'} - \epsilon_f - \epsilon_{f'})\,. \tag{29}$$

Here, W is the matrix element of the dynamically screened interaction potential $W(\omega)$:

$$W_{f,f'}^{i,i'}(\omega) = \left\langle i, i' \middle| W(\omega) \middle| f, f' \right\rangle = \int \mathrm{d}\mathbf{r}\,\mathrm{d}\mathbf{r}'\,\psi_i^*(\mathbf{r})\,\psi_{i'}^*(\mathbf{r}')\,W(\omega, \mathbf{r}-\mathbf{r}')\,\psi_f(\mathbf{r})\,\psi_{f'}(\mathbf{r}')\,. \tag{30}$$

Summing the probabilities of all possible excitations of the secondary electron weighted by the distribution function yields the total probability of the transition $i \to f$ of the primary electron with a reduction in energy:

$$P(i, f) = \sum_{i', f'} p_{f,f'}^{i,i'} g(\epsilon_{i'}) \left[1 - g(\epsilon_{f'})\right]\,. \tag{31}$$

Upon further summation over the lower states of f with their populations taken into account, we obtain the probability of transition per unit time, i.e., the relaxation rate:

$$\frac{1}{\tau(\epsilon_i)} = \sum_f P(i, f)\left[1 - g(\epsilon_f)\right]\,. \tag{32}$$

In Refs [99, 100, 106], various types of electron–electron scattering processes were considered, such as direct and exchange scattering, processes with the conservation of energy in the spin channel of the primary electron, and with energy transfer to states with the opposite spin. The realistic calculations are based on the assumption that elements averaged over the wave vector can be used instead of the matrix elements $W_{f,f'}^{i,i'}(\omega)$. This is the so-called 'random-**k**' approximation, which was first introduced in Refs [107, 108]. If the transitions $i \to i'$ and $f \to f'$ occur between states of the same type (e.g., d states), then the expression for the relaxation rate of an electron with an excess energy ϵ in this approximation is reduced to a formula with only one matrix element $M(\omega)$:

$$\frac{1}{\tau_\sigma(\epsilon)} = 2\pi \int_{E_\mathrm{F}}^{\epsilon} \mathrm{d}E'\,\rho_\sigma^{>}(E') \int_{E_\mathrm{F}-\omega}^{E_\mathrm{F}} \mathrm{d}E \times \left[\rho_\sigma^{<}(E)\,\rho_\sigma^{>}(E+\omega) + \rho_{-\sigma}^{<}(E)\,\rho_{-\sigma}^{>}(E+\omega)\right]\left|M(\omega)\right|^2, \tag{33}$$

where $\omega = \epsilon - E'$ is the energy lost by the primary electron, $\rho_\sigma^{>}(\epsilon) = [1 - g(\epsilon)]\,\rho_\sigma(\epsilon)$, and $\rho_\sigma^{<}(\epsilon) = g(\epsilon)\,\rho_\sigma(\epsilon)$, where $g(\epsilon)$ is the distribution function and $\rho(\epsilon)$ is the density of states. It can be assumed that in a narrow energy range, the matrix element M is constant. If the internal integral in Eqn (33) is only weakly dependent on the energy, then the relaxation rate is determined by the external integral

$$\frac{1}{\tau_\sigma(\epsilon)} \sim N_\sigma(\epsilon) = \int_{E_\mathrm{F}}^{\epsilon} \mathrm{d}E'\,\rho_\sigma^{>}(E')\,, \tag{34}$$

which represents a 'phase space' for a relaxing electron, i.e., the number of states allowed for transitions. The phase-space interpretation of the measurements of electron lifetimes was widely used in experimental works (see, e.g., Ref. [109]). The reliability of this approach was verified by the authors of this review by calculating the lifetimes in Al, Nb [110], Mo, Rh, Pd, Ag [111], and Fe, Ni, Pt, and Au [48] (see a discussion in Section 4). The general conclusion that follows from a comparison of the results obtained in the phase-space approximation with first-principle data is that the phase-space approximation correctly describes the dependence of the lifetimes on the electron energy and spin in a number of cases, but in general, the best results are obtained in terms of the random-**k** approximation [Eqn (33)].

In general, different states (of the s, p, or d type) can be present near the Fermi level. An example is given by the sufficiently complex band structures of nickel or iron (Fig. 7).

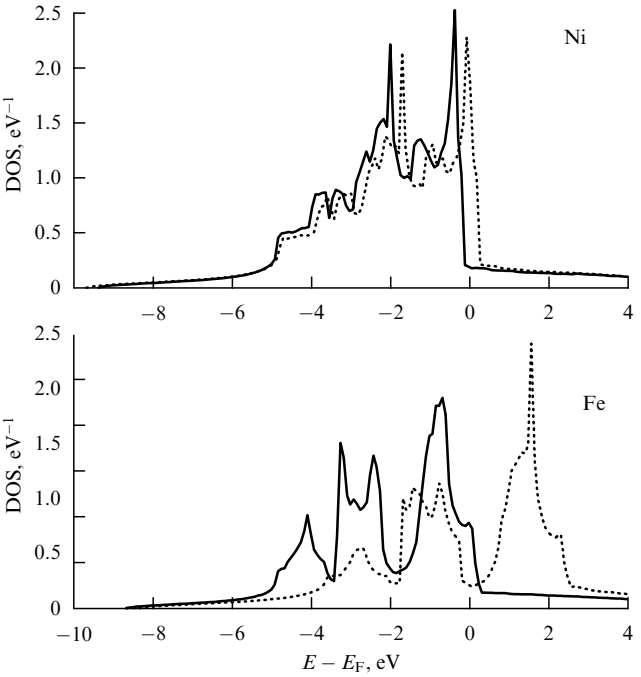

Figure 7. Density of states (DOS) in Fe and Ni [110]. Solid lines correspond to the DOS for spin-up electrons; the dashed lines are the DOS for spin-down electrons.

In the case of nickel, at the exchange splitting of the bands equal to 0.3 eV, the difference in the densities of states (DOS) for electrons with spins up and down can be neglected, i.e., it can be assumed that the occupied states are only states of the d type and that the empty states are nearly free states of the p type. Then the transitions of the primary electron are of the p → p type, while the excitations of the secondary electron are of the d → p type. Therefore, for Ni, we can use Eqn (33) with one matrix element $M \equiv M_{\mathrm{pp}}^{\mathrm{pd}}$ [with the arrangement of indices as in Eqn (30)]. In the case of iron, we can also assume that spin-up states below the Fermi level are d states, while those lying above the Fermi level are p states. However, spin-down d states also exist above the Fermi level; this is a peak in the DOS with a maximum at 1.7 eV. Therefore, we should introduce three different types of matrix elements (for details, see Ref. [100]). Analogous expressions can also be obtained for other objects, depending on their band structure. The matrix elements are determined by fitting the calculated relaxation rates to the experimental data. This method of evaluating relaxation rates was first used in [99, 100, 106] when studying the relaxation time and relaxation length for Fe, Ni, and Co. Similar methods with somewhat different approximations for the densities of states and matrix elements were also used in Refs [21, 23, 24, 102] for a number of ferromagnetic and nonmagnetic metals.

A more rigorous theory of relaxation of excited states must take the inhomogeneity of a system into account, i.e., at least, the presence of a surface, and also include the additional processes described in Section 2.1.2 for TR-2PPE spectroscopy. An analysis with transport and cascade processes taken into account was first carried out in [99, 100, 106]. Later, a more detailed analysis of the additional processes was performed in [22, 103, 112, 113] for Cu, Fe, Co, and Ni. In these works, the distribution function for an electron with an energy ϵ near the surface is characterized by the projection of the wave vector onto the surface ($k_{\parallel}$), the order number of the band (n), and the distance to the surface (z), i.e., $g_\sigma = g_\sigma(\epsilon, k_{\parallel}, n, z, t)$, and the Boltzmann equation is represented in the form

$$\frac{\partial g_\sigma}{\partial t} = P(t) - \frac{g_\sigma}{\tau^*} \,. \tag{35}$$

Here, $P(t)$ is the laser field intensity, which plays the role of a source function, and $\partial g_\sigma/\partial t$ contains terms that correspond to inelastic electron–electron scattering and to the additional processes, i.e.,

$$\frac{\partial g_\sigma}{\partial t} = \left(\frac{\partial g_\sigma}{\partial t}\right)^{\mathrm{opt}} + \left(\frac{\partial g_\sigma}{\partial t}\right)^{\mathrm{e-ph}} + \left(\frac{\partial g_\sigma}{\partial t}\right)^{\mathrm{inel}} + \left(\frac{\partial g_\sigma}{\partial t}\right)^{\mathrm{casc}} + \left(\frac{\partial g_\sigma}{\partial t}\right)^{\mathrm{trans}} + \left(\frac{\partial g_\sigma}{\partial t}\right)^{\mathrm{Au}} . \tag{36}$$

Because additional processes are included here, the time τ^* in this equation is not the lifetime but the relaxation time. In what follows, we omit details related to the presence of bands of the p and d types; they can be found in Refs [22, 103, 112, 113]. The term $(\partial g_\sigma/\partial t)^{\mathrm{opt}}$ corresponds to optically induced transitions of an electron from the excited to lower states, i.e., to transitions in which the role of the perturbation is played by the laser field. Since the laser field is weak (the fraction of excited atoms is $\sim 10^{-6}$), this term is negligibly small in comparison with the term $(\partial g_\sigma/\partial t)^{\mathrm{inel}}$, which depends on the screened electron–electron interaction potential W. We can also omit the small second term, which corresponds to the quasielastic electron–phonon interaction (a simple model in the random-**k** approximation was proposed for it in [112]). The term $(\partial g_\sigma/\partial t)^{\mathrm{inel}}$ is the rate of relaxation via inelastic electron–electron scattering, which was discussed above:

$$\left[\frac{\partial g_\sigma(\epsilon)}{\partial t}\right]^{\mathrm{inel}} = -\frac{g_\sigma(\epsilon)}{\tau_\sigma^{\mathrm{inel}}} \,. \tag{37}$$

Here, the time of inelastic processes is given by Eqns (33) or by similar equations in Refs [99, 100, 106]. The next term describes an increase in the population of the excited level due to the transitions of electrons from the higher levels populated as a result of the pumping pulse; it includes the time $\tau_\sigma^{\mathrm{casc}}$ that characterizes the intensity of the cascade processes:

$$\left[\frac{\partial g_\sigma(\epsilon)}{\partial t}\right]^{\mathrm{casc}} = \frac{1 - g_\sigma(\epsilon)}{\tau_\sigma^{\mathrm{casc}}} \,. \tag{38}$$

The expression for $\tau_\sigma^{\mathrm{casc}}$ can easily be obtained in the random-**k** approximation; it takes the densities of states and the distribution function into account and differs from Eqn (34) only in the integration limits:

$$\frac{1}{\tau_\sigma^{\mathrm{casc}}(\epsilon)} = 2\pi \int_{\epsilon}^{E_{\mathrm{F}}+h\nu} \mathrm{d}E' \, \rho_\sigma^{>}(E') \int_{E_{\mathrm{F}}-\omega}^{E_{\mathrm{F}}} \mathrm{d}E \times \sum_{\sigma'} \rho_{\sigma'}^{<}(E) \, \rho_{\sigma'}^{>}(E+\omega) |M|^2 \,. \tag{39}$$

As was shown in Section 2.1.2, in analyzing transport effects, we can neglect transport in directions parallel to the surface and examine only the transport perpendicular to the surface. The necessary expression is obtained with the use of the Liouville theorem [114]:

$$\left(\frac{\partial g_\sigma}{\partial t}\right)^{\mathrm{trans}} = -v_z \nabla_z g_\sigma \,. \tag{40}$$

The last term in Eqn (36) corresponds to the contribution of Auger processes (see Section 2.1.2). It satisfies an equation similar to Eqn (38) but with another characteristic time, $\tau_\sigma^{\mathrm{Au}}(\epsilon)$, which can also be obtained in the random-**k** approximation by analogy with Eqn (33). Namely, it can be shown that $\tau_\sigma^{\mathrm{Au}}(\epsilon)$ is given by the convolution

$$C_\sigma^{\mathrm{Au}}(\epsilon) = \int_{-\infty}^{0} \mathrm{d}E' \, \rho_\sigma^{<}(E') \int_{E_{\mathrm{F}}-h\nu}^{0} \mathrm{d}E \times \sum_{\sigma'} \rho_{\sigma'}^{<}(E) \, \rho_{\sigma'}^{>}(E+\omega) \,. \tag{41}$$

In this expression, the first integral accounts for all electrons that can be excited into a given energy level ϵ from the levels with a density of states $\rho_\sigma(E')$ due to the energy lost by the primary hole (i.e., by the energy that was generated by the pumping pulse). The second integral accounts for all possible ways of energy loss by the primary hole. The energy loss occurs when electrons 'fall' from states with the density $\rho_{\sigma'}(E+\omega)$ into hole-occupied states with the density $\rho_{\sigma'}(E)$; here, $\omega = \epsilon - E'$ is the energy lost by the hole. The smaller the lifetime of the primary hole $\tau_{\mathrm{h}}(\epsilon - h\nu)$, where $h\nu$ is the energy of the pumping photon, the greater the number of Auger electrons; therefore, we can assume that

$$\frac{1}{\tau_\sigma^{\mathrm{Au}}(\epsilon)} = R\tau_h(\epsilon - h\nu) C_\sigma^{\mathrm{Au}}(\epsilon) |M|^2 \,, \tag{42}$$

where R is an empirical constant. Because all the terms in Eqn (36) are now determined, we can solve Boltzmann equation (35) and calculate the correlation trace using Eqn (14) with trial values of the parameters $|M|$ and R. These parameters can then be refined via fitting to the experimental correlation trace.

3.2 First-principle approaches to the dynamics of electrons in an interacting free electron gas

The model of a free electron gas with interaction between the electrons (DFEG), also frequently called the Fermi liquid theory, is one of the simplest models of the many-body solid state theory. Nevertheless, it sufficiently well describes the dynamics of nearly free electrons in metals, for example, in aluminum or copper. In addition, it allows analyzing some physical phenomena that are ignored in more complex methods of the many-body theory. The properties of the electron gas in this theory depend on the electron density n_0, which is usually expressed through the electron density parameter r_s defined by the relation $1/n_0 = (4/3)\pi(r_s a_0)^3$; i.e., r_s is the radius of a sphere (in units of the Bohr radius a_0) that contains one electron. The basic results of the DFEG theory in the dynamics of electrons were obtained in the classic works of Quinn and Ferrell [25, 77] and Ritchie [78, 115]. A review of these works and of subsequent improvements in the theory was given in [40]; therefore, in this section, we give only some basic results of the theory and some remarks on the connections of the DFEG theory with other theories.

An expression for the lifetime of an excited electron in the DFEG theory can be obtained based of the perturbation theory, described in the foregoing section, with the application of some results of the many-body theory. If the initial and final states of free electrons in Eqns (29) and (30) are represented in the plane-wave form

$$\psi_{\mathbf{k}}(\mathbf{r}) = \frac{1}{\sqrt{\Omega}} \exp(\mathrm{i}\mathbf{k}\mathbf{r}) \tag{43}$$

with an energy $e_{\mathbf{k}} = k^2/2$ and a normalizing volume Ω, then Eqn (29) is reduced to

$$p_{f,f'}^{i,i'} = 2\pi \left|W(\mathbf{q},\omega)\right|^2 \delta(\mathbf{q} - \mathbf{k}_f' + \mathbf{k}_i')\,\delta(\omega - e_{\mathbf{k}_{f'}} + e_{\mathbf{k}_{i'}})\,, \tag{44}$$

where $W(\mathbf{q},\omega)$ is the Fourier transform of the screened interaction, which depends on the energy loss of the excited electron $\omega = e_{\mathbf{k}_i} - e_{\mathbf{k}_f}$ and the momentum loss $\mathbf{q} = \mathbf{k}_i - \mathbf{k}_f$. The Dirac δ functions ensure the energy and momentum conservation. Then the expression for the inverse lifetime becomes

$$\frac{1}{\tau(e_{\mathbf{k}_i})} = \frac{4\pi}{\Omega^2} \sum_{\mathbf{q}}^{\mathrm{cond}} \sum_{\mathbf{k}_i'} \left|W(\mathbf{q},\omega)\right|^2 g_{\mathbf{k}_i'}(1 - g_{\mathbf{k}_i'+\mathbf{q}}) \times \delta(\omega - e_{\mathbf{k}_i'+\mathbf{q}} + e_{\mathbf{k}_i'})\,. \tag{45}$$

The index 'cond' means that the summation over $\mathbf{q}$ obeys the condition $0 < \omega < e_{\mathbf{k}_i} - E_F$, because the primary electron cannot pass into an occupied state of the Fermi liquid. It follows from the many-body theory that the screened potential $W(\mathbf{q},\omega)$ in the free electron gas is related to the usual Coulomb potential $V(\mathbf{q})$ via the dielectric function $\epsilon(\mathbf{q},\omega)$ [79, 105]:

$$W(\mathbf{q},\omega) = \epsilon^{-1}(\mathbf{q},\omega) V(\mathbf{q})\,. \tag{46}$$

It also follows from the many-body theory that the sum over states in Eqn (45) is expressed through the imaginary part of the dielectric function obtained in the random-phase approximation (RPA) [116]:

$$\mathrm{Im}\,\epsilon^{\mathrm{RPA}}(\mathbf{q},\omega) = \frac{2\pi}{\Omega} V(\mathbf{q}) \sum_{\mathbf{k}} g_{\mathbf{k}}(1 - g_{\mathbf{k}+\mathbf{q}}) \delta(\omega - e_{\mathbf{k}+\mathbf{q}} + e_{\mathbf{k}})\,. \tag{47}$$

If we also express the screened potential through the RPA dielectric function, then, in the limit of an infinitely large normalizing volume, expression (45) becomes

$$\frac{1}{\tau(e_{\mathbf{k}})} = 2 \int^{\mathrm{cond}} \frac{\mathrm{d}\mathbf{q}}{(2\pi)^3} V(\mathbf{q})\, \mathrm{Im}\left[-\epsilon(\mathbf{q},\omega)\right]^{-1}, \tag{48}$$

where $\epsilon(\mathbf{q},\omega) = \epsilon^{\mathrm{RPA}}(\mathbf{q},\omega)$, and 'cond' again means that the integration in the $\mathbf{q}$ space is limited by the condition $0 < \omega = e_{\mathbf{k}} - e_{\mathbf{k}-\mathbf{q}} < e_{\mathbf{k}} - E_F$.

Quinn, Ferrell, and Ritchie were the first to study electron dynamics using the self-energy formalism of the many-body theory. In this formalism, the damping rate (inverse lifetime) of an excited state is determined by the imaginary part of the electron self-energy (see Section 3.3). To compute the self-energy, they used the method that is equivalent to the GW approximation discussed below. The final expression that they obtained is similar to Eqn (48), but with an *exact* dielectric function. An analogous expression was also obtained for the damping rate of holes, but with the integration region modified so as to include all occupied electron states that are accessible for holes to pass on them (see the details in review [40]). It is proven in the many-body theory that the dielectric function in the RPA approach becomes exact as $r_s \to 0$ [105]. But at finite values of r_s, the exact dielectric function is unknown; the use of some approximations is therefore unavoidable. The simplest approximation is to use Eqn (48) per se and insert the analytic expression for the RPA dielectric function obtained by Lindhardt (see textbook [105]) into it. At a finite r_s, the integral obtained in this approximation cannot be solved analytically, but Quinn and Ferrell obtained an analytic solution as $r_s \to 0$ in the case of low excess electron energy. It takes the form

$$\tau(E_i) = 263 r_s^{-5/2} (E_i - E_F)^{-2} \tag{49}$$

(in units of fs and eV). Hence, it follows that the so-called scaled lifetime $\tau(E_i - E_F)^2$ is independent of the energy and is determined only by the value of the parameter r_s. The energy dependence of the lifetime close to that following from Eqn (49) is observed for electron excitations in noble metals [117, 118]. Later, Ritchie [78] and Quinn [77] found an analytic solution as $r_s \to 0$, but with an energy far from the Fermi level (see [40]).

For real metals with nearly free electrons, the value of the parameter r_s is large (for example, 2.06 for aluminum); therefore, numerical methods are required for calculations. Such methods for the self-energy and lifetimes were first realized in the GW approximation in [119, 120]. However, in the concrete calculations for the interacting gas, the dielectric function was used only in the RPA. Such calculations in principle are similar to calculations in the GW approximation for real crystals, which are described in the following sections.

3.3 First-principle GW and *T*-matrix approaches

3.3.1 Self-energy, quasiparticle equation, and the Hedin equations. Modern calculations of the dynamics of single-particle excitations in real crystals are based on the self-energy formalism of the many-body theory [35, 36, 105, 121, 122]. In this formalism, the evolution of a system with a single extra electron or with a single hole added to the system of N interacting electrons is described by a single-particle Green's function defined as [35, 36]

$$G(\mathbf{x}t, \mathbf{x}'t') = -\mathrm{i}\langle N \left| T\Psi(\mathbf{x}t)\Psi^{\dagger}(\mathbf{x}'t') \right| N\rangle \,, \tag{50}$$

where $\mathbf{x} = (\mathbf{r}, \sigma)$ denotes spatial and spin coordinates, $|N\rangle$ is the wave function of the ground state of the system with interaction between electrons, $\Psi^{\dagger}$ and Ψ are the Heisenberg electron creation and annihilation operators, and T is the time ordering operator. At $t > t'$, the Green's function describes the evolution of the system with an electron added at the moment t', and at $t < t'$, it describes the evolution of the system with an electron added at the moment t.

For the Green's function of the system with the usual Coulomb interaction between the electrons $V_{\mathrm{c}}(\mathbf{r}, \mathbf{r}') = 1/|\mathbf{r} - \mathbf{r}'|$, there exists a formally rigorous equation of motion, which includes the two-particle Green's function [35, 36, 105]; but this equation cannot be solved at present. The problem is simplified by replacing the two-particle Green's function with the self-energy. A detailed description of the self-energy formalism can be found in monographs [35, 105], and the discussion in this section is therefore restricted to some points related to the dynamics of relaxation of excited states. In particular, it was shown that if the system is placed in a field with a weak electrostatic potential $\phi(\mathbf{x}, t)$, then the *exact* equation of motion for the Green's function can be written as

$$\left[\mathrm{i}\frac{\partial}{\partial t} - h(\mathbf{x}) - V(\mathbf{x}, t)\right] G(\mathbf{x}t, \mathbf{x}'t') - \int \mathrm{d}\mathbf{x}''\,\mathrm{d}t''\,\Sigma(\mathbf{x}t, \mathbf{x}''t'')\,G(\mathbf{x}''t'', \mathbf{x}'t') = \delta(\mathbf{x} - \mathbf{x}')\,\delta(t - t')\,, \tag{51}$$

where $h(\mathbf{x})$ is the kinetic energy of a quasiparticle, i.e., of an electron or hole, $\Sigma(\mathbf{x}t, \mathbf{x}''t'')$ is the self-energy of the quasiparticle, and $V(\mathbf{x}, t)$ is the total electrostatic potential

$$\begin{aligned} V(\mathbf{x}, t) &= \phi(\mathbf{x}, t) + V_{\mathrm{H}}(\mathbf{r}, t)\,, \\ V_{\mathrm{H}}(\mathbf{r}, t) &= \int \mathrm{d}\mathbf{r}'\,V_{\mathrm{c}}(\mathbf{r}, \mathbf{r}')\,\langle N \left| \Psi^{\dagger}(\mathbf{x}'t')\,\Psi(\mathbf{x}'t) \right| N\rangle \\ &= \int \mathrm{d}\mathbf{r}'\,V_{\mathrm{c}}(\mathbf{r}, \mathbf{r}')\,\rho(\mathbf{r}')\,. \end{aligned} \tag{52}$$

V_{H} in Eqn (52) is the Hartree electrostatic potential, which depends on the electron density ρ. Equation (51) is equivalent to the well-known Dyson equation [122]

$$G(\mathbf{x}t, \mathbf{x}'t') = G_0(\mathbf{x}t, \mathbf{x}'t') + G_0(\mathbf{x}t, \mathbf{x}''t'')\,\Sigma(\mathbf{x}''t'', \mathbf{x}'''t''')\,G(\mathbf{x}'''t''', \mathbf{x}'t')\,, \tag{53}$$

in which G_0 is the Green's function for a system without the interaction between the electrons, i.e., with a zero self-energy. It is understood that integration over repeated variables is performed.

In the absence of an external field ϕ, i.e., when the properties of the system depend not on the values of t and t' but on $t - t'$, Eqn (51), as a result of a time Fourier transformation, is reduced to the form

$$\left[\omega - h(\mathbf{x}) - V_{\mathrm{H}}(\mathbf{x})\right] G(\mathbf{x}, \mathbf{x}', \omega) - \int \mathrm{d}\mathbf{x}''\,\Sigma(\mathbf{x}, \mathbf{x}'', \omega)\,G(\mathbf{x}'', \mathbf{x}', \omega) = \delta(\mathbf{x} - \mathbf{x}')\,. \tag{54}$$

The general approach to the calculation of the Green's function consists in the use of the spectral representation

$$G(\mathbf{x}, \mathbf{x}', \omega) = \sum_k \frac{\psi_k(\mathbf{x}, \omega)\,\psi_k^*(\mathbf{x}', \omega)}{\omega - E_k(\omega)}\,, \tag{55}$$

where ψ_k are the wave functions of quasiparticle states. It can be shown that they satisfy the quasiparticle equation

$$\left[E_k(\omega) - h(\mathbf{x}) - V_{\mathrm{H}}(\mathbf{x})\right] \psi_k(\mathbf{x}, \omega) - \int \mathrm{d}\mathbf{x}'\,\Sigma(\mathbf{x}, \mathbf{x}', \omega)\,\psi_k(\mathbf{x}', \omega) = 0\,. \tag{56}$$

The eigenvalues of this equation (quasiparticle energies) are complex: $E_k = \mathrm{Re}\,E_k + \mathrm{i}\,\mathrm{Im}\,E_k$. It follows from expansion (55) that the imaginary part of G (spectral function) consists of a set of Lorentz peaks with maxima at frequencies $\omega_k = \mathrm{Re}\,E_k$ and the FWHM equal to $\Gamma_k = 2\,\mathrm{Im}\,E_k$. It is shown in the many-body theory that for the electron Green's function, these peaks exactly correspond to the energies of excited states of the $(N+1)$-electron system (with one extra electron), and for the hole Green's function, to the energies of excited states of the $(N-1)$-electron system (i.e., with one hole). It has also been proven that the time evolution of the Green's function at the energy $\omega = E_k$ follows the law $\exp(-\Gamma_k t)$, i.e., solving Eqn (56), we obtain the damping rate of the excited state Γ_k and the lifetime $\tau_k = 1/\Gamma_k$.

For solving Eqn (56), numerical methods are normally used, based on the electron density functional theory (DFT) [123]. The DFT methods allow obtaining single-particle wave functions $\psi_{\mathbf{q},\sigma}$ and the eigenvalues $e_{\mathbf{q},\sigma}$ ($\mathbf{q}$ is the wave vector), i.e., solutions of the Kohn–Sham equation. Estimates of the lifetime cannot be obtained from the Kohn–Sham equation; however, the excitation energies are quite frequently obtained correctly within the DFT. It is therefore assumed that the Kohn–Sham wave functions $\psi_{\mathbf{q},\sigma}$ are a good approximation of quasiparticle wave functions ψ_k and that the quasiparticle energies differ from the Kohn–Sham energies only in small corrections due to the self-energy. Substituting $\psi_{\mathbf{q},\sigma}$ for ψ_k, redefining the self-energy as $\Delta\Sigma_\sigma(\omega) = \Sigma_\sigma(\omega) - V_\sigma^{xc}$, and calculating averages over the states $\psi_{\mathbf{q},\sigma}$, we can write the quasiparticle equation in the absence of spin mixing as

$$E_{\mathbf{q},\sigma}(\omega) = e_{\mathbf{q},\sigma} + \Delta\Sigma_{\mathbf{q},\sigma}(\omega)\,, \tag{57}$$

where $\Delta\Sigma_{\mathbf{q},\sigma}(\omega) = \langle \psi_{\mathbf{q},\sigma} | \Delta\Sigma_\sigma(\omega) | \psi_{\mathbf{q},\sigma} \rangle$. In calculations, it is frequently assumed that $\omega = e_{\mathbf{q},\sigma}$; this is the heart of the so-called 'on-shell' approximation [117, 124, 125]. Another way is to keep only the linear part of the dependence of the self-energy on the frequency ω near the energy $e_{\mathbf{q},\sigma}$. In this approximation, the self-energy corrections to the Kohn–Sham energies take the form

$$\Delta e_{\mathbf{q},\sigma} \equiv E_{\mathbf{q},\sigma} - e_{\mathbf{q},\sigma} = Z_{\mathbf{q},\sigma}\Delta\Sigma_{\mathbf{q},\sigma}(e_{\mathbf{q},\sigma})\,, \tag{58}$$

where

$$Z_{\mathbf{q},\sigma} = \left[1 - \frac{\partial \Delta\Sigma_{\mathbf{q},\sigma}(\omega)}{\partial\omega}\right]^{-1}_{\omega = e_{\mathbf{q},\sigma}} \tag{59}$$

is the renormalization factor of the Green's function. The Lundqvist calculations for the gas of the interacting electrons [120] in a sufficiently wide range of the parameter r_s (about 2–5) and energy (± 1.5 hartree with respect to E_F) showed that Z is a complex function slowly varying with the momentum, with its real part close to 0.7. The imaginary part of Z is much less than the real part; therefore, it is usually neglected. Below, this approximation is called the 'computed-Z' approximation. If we assume that $Z = 1$, we obtain the 'on-shell' approximation. Finally, the damping rate of the quasiparticle state (electron or hole) is calculated as

$$\frac{1}{\tau_{\mathbf{q}\sigma}} = 2|\mathrm{Im}\,\Delta e_{\mathbf{q},\sigma}|\,. \tag{60}$$

Because the computed-Z approximation is mathematically more correct, it might be assumed that the lifetimes computed in this approximation must be more precise. However, the concrete calculations for a number of metals discussed in Section 4 do not confirm this.

Because the Green's function G, according to Eqn (55), is determined by quasiparticle energies and because the quasiparticle energies themselves depend on the self-energy Σ, the quantities G and Σ must be self-consistent. A formally exact set of equations, which in principle allows obtaining a self-consistent solution for G and Σ, was obtained by Hedin [36]. The derivation of these equations [36, 37, 122] is based on the analysis of the response of the system to a weak external field $\phi(\mathbf{x}, t)$. Below, we use abbreviations of the form $(1) = (\mathbf{x}_1, t_1) = (\mathbf{r}_1, \sigma_1, t_1)$. In the Hedin equations, the self-energy is represented in the form of an expansion into a series in the dynamic screened electron–electron interaction potential

$$W(12) = \int v_C(13)\epsilon^{-1}(32)\mathrm{d}(3)\,, \tag{61}$$

where $v_C(13) = V_C(\mathbf{r}_1, \mathbf{r}_3)\,\delta(t_1 - t_3)$ is the usual Coulomb potential. The inverse dielectric function ϵ^{-1} is a generalization of the classical dielectric function. It describes the response of the total internal field $V = \phi + V_H$ to a small applied external field ϕ and is expressed in terms of a functional derivative

$$\epsilon^{-1}(12) = \frac{\delta V(1)}{\delta\phi(2)} = \delta(1-2) + \int \mathrm{d}(3) v_C(13)\,\frac{\delta\rho(3)}{\delta\phi(2)}\,. \tag{62}$$

The second part of this equation follows from Eqn (52). Equation (62) contains the so-called response function

$$R(12) = \frac{\delta\rho(1)}{\delta\phi(2)}\,, \tag{63}$$

which describes the reaction of the electron density to an applied *external* field. One additional quantity used in the Hedin equations is the irreducible polarization function, which is connected with ϵ by the relation

$$\epsilon(12) = \delta(1-2) - \int \mathrm{d}(3) v_C(13) P(32)\,. \tag{64}$$

It represents a change in the electron density with a change in the *total* field $(\phi + V_H)$:

$$P(12) = \frac{\delta\rho(1)}{\delta V(2)}\,. \tag{65}$$

Equations (52), (62), and (65) immediately imply a relation between R and P,

$$\begin{aligned} R(12) &= \int \mathrm{d}(3) P(13)\epsilon^{-1}(32) \\ &= P(12) + \int \mathrm{d}(3)\mathrm{d}(4) P(13) v_C(34) R(42)\,. \end{aligned} \tag{66}$$

The introduction of the polarization function allows representing the screened potential as

$$W(12) = v_C(12) + \int \mathrm{d}(3)\mathrm{d}(4) W(13) P(34) v_C(42) \tag{67}$$

or as

$$W(12) = v_C(12) + \int \mathrm{d}(3)\mathrm{d}(4) v_C(13) R(34) v_C(42)\,. \tag{68}$$

Finally, a vertex function is introduced in the Hedin approach as

$$\Gamma(12;3) = -\frac{\delta G^{-1}(12)}{\delta V(3)}\,. \tag{69}$$

With this notation, the Hedin equations take the form

$$\Sigma(12) = \mathrm{i}\int \mathrm{d}(3)\mathrm{d}(4) W(13) G(14) \Gamma(42;3)\,, \tag{70}$$

$$W(12) = v_C(12) + \int \mathrm{d}(3)\mathrm{d}(4) W(13) P(34) v_C(42)\,, \tag{71}$$

$$P(12) = -\mathrm{i}\int \mathrm{d}(3)\mathrm{d}(4) G(23) G(42) \Gamma(34;1)\,, \tag{72}$$

$$\begin{aligned} \Gamma(12;3) = \delta(12)\delta(13) &+ \int \mathrm{d}(4)\mathrm{d}(5)\mathrm{d}(6)\mathrm{d}(7)\,\frac{\delta\Sigma(12)}{\delta G(45)} \\ &\times G(46) G(75) \Gamma(67;3)\,. \end{aligned} \tag{73}$$

The Hedin equations are extremely complicated; their exact solution is impossible even in the model of a free electron gas. Instead, they can be used to generate series that represent expansions of Σ, P, and Γ in powers of the screened potential W. A systematic procedure for such constructions is described in textbook [122]. After this, we can drop supposedly small terms of the series (or sum up the summable series) and solve the equations.

We note the general nature of the Hedin equations. Because the self-energy depends on two spin coordinates, the equations in principle are applicable to nonmagnetic and magnetic systems, to systems without mixing and with mixing of spin coordinates. In Ref. [126], analogous equations were obtained in terms of the Matsubara Green's functions, i.e., for finite temperatures. In Ref. [127], a method of introducing spin–orbit interaction into the Hedin equations was suggested.

3.3.2 GW approximation. If we assume $\Sigma = 0$ as the initial approximation for the calculations of the vertex function Γ, then we obtain $\Gamma(12;3) = \delta(12)\delta(13)$. This considerably

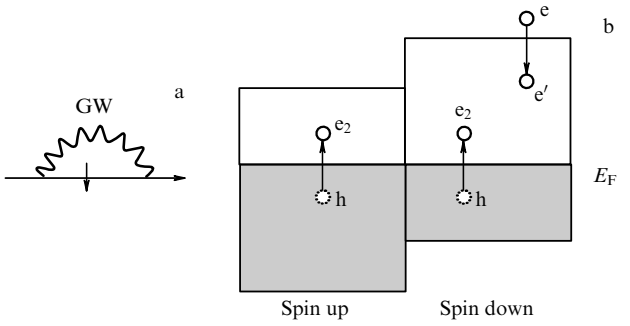

Figure 8. (a) Self-energy Feynman diagram in the GW method; the straight line represents the Green's function and the wavy line, the screened potential. (b) A schematic representation of electron transitions that are taken into account in the lifetime calculations by the GW method; $e \to e'$ corresponds to the process of damping the excitations of primary electrons; $h \to e_2$ is the processes of the excitation of secondary electron–hole pairs in two spin channels (see text).

simplifies the Hedin equations; they acquire the form

$$\Sigma(12) = iW(12)G(12)\,, \tag{74}$$

$$W(12) = v_C(12) + \int d(3)d(4)W(13)P(34)v_C(42)\,, \tag{75}$$

$$P(12) = -iG(12)G(21)\,. \tag{76}$$

Together with Eqns (62)–(68), these equations represent the so-called GW method, which is sufficiently simple for programming and for concrete calculations. The self-energy in the GW method contains the screened potential only in the first order; the terms of higher orders in W are omitted. Usually, the self-energy in the GW approximation is interpreted as the interaction energy of a quasiparticle (electron or hole) with the polarization field produced by the quasiparticle itself. It is described by the Feynman diagram shown in Fig. 8. For concrete calculations, a Fourier transformation from time to frequency coordinates is made for all the quantities involved, and the quantities that depend on spatial coordinates are expanded into series in the full sets of basis orbitals. Because the exact screened potential is unknown, the polarization and then ϵ and W are usually calculated using the Green's function without interaction, G_0. This is equivalent to the RPA, in which

$$P_0(12) = -iG_0(12)G_0(21)\,. \tag{77}$$

The Green's function G_0 can be constructed using Eqn (55) by substituting the wave functions and energies obtained from the DFT into it. The thus obtained version of the GW method is usually designated as G_0W_0.

We omit consideration of the diverse options for improving the GW method based on the introduction of vertex corrections to Γ in terms of the DFT, i.e., by going from the GW to the GWΓ method. A review of these works can be found in [37–39]. The results of calculations in the GWΓ approximation are on the whole contradictory. The GWΓ approach was mainly used for the introduction of corrections into band calculations done in the DFT methods. Some improvements in the energies of bands in the GWΓ method compared to the results of GW calculations were noted for Li, Na, and Al in [128] and for diamond, Si, and Ge in [129]. But for the energy gap, the GWΓ method gives values either very close to G_0W_0 results (Al [130]) or worse than those obtained in the G_0W_0 approximation (diamond, Si, Ge, LiCl [129]). It was shown in Ref. [131] that the influence of vertex corrections on the lifetimes in Cu, Ag, and Au is very small; however, it is unclear whether the accuracy of the calculation of the Γ corrections based on the DFT was sufficient in this case.

Meanwhile, an analysis of the basic expressions of the GW method in the frequency representation allows comparing it with the theory of scattering, revealing physical processes disregarded in the GW method, and outlining ways to improve it. The self-energy in this method is diagonal in spin and can be represented in the form

$$\Sigma_\sigma(\mathbf{r}, \mathbf{r}', \omega) = \frac{i}{2\pi}\int d\omega'\, G_\sigma(\mathbf{r}, \mathbf{r}', \omega + \omega')\, W(\mathbf{r}, \mathbf{r}', \omega')\,. \tag{78}$$

By expanding the self-energy and all the related quantities (P, R, ϵ, ϵ^{-1}) into series in some complete basis of Bloch functions $B_{\mathbf{k}i}$, we can calculate the expectation value $\mathrm{Im}\,\Sigma_{\mathbf{q},n,\sigma}(\omega) = \langle\psi_{\mathbf{q},n,\sigma}|\mathrm{Im}\,\Sigma_\sigma(\omega)|\psi_{\mathbf{q},n,\sigma}\rangle$, $\omega \simeq e_{\mathbf{q},n,\sigma}$, that determines the lifetime of a quasiparticle in the $\psi_{\mathbf{q},n,\sigma}$ state. For the electron excitations ($\omega > E_F$), it is equal to

$$\begin{aligned}\mathrm{Im}\,\Sigma_{\mathbf{q},n,\sigma}(\omega) = -\sum_{\mathbf{k}}\sum_{n'}^{\mathrm{unocc}}\sum_{i,j}\mathrm{Im}\,W_{i,j}(\mathbf{k}, \omega - e_{\mathbf{k}-\mathbf{q},n',\sigma})\\ \times\langle\psi_{\mathbf{q},n,\sigma}\psi_{\mathbf{k}-\mathbf{q},n',\sigma}|B_{\mathbf{k}i}\rangle\langle B_{\mathbf{k}j}|\psi_{\mathbf{k}-\mathbf{q},n',\sigma}\psi_{\mathbf{q},n,\sigma}\rangle\\ \times\Theta(\omega - e_{\mathbf{k}-\mathbf{q},n',\sigma})\,.\end{aligned} \tag{79}$$

The polarization matrix in the RPA in the Bloch-function basis is written as

$$\begin{aligned}\mathbf{P}^0_{i,j}(\mathbf{q},\omega) = \sum_{\sigma,t,\mathbf{k}}\sum_{n}^{\mathrm{occ}}\sum_{n'}^{\mathrm{unocc}}\frac{1}{t\omega - e_{\mathbf{k}+\mathbf{q},n',\sigma} + e_{\mathbf{k},n,\sigma} + i\delta}\\ \times\langle B_{\mathbf{q},i}\psi_{\mathbf{k},n,\sigma}|\psi_{\mathbf{k}+\mathbf{q},n',\sigma}\rangle\langle\psi_{\mathbf{k}+\mathbf{q},n',\sigma}|\psi_{\mathbf{k},n,\sigma}B_{\mathbf{q},j}\rangle\,,\end{aligned} \tag{80}$$

where $t = 1, -1$. The other equations of the method (in matrix notation) take the form

$$\mathbf{R}(\omega) = \mathbf{P}^0(\omega) + \mathbf{P}^0(\omega)\mathbf{v}_C\mathbf{R}(\omega)\,, \tag{81}$$

$$\epsilon(\omega) = 1 - \mathbf{v}_C\mathbf{P}^0(\omega)\,, \tag{82}$$

$$\epsilon^{-1}(\omega) = 1 + \mathbf{v}_C\mathbf{R}(\omega)\,, \tag{83}$$

$$\mathbf{W} = \epsilon^{-1}(\omega)\mathbf{v}_C\,. \tag{84}$$

For the screened interaction, we therefore have

$$\begin{aligned}\mathrm{Im}\,\mathbf{W}(\omega) &= \mathbf{v}_C\,\mathrm{Im}\,\mathbf{R}(\omega)\mathbf{v}_C\\ &= \mathbf{v}_C\,\mathrm{Im}\left[1 - \mathbf{P}^0(\omega)\mathbf{v}_C\right]^{-1}\mathbf{P}^0(\omega)\mathbf{v}_C\,.\end{aligned} \tag{85}$$

In the 'on-shell' approximation, we have $\omega = e_{\mathbf{q},n,\sigma}$. The poles of the function $[1 - \mathbf{PV}]^{-1}$ determine plasmon energies. Usually, these energies are considerably higher than the maximum energies of the quasiparticles under consideration, ~ 3 eV in the TR-2PPE method. Only in MgB_2 are they about 2 eV [132]; in silver, they are approximately 3.8 eV [133]. Consequently, in the calculations of lifetimes at low energies, it is possible to neglect plasmon poles and to assume that the damping of excitations is accompanied only by the excitation of secondary electron–hole pairs with energies corresponding to the zeros of the denominators in (80). In this approximation, we have

$$\mathrm{Im}\,\mathbf{W}(\omega) = \mathbf{v}_C\,\mathrm{Im}\,\mathbf{P}^0(\omega)\mathbf{v}_C\,. \tag{86}$$

With the approximation of a single matrix element used in Eqn (79), which includes the factored matrix element $W_{ij} = W_{00}\delta_{0j}\delta_{0i}$ and integrals of the form $\langle\psi\psi|B\rangle$, i.e., the random-**k** approximation, we can obtain an equation for the damping rate of a state similar to Eqn (33) at the zero temperature. A good agreement between the lifetimes calculated by the G_0W_0 method and by the methods of scattering theory was demonstrated in Refs [110, 111].

Thus, according to the GW approximation, the process of damping the excitations of primary electrons is accompanied by the process of excitation of secondary electron–hole pairs in both spin channels (see Fig. 8). The energy and the momentum lost by the primary electrons are transferred to the secondary quasiparticles. In this case, the interaction between the primary electrons and the secondary quasiparticles is ignored. However, this interaction can be important in the case of ferromagnets, where the interacting electrons and holes from different spin channels can form spin waves. This limitation is bypassed in the GW+T method described in the next sections.

3.3.3 The *T*-matrix approximation. The concept of the T matrix was introduced as a tool for describing the evolution of a system that includes two interacting quasiparticles [134]. The T matrix enters the integral equations that describe the evolution of a two-particle propagator [104, 121, 135, 136]. There exists an intimate relationship between the T matrix and the self-energy, which follows from the Hedin equations. Namely, if we substitute the T matrix instead of the screened potential in the self-energy of a quasiparticle calculated in the GW approximation, we obtain a new self-energy that corresponds to the evolution of the quasiparticle accompanied by the emission of bosons. For nonmagnetic systems, excitons can serve as such bosons; for magnetic systems, these are magnons. Even if the interaction described by the T matrix is insufficiently strong to ensure the emission of bosons with a large lifetime, it nevertheless can noticeably change the spectral properties and the dynamics of electrons.

The dynamics of electrons in metals accompanied by generation of spin waves have been studied on a semiempirical level in Refs [98, 137, 138]. The effect of the T matrix on the spectral properties of nickel was studied in [139]. Later, a first-principle variant of the T-matrix theory was developed, which was applied to calculations of magnons in Fe and Ni [126, 140] and of a plasmon satellite in Ni [45]. A more complete first-principle variant of the theory adapted to studying electron dynamics was published in [47].

In the theory of the evolution of two interacting quasiparticles, the T matrix is defined as a solution of the Bethe–Salpeter equation

$$T_{\sigma_1,\sigma_2}(1,2|3,4) = W(1,2)\delta(1-3)\delta(2-4) + W(1,2)\int \mathrm{d}(1')\mathrm{d}(2')K_{\sigma_1,\sigma_2}(1,2|1',2')T_{\sigma_1,\sigma_2}(1',2'|3,4) \quad (87)$$

[in this section, we use abbreviations of the form $(\mathbf{r}_1, t_1) = 1$]. The corresponding Feynman diagrams in the case with the interaction between an electron and a hole are shown in Fig. 9a. The kernel K of integral equation (87) is the electron–hole propagator for noninteracting particles, i.e., the product of the electron and hole Green's functions

$$K^{\mathrm{eh}}_{\sigma_1,\sigma_2}(1,2|1',2') = \mathrm{i}G_{\sigma_1}(1,1')G_{\sigma_2}(2',2)\,. \quad (88)$$

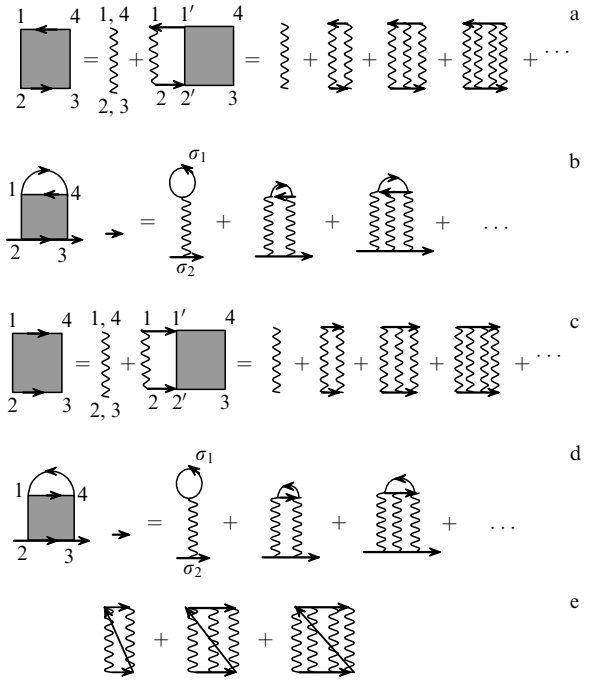

Figure 9. Feynman diagrams: (a) for the Bethe – Salpeter equation with the interaction between an electron and a hole; (b) for the direct term in the expression for the self-energy in the T-matrix method with the electron–hole interaction; (c) for the Bethe – Salpeter equation with the electron–electron interaction; (d) for the direct term in the self-energy with the electron–electron interaction; and (e) for the exchange term of self-energy. The arrows denote the Green's functions and the wavy lines are the screened interaction.

Substituting the T matrix instead of the screened interaction in the expression for the self-energy in the GW approximation, we obtain a direct T-matrix term of the self-energy for the electron–hole interaction, whose diagram for the electron excitation is shown in Fig. 9b. This term corresponds to a process in which the quasiparticle loses part of its energy and momentum, which are transferred to the generated electron–hole pair (to a Stoner pair or to a spin wave if the electron and hole have different spin projections). The second type of kernel is the kernel of the electron–electron interaction, i.e., the product of two electron Green's functions:

$$K^{\mathrm{ee}}_{\sigma_1,\sigma_2}(1,2|1',2') = \mathrm{i}G_{\sigma_1}(1',1)G_{\sigma_2}(2',2)\,. \quad (89)$$

The T matrix and self-energy diagrams corresponding to this propagator are given in Fig. 9c. In contrast to the electron–hole interaction, two types of self-energy arise in the case of the electron–electron interaction. The first (direct) type is shown in Fig. 9d; it is analogous to the direct electron–hole interaction. The second (exchange) type appears upon the exchange of points 3 and 4 in the diagram for the direct term (Fig. 9e). Similar diagrams also exist in the series for the self-energy that follow from the Hedin equation. Below, we discuss only the self-energy of electrons; additional information on the holes can be found in [47]. There is an essential difference between the self-energy of the direct electron–hole or electron–electron interaction and the self-energy of the exchange interaction. In the direct term, the spin coordinate σ_2 of the relaxing electron can be equal to or be opposite to the spin coordinate σ_1 of the electron or hole in the polarization loop. Thus, the direct T-matrix term describes the electron–

electron and electron–hole interaction between the quasiparticles with the identical or opposite spin. The exchange term acts only between electrons with like spins, by analogy with the usual Hartree–Fock method.

Explicit expressions for the self-energy are obtained according to the usual Feynman rules [122, 105]. For the electron–electron interaction, the direct self-energy term is written as [45]

$$\Sigma^d_{\sigma_2}(4,2) = -\mathrm{i}\sum_{\sigma_1}\int \mathrm{d}1\,\mathrm{d}3\, G_{\sigma_1}(1,3)T_{\sigma_2,\sigma_1}(1,2|3,4)\,, \quad (90)$$

and the exchange term as

$$\Sigma^x_{\sigma_2}(4,2) = \mathrm{i}\int \mathrm{d}1\,\mathrm{d}3\, G_{\sigma_2}(1,3)T_{\sigma_2,\sigma_2}(1,2|4,3)\,. \quad (91)$$

For the electron–hole interaction, the Green's function in Eqn (90) is replaced by the function $G_{\sigma_1}(3,1)$.

At a low excitation energy, we can assume the static approximation $W(1,2) = W(\mathbf{r}_1,\mathbf{r}_2)\delta(t_1-t_2)$ for W in Eqn (87). In the general case, the Fourier transform $W(\omega)$ of the screened potential is frequency dependent, whereas in the static approximation, $\omega = 0$. In the calculations of the T matrix and self-energy, it is also possible to accept a local approximation, i.e., to assume that $1 = 2$, $1' = 2'$, and $3 = 4$ in Eqns (87), (90), and (91). This approximation, suggested in Ref. [140], is good at least for transition metals, which is confirmed by the successful calculations of the dispersion of magnons in iron and nickel. With this approximation, the kernels transform into functions similar to polarization, for example, $K^{\mathrm{eh}}_{\sigma_1,\sigma_2}(1,1') = \mathrm{i}G_{\sigma_1}(1,1')G_{\sigma_2}(1',1)$; they depend only on two coordinates, which leads to a significant simplification of the calculations. In addition, the exchange self-energy $\Sigma^x_{\sigma_2}$ is canceled in this approximation by the part of the direct self-energy $\Sigma^d_{\sigma_2}$ with the same spin coordinate, which also leads to a simplification of the calculations.

The Fourier transform of the Bethe–Salpeter equation has the form

$$T_{\sigma_1,\sigma_2}(\mathbf{r}_1,\mathbf{r}_2,\omega) = W(\mathbf{r}_1,\mathbf{r}_2,0) + W(\mathbf{r}_1,\mathbf{r}_2,0)\int \mathrm{d}\mathbf{r}_{1'}\, K_{\sigma_1,\sigma_2}(\mathbf{r}_1,\mathbf{r}_{1'},\omega)T_{\sigma_1,\sigma_2}(\mathbf{r}_{1'},\mathbf{r}_2,\omega)\,, \quad (92)$$

where 0 means that we accepted the static approximation $\omega = 0$. The explicit expressions for the Fourier transforms of the kernels and the imaginary part of the self-energy are given in Refs [45, 140, 47]. Upon expansion of all quantities into series in the functions of a certain complete basis, expressions are obtained for the T-matrix part of the self-energy, i.e., for the contribution of the T matrix to the damping rate of the excited state [47]. According to Eqn (92), the T matrix in the complete basis is expressed as

$$\mathbf{T}_{\sigma_1,\sigma_2}(\omega) = \left[1 - \mathbf{W}\mathbf{K}_{\sigma_1,\sigma_2}(\omega)\right]^{-1}\mathbf{W}\,. \quad (93)$$

If we introduce susceptibilities as the quantities defined by the matrices

$$\mathbf{R}_{\sigma_1,\sigma_2} = \mathbf{K}_{\sigma_1,\sigma_2}\left[1 - \mathbf{W}\mathbf{K}_{\sigma_1,\sigma_2}\right]^{-1}, \quad (94)$$

then the expression

$$\operatorname{Im}\mathbf{T}_{\sigma_1,\sigma_2}(\omega) = \mathbf{W}\operatorname{Im}\mathbf{R}_{\sigma_1,\sigma_2}(\omega)\mathbf{W} \quad (95)$$

holds for the imaginary part by analogy with Eqn (86). If the matrices are approximated by their leading elements, then

$$\operatorname{Im} R_{\sigma_1,\sigma_2} = \frac{\operatorname{Im} K_{\sigma_1,\sigma_2}}{\left(1 - W\operatorname{Re} K_{\sigma_1,\sigma_2}\right)^2 + \left(W\operatorname{Im} K_{\sigma_1,\sigma_2}\right)^2}\,, \quad (96)$$

i.e., the contributions of the T matrix to the self-energy are determined by the longitudinal $(R_{\sigma,\sigma})$ and transverse $(R_{\sigma,-\sigma})$ susceptibilities. For paramagnetic crystals, these susceptibilities are identical.

It follows from Eqn (96) that the susceptibilities have poles of two types. The poles of $\operatorname{Im} K_{\sigma_1,\sigma_2}$ correspond to the formation of electron–hole pairs with a hole in the spin channel σ_2 and an electron with a spin σ_1 (Stoner pairs at $\sigma_1 \neq \sigma_2$). An essential advantage of the T-matrix approach in comparison with the GW approach is that the poles of the function $[1 - WK]^{-1}$ are also taken into account, which can be important at low energies. This is, for example, the case for ferromagnetic metals, where $\operatorname{Im} R_{-1/2,1/2}$ is the spectral function of the excitation of spin waves. As is shown in Section 4.5, in the range of magnon energies, i.e., about 0.5 eV, the contribution of the T matrix to the self-energy is greater than the contribution of the GW term. We also show in what follows that the T-matrix term with the electron–hole interaction, although less important than the GW term, gives a noticeable contribution to the damping rate of electron excitations in paramagnetic metals such as Ta, Mo, and Rh, leading to a better agreement with experiment. Of large importance is also the T-matrix contribution to the lifetime of electrons in ytterbium [50, 66].

3.3.4 GW + *T* approximation. The GW+T method is an alternative method (with respect to the above-mentioned GWΓ approach) of including terms of higher orders in W into the self-energy. The idea of combining the GW and T-matrix approaches was first proposed in [141], where it was noted that it would be incorrect to simply add the GW and T-matrix self-energies. Indeed, by constructing a series of self-energy diagrams corresponding to the Hedin equations, for example, according to the algorithm suggested in [122], it can be easily shown that the T-matrix term of the first order in W is absent in the Hedin equations, as is the second-order term, which contains the polarization loop [the so-called double-counting term, which is denoted as $D(P)$ below]. In the simplified notation, this term takes the form $GWPW$. In calculating lifetimes with a static screened potential, we can neglect the first-order Hartree-like term of the self-energy because this term does not have an imaginary part. It would then be simplest to calculate the $D(P)$ term separately and subtract it from the self-energy $\Sigma^{\mathrm{GW}} + \Sigma^T$. Another approach, suggested in [141] and realized for the first time in [68], is to sum the T-matrix terms starting with the term proportional to W^3. The problems in the calculation of the $D(P)$ term were revealed in the first calculations of the self-energy and spectral function of nickel [45]. It was shown that this way of eliminating double counting leads to a situation where the spectral function is negative for some energies, which makes no physical sense. Subsequent calculations showed that with this treatment of double counting, nonphysical results can also appear for the lifetime [47]; indeed, when the T-matrix terms are small (for example, for palladium), this method of the correction for double counting leads to an increase in the lifetime.

A more correct method of compensating double counting was suggested in [45]. It was shown that the self-energy in the GW method contains a term similar to $D(P)$, which, however, is determined not by the polarization function but by the response function; below, it is denoted by $D(R)$. This term compensates double counting in the GW part and in the T part of the self-energy with the electron–hole interaction taken into account. But if the T-matrix terms with the electron–electron interaction are included, the second-order term in W should be compensated again. If we take into account that the exchange T-matrix term is canceled by the direct spin-diagonal part of the T-matrix self-energy, then the second term of the double counting must be equal to $D(P)/2$. Thus, in the GW+T approach, the self-energy is defined as $\mathrm{Im}\,\Sigma^{\mathrm{GW}+T} = \mathrm{Im}\,\Sigma^{\mathrm{GW}} + \mathrm{Im}\,\Sigma^{T} - \mathrm{Im}\,\Sigma^{D(R)} - \mathrm{Im}\,\Sigma^{D(P)/2}$. The electron–electron term is usually small in comparison with the electron–hole one; therefore, this term and $\mathrm{Im}\,\Sigma^{D(P)/2}$ are omitted. The concrete formulas for computing the double-counting terms are given in Ref. [47].

3.4 Basis functions and programs for calculations

The concrete details of computer programs for the calculation of the relaxation characteristics for electrons or holes are to a considerable extent determined by the type of basis functions that are used for the representation of the band states and many-body characteristics of solids (polarization, response function, etc.). From this standpoint, two groups of computational methods should be distinguished.

3.4.1 Methods based on the expansion into plane waves. Two methods of this type have been suggested, both in the framework of the GW approximation. The first was used for calculations of the lifetimes of electrons in copper and aluminum [117], magnesium and beryllium [125], holes in copper [124, 88], and electrons in gold [142]. In this method, which is based on the pseudopotential band method of augmented plane waves (APWs), the Kohn–Sham equation is solved using the standard exchange–correlation potential and the electron–ion pseudopotential for the band states that are expanded into a large number of plane waves (600 – 900). Because the subsequent GW calculations with such a long basis (APW GW) are very hindered, a so-called 'local-field' approximation is used. This approximation ignores the off-diagonal elements of the dielectric matrix, i.e., the $\epsilon_{\mathbf{GG}'}$ elements with unequal wave vectors $\mathbf{G}$ and $\mathbf{G}'$, which allows avoiding the inversion of matrices that are too large. The rationality of this approximation is confirmed by a comparison with the results obtained in the basis of linear 'muffin-tin' orbitals, in which calculations without the local-field approximation meet with no problems. The lifetimes are calculated in the 'on-shell' approximation, i.e., avoiding calculations of the renormalization factor.

Another version of the GW method [143] was developed for the basis of plane waves in the framework of the Matsubara formalism of Green's functions for finite temperatures [105, 121]. In this version, the Fourier transforms of the Green's function and self-energy are determined for imaginary frequencies, i.e., instead of the integration over real frequencies in the equation for the self-energy (78), a summation over imaginary Matsubara frequencies is performed. In practice, the Green's function is calculated for imaginary frequencies, which is corrected for the self-energy effect, and then its analytic continuation to the real axis is found. The imaginary part of the Green's function on the real axis is the spectral function of excited states. The position of the peaks of this function determines the energies of excited states, and the width of the peaks determines the damping rate. The lifetimes for Al and Cu calculated using this scheme [143] are in qualitative agreement with the experimental data, but noticeably differ from the results of calculations with other methods (see Sections 4.1, 4.2).

The main obstacle for a wide use of methods based on plane waves is the large length of the basis, which hampers their use for objects with localized electron states. In such cases, a more efficient way may be the use of the methods discussed in Section 3.4.2 with the basis states coordinated with the effective potential in the crystal.

3.4.2 Methods based on expansion into partial waves. Partial waves are functions that are approximate solutions of the Kohn–Sham equations for an approximate potential in a crystal. They are constructed via sufficiently complex procedures, but they result in a number of advantages in comparison with plane-wave methods. To construct partial waves, the space of the crystal is divided into specific muffin-tin spheres, in which the potential is considered spherically symmetric, and the interstitial space between the spheres, in which the potential is considered constant. The partial waves are solutions of the Kohn–Sham equation inside the muffin-tin spheres smoothly coupled to solutions in the interstitial space. Such solutions depend on the energy and can be chosen in different ways. In particular, one can take a linearized solution, which is exact in the sphere of some atom for an average energy of the occupied bands and linearly changes with the deviation from this energy (the 'head' of the orbital). If this solution is smoothly coupled on the sphere to the solution in the interstitial space, which decreases with the distance from the center of this sphere (the 'tail'), and if the tail is expanded into solutions of the Kohn–Sham equations in other spheres, then we obtain a linear muffin-tin orbital (LMTO) [144]. But if the linearized Kohn–Sham solutions in the spheres are coupled to plane waves in the interstitial space, we obtain the so-called linear augmented plane wave (LAPW) [144].

The fastest calculations of the band structure are achieved in terms of the tight-binding LMTO method (TB-LMTO). A description of very ingenious methods of constructing such orbitals can be found in Ref. [145]. It is shown there that the interstitial solution can be chosen such that the value of the tail of the TB-LMTO in the atomic spheres nearest to the 'head' sphere is an order of magnitude smaller than the TB-LMTO value in the head sphere, and for atoms of the third coordination shell, the tail is completely negligible. With such atomic-like orbitals, sufficiently exact Kohn–Sham solutions for close-packed structures are obtained with a minimum s, p, d, f set of basis orbitals. An additional acceleration of calculations is achieved by the use of the atomic-sphere approximation (ASA), in which spheres of an increased volume, which cover the entire volume of the crystal, are introduced instead of the nonoverlapping muffin-tin spheres, and the calculation of the matrix elements of the Hamiltonian is performed only over the atomic spheres.

The method of constructing a complete but very short basis set for many-body calculations based on the LMTO method was suggested in [146]. The idea in [146] follows from expressions (79) and (80) for the polarization; because the polarization matrix elements are determined by the products of the band states, the basis in the LMTO approach should be

constructed from the products of LMTOs. Because the products of LMTOs are not mutually orthogonal and can be linearly dependent in general, an orthonormalized basis of the so-called 'product orbitals' should be constructed via the orthogonalization of the matrix of the overlap integrals of the products of LMTOs. Linear dependences can then be eliminated by the removal of product orbitals with small weights (which can be estimated in terms of the appropriate eigenvalues of the overlap matrix). The number of the thus obtained product orbitals sufficient for calculations of the dynamics of electrons is 40 – 50 for atoms with valence s, p, d orbitals and 70 – 100 for atoms with s, p, d, f orbitals.

The majority of calculations for the dynamics of electrons discussed in the subsequent sections were performed in the basis of product orbitals. These are TB-LMTO GW calculations for the lifetime of excited electrons in Cu, Ag, Au [147], Nb, Mo, Rh, Pd, Ag [111], Nb, and Al [110]. The results of TB-LMTO GW+T calculations were published for the lifetime of electrons in Fe and Ni [46, 148], Pd, Ta, Al [47], V, Nb, Ta, Mo, W, Rh, and Ir [149], and for the mean free path of electrons in Fe, Ni, Pt, and Au [48]. TB-LMTO GW calculations were also made with spin–orbit interaction for the time and length of spin depolarization in Al, Cu, Au, Nb, and Ta [127].

Calculations in the basis of products of orbitals are fastest and sufficiently precise for the close-packed structures or structures that can be artificially made close-packed by the introduction of additional atomic spheres into the interstitials with a basis but without an atomic core (extraspheres). However, for many structures, for example, for layered ones, this is impossible, and then more complex methods are required. One such method, based on the full-potential LMTO band method (FP-LMTO) was developed in [150, 151]. In contrast to the TB-LMTO method, the FP-LMTO method is based on the geometry of a potential with nonoverlapping muffin-tin spheres. The basis functions used in this method have a large spatial extent; the way of constructing them and the methods of computing matrix elements of the Hamiltonian in this basis are described in [151]. To increase the accuracy of calculations, 'floating' orbitals can be introduced with the centers in the extraspheres, as can 'local orbitals' with the centers in the real atoms. The Kohn–Sham equation in the FP-LMTO method is solved for the full potential rather than the potential that is spherically symmetric in the atomic spheres, as in the TB-LMTO method.

The many-body method based on the band FP-LMTO method is a self-consistent GW method. As the TB-LMTO GW method, the FP-LMTO GW method involves product orbitals localized inside the atomic spheres, but with a basis extended by adding plane waves necessary for calculating the interstitial parts of the matrix elements (for details, see [151]). Eventually, a method was obtained that works more slowly than the GW method on the basis of TB-LMTO orbitals, but has a wider field of application and involves no additional approximations except the GW approximation itself. The method was widely used for calculating energy band structures with self-energy corrections [151], but there are only two examples of the application of the method to the dynamics of excitation damping; these are works [152] for holes in Cu and Au and [153] for holes in Ag.

In Ref. [154], a modified GW method was also developed in the basis of LAPW partial waves (LAPW GW). It was used in the calculation of lifetimes for Al, Cu, Au, and Pd. The results of calculations are compared with the results of TB-LMTO GW calculations in Section 4.1.

4. Some concrete results of studies of the femtosecond dynamics of electrons in metals

4.1 The dynamics of electrons in aluminum

The energy band structure of aluminum is well known (see, e.g., Ref. [155]). This metal has a relatively low density of states, which is very close to that in a free electron gas with the electron density value $r_s = 2.06$, which follows from its crystal structure. Therefore, aluminum is a good object for testing the theory of the dynamics of excited states. The relaxation times of excited electrons in aluminum were first determined by the TR-2PPE method in [156]. Recently, new measurements of relaxation times were carried out, in which the contributions from the cascade electrons, transport, and photon scattering were excluded [81]. At energies above 1.2 eV, the results obtained in [81] almost coincide with the data obtained previously in [156]; therefore, at this energy, the results in [156] can be considered to be confirmed and to be related to the relaxation via electron–electron scattering only. The divergences between the data of these works at energies below 1.2 eV are ascribed in [81] to problems with the vacuum in the experiments in [156].

The first calculations of the lifetime of excited electrons were performed in Refs [143, 157] by the GW method in the Matsubara formalism of Green's functions. Their results differ substantially from the results of later, more correct calculations, and we do not discuss them in what follows. The more complete calculations of lifetimes, with the averaging over the directions of the momenta for each excess energy of an electron, were performed by the APW GW method in [125]. Calculations by the GW method in the TB-LMTO [110] and LAPW [154] bases then followed. Self-energy terms of a higher order in W were included in calculations by the GW+T method in [47].

The results of measurements and first-principle calculations of the lifetime in aluminum are shown in Fig. 10. The lifetimes averaged over the wave vector that were calculated in the plane-wave basis almost coincide with the data obtained in the TB-LMTO basis and in the DFEG theory. Furthermore, these data are very close to the results of calculations in the random-**k** model [110]. The lifetimes calculated in the LAPW basis are somewhat higher, but with increasing the energy of the excited electron, they demonstrate quite a similar tendency. However, all the calculations (carried out in the framework of the G_0W_0 version of the method, i.e., using the RPA and Green's function uncorrected for the self-energy) give lifetimes noticeably greater than both the old and new experiments.

A noticeable improvement in the first-principle results was achieved when higher-order terms in the screened potential were included into the self-energy in the framework of the GW+T approach. After the inclusion of T-matrix terms with the electron–hole interaction, the estimated lifetime becomes only 20 – 30% higher than the experimental value. After the inclusion of T-matrix terms with the electron–electron interaction, the estimated lifetimes with an excess energy above 1 eV practically coincide with the experimental values, but at energies below 1 eV, they become lower [81]. It is therefore obvious that the self-energy terms of higher orders in W should also be taken into account, but the problem of

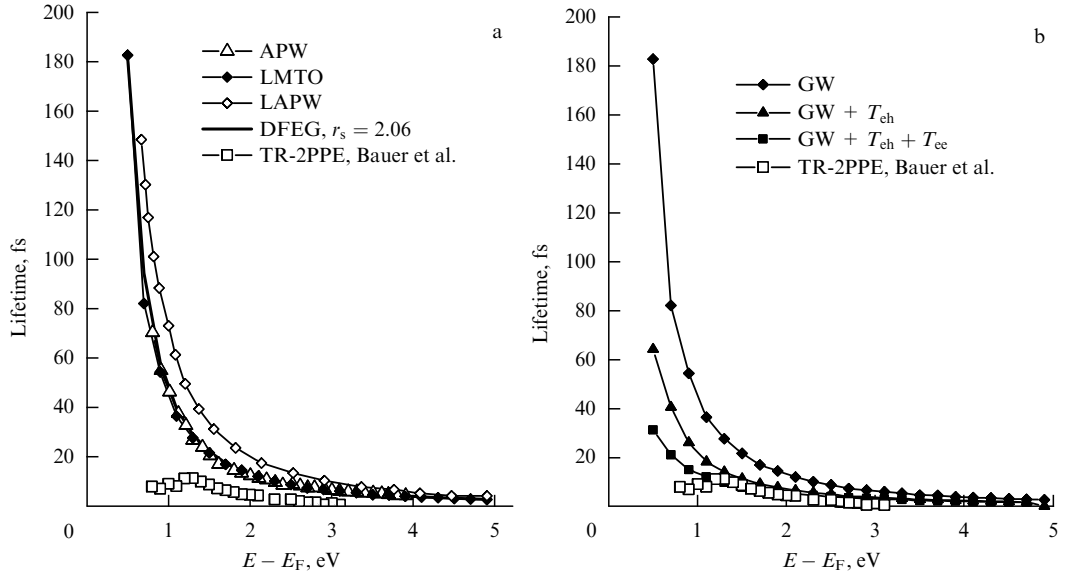

Figure 10. Results of experiments and first-principle calculations for the lifetime of excited electrons in aluminum: (a) triangles, APW GW results [125]; solid rhombi, LMTO GW results [110]; open rhombi, LAPW GW results [154]; continuous bold line, results of calculations within the DFEG theory; (b) rhombi, LMTO GW results [110]; triangles, LMTO GW+T results with the electron–hole interaction included in the T matrix [47]; solid squares, LMTO GW+T results with the electron–hole and electron–electron interactions included in the T matrix [47]; open squares, the experimental TR-2PPE results in [156] in both (a) and (b).

their correct calculation has not yet been completely solved. The first-principle calculations carried out for aluminum are not perfect. Possible ways of improving the theory are calculations of the screened potential beyond the RPA and the inclusion of self-energy effects into the Green's function, i.e., self-consistency. Another possibility is also offered by the GWΓ method. It was asserted in [158, 159] that the approximation of the static screened potential used in the T-matrix calculations for materials with nearly free electrons overestimates the T matrix by a factor of approximately 1.5; however, the calculations with a reduced T matrix led to results that were only slightly better than the GW calculations in the RPA. Further efforts are required in this research direction.

4.2 The dynamics of electrons in copper, silver, and gold

Figure 11 displays the total densities of states for copper, silver, and gold obtained by the TB-LMTO method [147]. The high peaks in the density of states belong to bands of the d type; they lie in the energy ranges -6 to -1.5 eV for copper, -6.3 to -2.6 eV for silver, and -7.5 to -1.6 eV for gold. The states with the lower energy are mainly formed from valence s orbitals of metals, and those with the higher energy, from valence p orbitals. Therefore, it can be expected that the dynamics of the relaxation of electron excitations in these metals must be similar to the dynamics in metals with nearly free electrons. This assumption, as we show below, is justified only partially in view of the complexity of relaxation processes, which include inelastic scattering and a number of additional processes.

We note that the energy of the d zones for these metals is not calculated entirely correctly, which is a disadvantage of all band methods of the density functional theory. A comparison with the photoemission spectroscopy data shows that the energies of the d bands are overstated by 0.5 eV in copper, by 1.2 eV in silver, and by 0.9 eV in gold. Attempts to correct the energies of the d bands by self-energy methods of the many-body theory have not led thus far to positive results. In Ref. [147], we studied the effect of the energy of d bands on

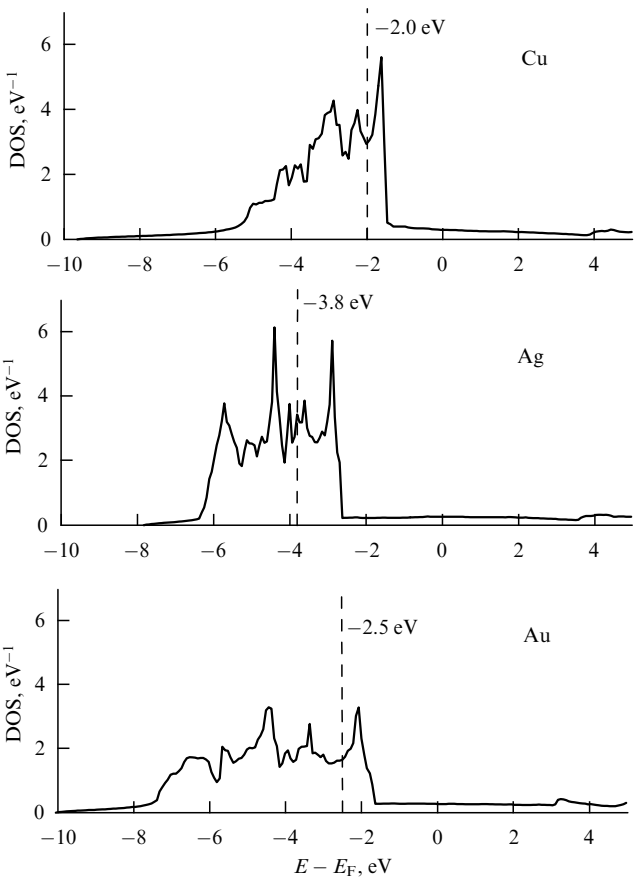

Figure 11. Densities of states (DOS) in Cu, Ag, and Au calculated by the TB-LMTO method. Dashed lines show the experimental values of the maximum energy of the d bands [8].

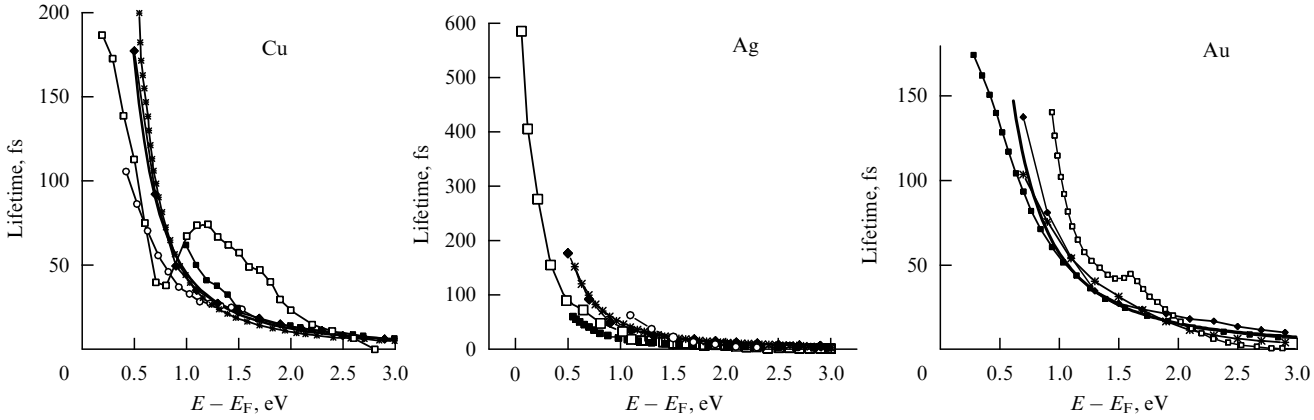

Figure 12. Experimental relaxation times and calculated lifetimes for Cu, Ag, and Au. For copper, the open squares correspond to the TR-2PPE data in [160]; open circles, to the TR-2PPE data in [28]; solid squares, to the calculated APW GW results in [117]; solid rhombi, to the calculated LMTO GW results in [147]; asterisks, to the calculated APW GW data in [143]; and the solid line, to the data calculated within the DFEG theory. For silver, the open squares correspond to the TR-2PPE data in [162]; open circles, to the TR-2PPE data in [80]; solid squares, to calculated APW GW lifetimes in [131]; the solid line, to the lifetimes calculated within the DFEG theory; asterisks, to the lifetimes estimated in the random-**k** approximation by Zhukov et al.; and solid rhombi, to the calculated LMTO GW results in [147]. For gold, the open squares correspond to the TR-2PPE results in [80]; the solid line, to the lifetimes estimated within the DFEG theory; solid squares, to the lifetimes borrowed from the APW GW calculations in [118]; solid rhombi, to the lifetimes taken from the LMTO GW calculations in [147]; and asterisks, to the results of calculations in the random-**k** approximation.

the lifetimes of electron excitations. The energy of the bands was varied by changing the specific parameter of the LMTO method, the so-called generalized principal quantum number of d orbitals. It was shown that this influence is insignificant.

Experimental studies of the relaxation time of electron excitations in Cu, Ag, and Au were mainly performed by the TR-2PPE method. The first studies for copper [19, 26] showed a monotonic decrease in the relaxation time with increasing the electron energy, as is expected from the DFEG theory; this decrease was not confirmed later, however. On the contrary, a nonmonotonic change in the relaxation time with a sharp increase at energies from 1.5 to 2.5 eV was observed in [160] (Fig. 12). The presence of this effect was confirmed in Refs [161] and [32]. The authors ascribed this phenomenon to the effect of the generation of Auger electrons upon filling the primary holes in the d zone, i.e., to the 'd-band catastrophe' (see Section 2.1.2). The magnitude of this effect depends on the energy of the pumping photon. Because the maximum energy of the d bands in copper is smaller by 2 eV than the Fermi energy, this effect should be absent at energies of the pumping photon less than 2 eV. This is completely confirmed by the data in [28] obtained at the pumping photon energy 1.63 eV. The results obtained in [160] and [28] are given in Fig. 12, together with the lifetimes calculated in the GW approximation. The first calculated lifetimes obtained in [117] are insufficiently reliable, because at energies below 1.5 eV, they differ from the later data in a way that is difficult to explain. But the almost complete agreement of the results obtained independently in the plane-wave basis in [143] and by Zhukov et al. in the LMTO basis show the reliability of later calculations. The results of LMTO GW calculations are far from the lifetimes that can be obtained using the DFEG theory at $r_s = 2.65$, which follows from the number of s electrons and the lattice parameter. However, by varying r_s, good agreement can be obtained between the results of the DFEG theory and LMTO GW calculations at $r_s = 2.1$.

Because the experimental relaxation times obtained in [28] are free of the effects caused by Auger electrons, it is instructive to compare them with computed lifetimes. It is evident that agreement is observed at the excess energies of electrons above 1.2 eV. At lower energies, the calculated lifetimes are noticeably higher than the relaxation time. The most probable factor that can be responsible for this difference is the transport of electrons from the irradiated spot, which reduces the relaxation time. From the theoretical standpoint, errors can appear in the calculations due to the use of the noninteracting Green's function G_0, as well as the use of the RPA in the calculations of the screened interaction and the neglect of the self-energy terms of higher orders in W.

The relaxation times of excited electrons in silver in the widest energy range were studied by the TR-2PPE method in [162]. At energies below 0.5 eV, they are close to the earlier results in [163], and at energies greater than 1.5 eV, they are confirmed by the data in [164]. However, at energies between 0.5 and 1.5 eV, the relaxation times obtained by Aeschlimann [80] are higher than the relaxation times according to Wolf [162]. This is explained by the different conditions of conducting the experiments; Wolf's experiments were carried out on thick metallic films, whereas the measurements of Aeschlimann were performed on thin (from 10 to 30 nm) (100) films on magnesium oxide. This prevents the transport of excited electrons and results in an increase in the relaxation time with decreasing the thickness of the film. On the other hand, because the experiments were conducted at energies of the pumping photons approximately equal to 3.3 eV, the effect of Auger electrons can be excluded because the energy of the d bands is too low, lower than −3.8 eV.

Two first-principle calculations of the lifetime of excited electrons with averaging over the wave vector have been performed; these are the APW GW calculation in [131] and the LMTO GW calculation in [147]. The APW lifetimes appear to be incorrect, because, in spite of the similarity of the band structures of noble metals, they are 2–3 times less than the lifetimes for copper and gold. The LMTO lifetimes are somewhat lower than the relaxation times given by Aeschlimann, which can be explained by the positive contribution from cascade electrons. The relaxation times calculated by Wolf are less than the lifetimes obtained in LMTO calculations, apparently because of the transport effects.

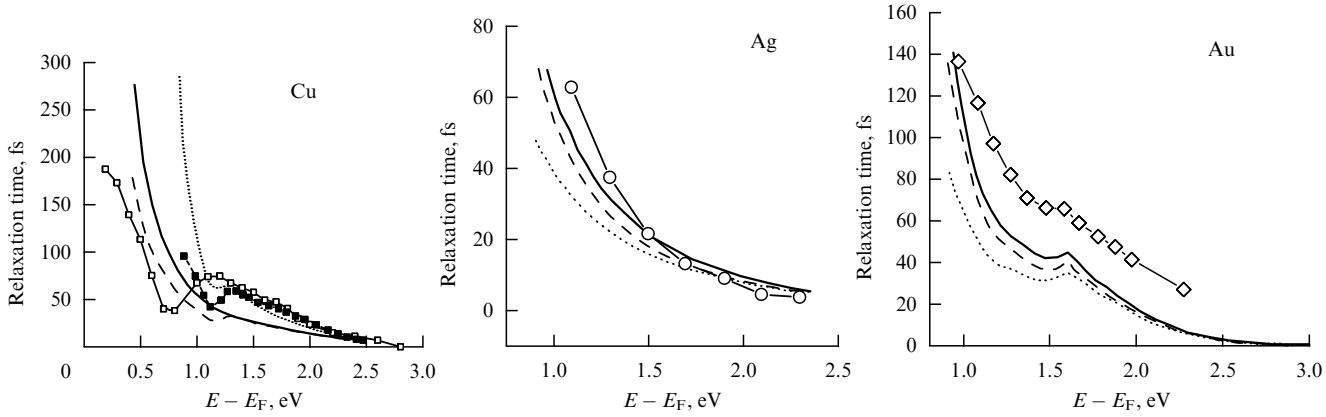

Figure 13. Relaxation times of excited electrons in Cu, Ag, and Au calculated within the Boltzmann theory (see Section 3.1). For copper [22, 103, 113], the solid line corresponds to calculations performed with only inelastic scattering taken into account; dotted line, the effect of cascade electrons is added; dashed line, the transport effect is subtracted; solid squares, the effect of Auger electrons is added; open squares, experimental data of Pawlik et al. For silver [80], the dotted line corresponds to calculations performed for a bulk sample with allowance for inelastic scattering and the transport effect; dashed line, analogous results for a film 30 nm thick; solid line, analogous results for a film 15 nm thick; open circles, experimental relaxation times for a film 15 nm thick. For gold [80], the dotted line corresponds to calculations with inelastic scattering and the transport effect for a bulk sample; dashed line, analogous results for a film 26 nm thick; solid line, analogous results for a film 10 nm thick; and open rhombi, experimental relaxation times for a film 10 nm thick.

For gold, the relaxation times of electron excitations were measured by Aeschlimann et al. using thin (111) Au films on MgO, which allowed, as in the case of silver, eliminating transport effects. The lifetimes were calculated by the APW GW method in [118] and in the LMTO GW approach in [147]. The second set of results is more reliable, because the results in [118] are not extrapolated to the infinite lifetime at the zero excess energy of an excited electron. However, at the excess energy of electrons above 1 eV, the correspondence between the results of these calculations is satisfactory. As in the case of silver, the estimated lifetimes are less than the experimental relaxation times. This can be partly explained by the effect of cascade electrons. But because the maximum energy of the d bands is 2.5 eV away from the Fermi level, which is less than the energy of the pumping photon, the generation of Auger electrons, which increases the relaxation time, should also be efficient. Indeed, the experimental energy dependence of the relaxation time exhibits a local maximum at 1.7 eV.

Figure 13 displays the results of the estimation of relaxation times for Cu, Ag, and Au according to the Boltzmann theory. For copper, data are given that are obtained by the successive inclusion of the $\partial g_\sigma/\partial t$ terms in Eqn (36), which describes different mechanisms of changes in the population of the excited level. The relaxation times calculated with only the 'inel' term in Eqn (36) are in good agreement with the results of LMTO GW calculations. The inclusion of the effect of cascade electrons (the 'casc' term) that fall onto a given excited level from the higher levels, substantially increases the relaxation time, but the effect of electron transport from the irradiated zone almost completely compensates the cascade effect. When taking the effect of Auger electrons into account (the 'Au' term), a local maximum at 1.3 eV appears in the dependence of the relaxation time on the electron energy. It corresponds to the maximum in the experimental curve near 1.2 eV. On a qualitative level, the calculated energy dependence of the relaxation time corresponds to the experimental data. However, there are significant quantitative differences; an increase in the relaxation time with decreasing $E - E_F$ in the calculation is observed beginning at 1.15 eV, whereas in the experiment, it occurs at 0.75 eV.

The calculations within the Boltzmann theory for Ag and Au were carried out in [80]. The calculations included 'inel,' 'transp,' and 'Au' terms, but the effect of cascade electrons was omitted. The calculations of the transport effect were carried out for both a bulk crystal and thin films. For both Ag and Au, a reduction in the transport effect with decreasing the film thickness was noted. As is expected from the experiment and the band structure, no effect of Auger electrons is present in silver, but it substantially increases the relaxation time in gold and leads to the appearance of a local maximum at 1.6 eV. Because the first-principle GW approach includes only the inelastic scattering, the lifetimes estimated according to the LMTO GW method prove to be considerably less than the experimental values and than the lifetimes calculated according to the Boltzmann theory.

4.3 The dynamics of holes in copper, silver, and gold

It can be expected that the relaxation time of holes in the d states of noble metals, because of their smaller spatial extent, can differ noticeably from the lifetimes of electrons or holes in nearly free states. Therefore, the dynamics of holes in d bands have attracted the attention of many researchers. The first measurements of the relaxation times of d holes were carried out in [165] by the ARPES method. They showed a decrease in the relaxation time from the upper to the lower states of the d band, but the values of the relaxation time were 5–7 times less than the results of later measurements. It is remarkable that the first correct results on the dynamics of holes were obtained not by the ARPES method, which is suitable for such measurements in its physical essence, but by the TR-2PPE method, which was developed for studying the dynamics of electron excitations. The corresponding modification of the three-level model and related measurements were performed in [32, 33, 74, 75]. The problem of this approach is that it results in an averaged relaxation time, without resolution in the hole energy. Therefore, we restrict ourselves to the examination of more complete data obtained only by the ARPES method.

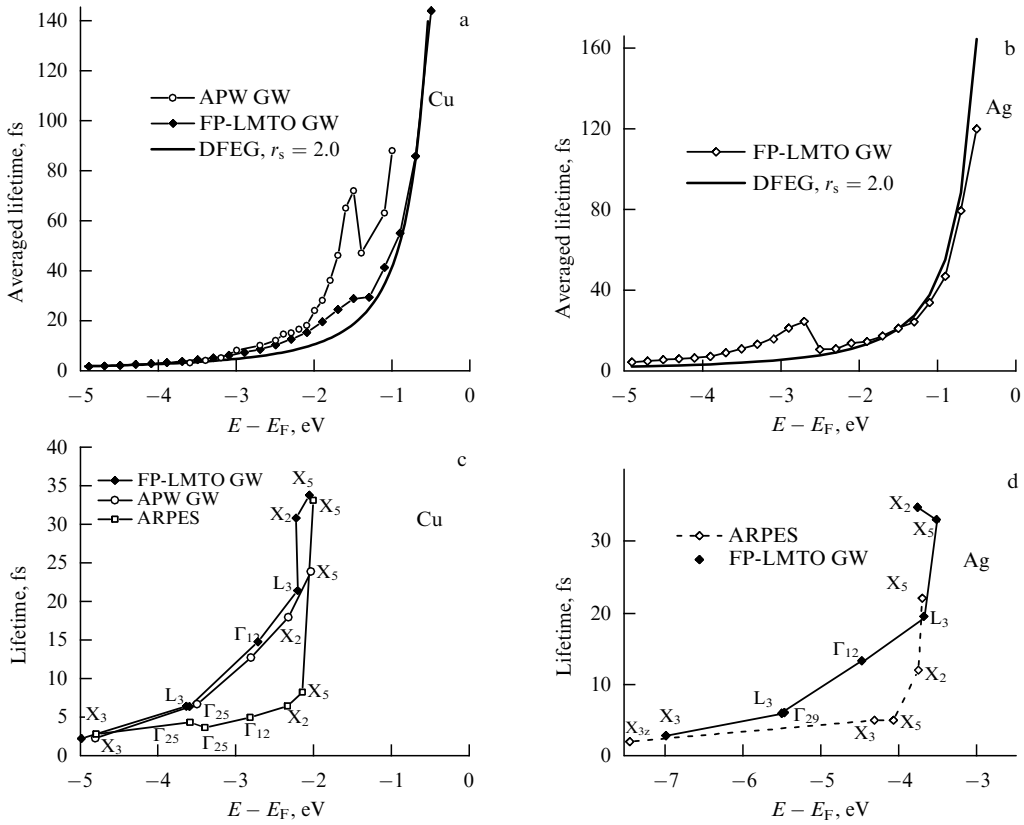

Figure 14. Experimental and theoretical lifetimes for excited holes in copper and silver. (a, b) Calculated lifetimes averaged over the wave vector. APW GW are the results in [124, 125]; FP-LMTO GW are the results in [152]; DFEG are the results of calculations within the theory of an interacting electron gas at $r_s = 2.0$. (c, d) Lifetimes for some states at the symmetry points of the Brillouin zone. Here, FP-LMTO GW are the results in theoretical works [152, 153]; APW GW are the results of calculations performed in [88]; and ARPES are the experimental results in Refs [88, 89].

The first relaxation times with resolution in the energy of holes were calculated in [31] from the high-resolution ARPES spectra obtained for copper in [166]; they were equal to 26 fs for states near the upper edge of the d band and ~ 3.5 fs for the bottom edge of the band. More complete studies were carried out by Gerlach et al. for states at the points Γ and X of the Brillouin zone (BZ) of copper [88] and for states at the point X of the BZ of silver [89]. One of these high-resolution spectra is given in Fig. 5. The measurements were performed at different temperatures and the results were extrapolated to 0 K, which allowed eliminating the contribution of the electron–phonon interaction to the linewidth, i.e., to the inverse relaxation time. Furthermore, the authors of [88, 89] carried out measurements for different durations of annealing, i.e., for samples with different concentrations of defects. The concentration of defects w was estimated from the widths of the diffraction lines of low-energy electrons; the relaxation times were then extrapolated to $w = 0$. The data obtained by Gerlach et al. are free from the effects of the electron–phonon interaction and the imperfection of the sample, and can therefore be compared with the first-principle lifetimes.

For copper, the first calculations of the lifetime of holes (not entirely successful) were performed by the APW GW method (with averaging over the wave vectors) in [124, 125]. Then, calculations performed within the TB-LMTO GW [147] and FP-LMTO GW [152] approximations appeared. The lifetimes for the states at the points X and Γ were also calculated by the APW GW method in [88]. For silver, the lifetime of holes was calculated by the TB-LMTO GW [147] and FP-LMTO GW [153] methods. The results of the experimental studies and first-principle calculations are given in Fig. 14.

It is obvious from Fig. 14 that according to the FP-LMTO GW calculations, the average lifetimes of holes in the nearly free hole states agree well with the data of the DFEG theory at $r_s = 2.0$, at which the lifetimes of the nearly free electron excitations are also described satisfactorily. But the results of the APW GW calculations for copper [124, 125] are almost 2 times higher. For the holes in the d bands, a deviation from the DFEG model is confirmed, but the magnitude of the deviation is much higher in the APW GW than in the FP-LMTO GW calculations. For silver, the lifetimes calculated for the states at the L, Γ, and X points within the FP-LMTO approach agree with the results of APW GW calculations, except for the states X_5 and X_2 at the top of the d band. However, the calculation data for both copper and silver are considerably higher than the experimental data. Thus, on the qualitative level, the first-principle calculations correctly describe the lifetimes of the hole d states, confirming their decrease in going from the top of the d band to the bottom of the band; however, there are noticeable differences between the experimental data and the results of calculations in the GW approximation.

4.4 The dynamics of electrons in nonmagnetic transition metals

The first experimental studies of the relaxation time of electrons in transition metals were performed for tantalum

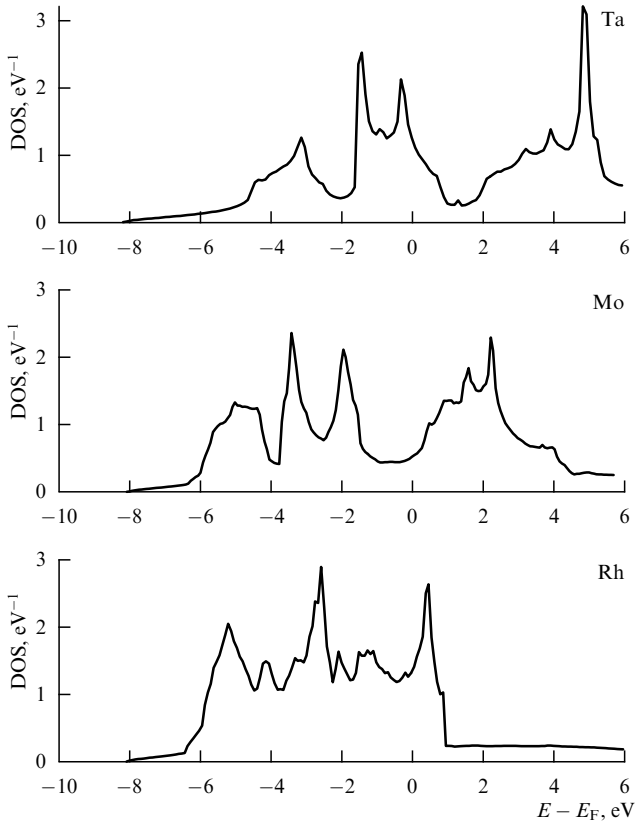

Figure 15. Densities of states in Ta, Mo, and Rh calculated by the LMTO method in the basis of tight-binding orbitals (TB-LMTO).

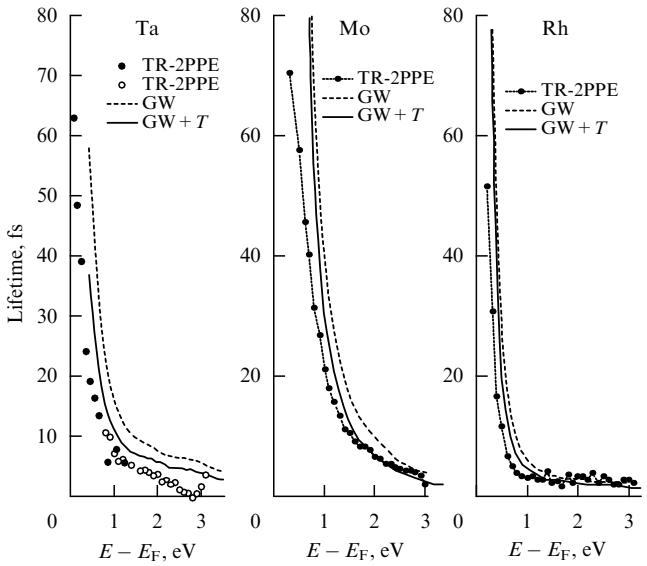

Figure 16. Experimental relaxation times and first-principle lifetimes of excited electrons in Ta, Mo, and Rh. For tantalum, the solid circles correspond to experimental TR-2PPE results in [163]; open circles, to the TR-2PPE data in [81]; the dashed line, to the LMTO GW results in [149]; the solid line, to the LMTO GW+T results in [149]. For molybdenum and rhodium, solid circles correspond to the TR-2PPE results in [68]; the dashed and solid lines, to the LMTO GW and LMTO GW+T results, respectively, of the same work [68].

in [27, 163]. Later, the relaxation times were studied by the TR-2PPE method for Ta [49] and Mo and Rh [68]. The first calculations of the lifetime with averaging over the wave vector were carried out by the TB-LMTO GW method for Nb [110, 111] and Mo, Rh, and Pd [111]. In Ref. [167], the APW GW method was used to calculate the lifetime of electrons at some symmetrical points in the Brillouin zones of Y, Rh, Nb, Mo, and Pd. Then, two first-principle calculations by the GW+T method for Ta [49, 47], Pd [47], and Pt [48] appeared. Later, a new version of the GW+T method, with the summation of the T matrix beginning with the term proportional to W^3, was used in the calculations for Mo and Rh [68] and V, Nb, Mo, Rh, and Ir [149].

Some information on the dynamics of relaxation of electrons in transition metals can be derived from the densities of states, which are given in Fig. 15 for the most studied cases of Ta, Mo, and Rh. In all these cases, the Fermi level lies in the region of a high density of d states; therefore, shorter lifetimes can be expected for both electrons and holes in these metals. Because of the short lifetime of holes, the influence of Auger electrons must be weak. Since the d-band electrons have a large effective mass and a low velocity (in comparison with nearly free electrons), it may be expected that the transport effects are also weak. This is completely confirmed by the results of experiments in [81], which have shown the absence of noticeable changes in the correlation traces upon changes in the thicknesses of Ta, Mo, and Rh films. For the transition metals, in view of the absence of the above-mentioned secondary processes, it is possible to expect better correspondence (than for the noble metals) between the experimental relaxation times and the first-principle lifetimes.

Figure 16 displays the experimental and calculated data on the dynamics of electrons in tantalum, molybdenum, and rhodium. It is evident that already at the GW level, the first-principle calculations agree well with the experimental tendencies. Moreover, even some fine details are reproduced, such as a smooth change in the lifetime with increasing the state energy in molybdenum, the presence of a bend in this curve at 1 eV in tantalum, and a sharp bend at 1 eV in rhodium. The contribution of the T matrix to the self-energy somewhat reduces the lifetimes, bringing them into better correspondence with experiment. However, in contrast to the case of aluminum, the T-matrix contributions are inessential in general. A qualitative explanation of this circumstance is given in Ref. [47]. In view of the high density of states near the Fermi level, the electron–electron interaction is more effectively screened in the transition metals. As a result, the screened potential W in the transition metals is noticeably lower than in aluminum, which, in view of Eqn (93), ensures the smallness of the T matrix.

4.5 The dynamics of electrons in magnetic transition metals

The first studies of the dynamics of the relaxation of excited electrons in magnetic metals were performed for Co by the TR-2PPE method [109]. The scheme of the experiment was similar to that depicted in Fig. 2; however, the experiments were conducted with time and spin resolution, which allowed determining the spin-dependent relaxation times. Analogous studies were then carried out for iron and nickel [22].

The first theoretical estimations of the dynamics of excited electrons in ferromagnetic metals were performed in [99, 100, 106] in the framework of the semiempirical scattering theory. For Fe, Co, and Ni, the energy dependence of the spin polarization of excited electrons, the mean free path, and the spin asymmetry of the lifetime (i.e., the ratio of the lifetime of

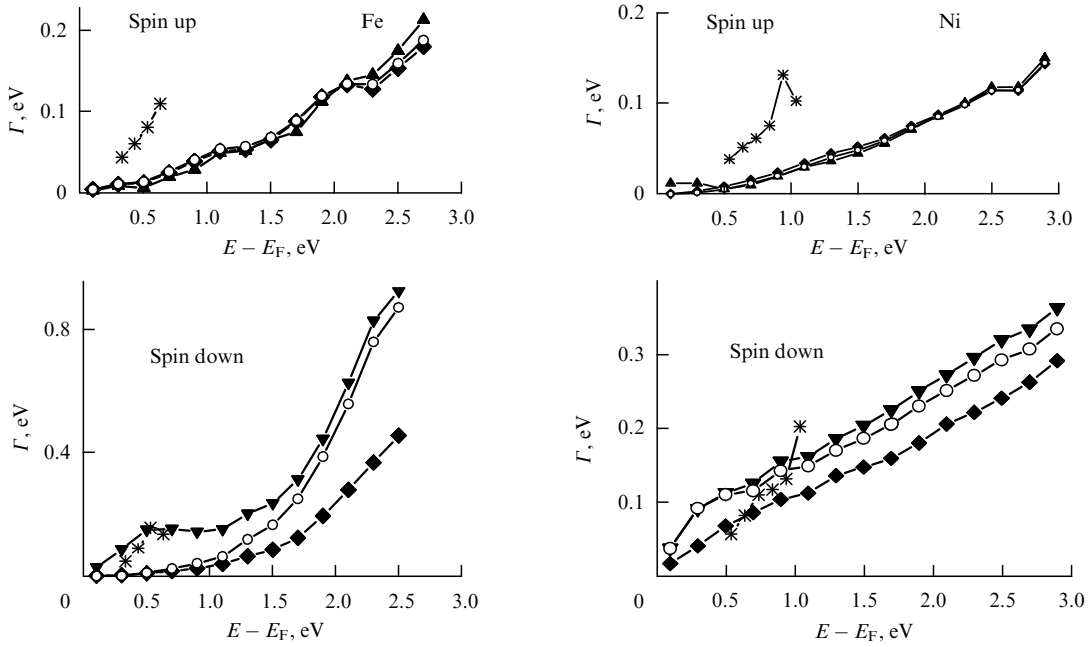

Figure 17. Calculated [46] and experimental [22] (asterisks) inverse lifetimes (damping rates) Γ for iron and nickel. The solid rhombi show the GW contributions to Γ; open circles, the sums of the GW and spin-diagonal T-matrix contributions to Γ; solid triangles, the totals of all contributions to Γ, i.e., of the GW contributions and T-matrix spin-diagonal and spin-off-diagonal contributions.

electrons with spin up to the lifetime of electrons with spin down) were studied. Later, in [22], the relaxation time of electrons in Fe, Co, and Ni was studied using the Boltzmann theory and, unlike in [99, 100, 106], transport processes, cascade processes, and the generation of Auger electrons were introduced into the consideration. The scattering theory with a somewhat different choice of parameters was also used for calculations of the lifetime in [21].

On the whole, a correct choice of the theory parameters leads to a correct description of the tendencies in changes in the relaxation characteristics. However, all the above-noted approaches have one common shortcoming: they are all based on the first Born approximation, and hence do not account for a multiple interaction of particles. As a consequence, they ignore energy losses by electrons in magnets via the generation of spin waves. As was shown in Section 3.3.3, such processes can be taken into account in terms of the T-matrix theory. At the model level, the T-matrix formalism for the self-energy and spin magnetic susceptibility was developed in [137]. A more realistic approach, based on the RPA and a modified Hubbard Hamiltonian, was developed in [98, 138, 168–170]. Apart from the correlation Hubbard term, the Hamiltonian considered there included an exchange term, computed using first-principle d orbitals. The authors calculated the energy of spin waves, spin-dependent electron lifetimes, and the mean free path. However, their approach was not entirely a first-principle one.

A many-body formalism for the spin susceptibility and the self-energy of electrons in ferromagnets based on the Matsubara Green's functions was suggested in [45, 126, 140]. The first completely first-principle calculations of a self-energy and lifetimes of excited electrons, including both the longitudinal and transverse T-matrix terms, were performed in [46] for Fe and Ni (see the description of the method in Section 3.3.3). The authors then calculated the mean free path of electrons in Fe and Ni [48]. The main results in [46] are given in Fig. 17. Because interesting effects are observed at low energies, the results are shown for the inverse lifetime Γ, i.e., the damping rate, equivalent to the spectral linewidth.

The possibility of the generation of spin waves upon energy loss by primary electrons in ferromagnets is determined by the conservation law of the total spin. Upon the appearance of a spin wave, the magnetic moment of a ferromagnet decreases by two Bohr magnetons [114], and therefore the transition of a primary electron must also occur with an increase in its spin momentum by two Bohr magnetons. Consequently, only spin-down electrons can lose energy, generating spin waves. This completely corresponds to the results of calculations of the damping rate Γ for iron. It is seen that Γ for spin-up electrons in iron is determined by the GW contribution, whereas both the spin-diagonal and spin-off-diagonal T-matrix contributions to Γ are negligible. The calculated damping rate of spin-up electrons is noticeably higher than the experimental value. Because the experiments were conducted using oriented thick films grown on a Cu(001) surface, the probable factor responsible for this difference can be the electron transport from the irradiated zone.

The calculations show that the damping of spin-down electrons in iron is the case where both spin-diagonal and spin-off-diagonal T-matrix terms are important. The spin-diagonal terms are small at electron energies below 1 eV, but they become significant at higher energies. This is explained by an increase in the propagator $K_{-1/2,-1/2}$ related to the excitation of secondary electrons from spin-down states, which form a peak in the density of states with a maximum near -1 eV, to states that form a peak at approximately $+1$ eV (see Fig. 7). On the contrary, spin-off-diagonal terms, which correspond to the relaxation that is accompanied by the generation of spin waves, are important at electron energies below 1 eV; in the $\Gamma(E - E_F)$ dependence, they yield a maximum at approximately 0.5 eV.

The processes of damping of spin-up electrons in nickel are similar to those in iron; the contribution of the T-matrix terms is also small, and the calculated damping rate is lower than in experiment, probably for the same reasons. However, the processes of damping of spin-down electrons in iron and nickel differ noticeably. In nickel, the spin-diagonal T-matrix terms increase noticeably with increasing the electron energy near 0.3 eV. This is related to the excitation of spin-down electrons in the limits of a band with a high density of states, in which the Fermi level is located (see Fig. 7). In this case, charge-density waves rather than magnons are generated. However, the contribution of spin-off-diagonal T-matrix terms, which are related to the generation of spin waves, is much less in Ni than in Fe. Qualitatively, this is explained by the difference in the screened potential. For a wave vector close to zero, the leading matrix element of this potential W_{11} is equal to 1.3 Ry for iron (where Ry is the Rydberg energy), and to only 0.63 Ry for nickel. According to Eqn (95), the ratio of the damping rates for Fe and Ni at close spectral functions $\mathrm{Im}\, R_{1/2,-1/2}$ is

$$\frac{\Gamma_{1/2,-1/2}(\mathrm{Ni})}{\Gamma_{1/2,-1/2}(\mathrm{Fe})} \sim \frac{W_{11}^2(\mathrm{Ni})}{W_{11}^2(\mathrm{Fe})}\,,$$

and therefore the magnitude of $\Gamma(\mathrm{Ni})$ is considerably lower than $\Gamma(\mathrm{Fe})$.

Thus, the first-principle GW+T calculations show that the effects of the T matrix, which correspond to the generation of magnons in iron and of charge-density waves in nickel, are important for the relaxation of excited electrons with energies below 1 eV. We show in what follows that they are also important for the mean free path at electron energies below 1 eV, whereas the GW term is prevalent at higher energies.

4.6 The mean free path of excited electrons in metals

The mean free path of excited electrons that is computed in the first-principle approaches in a state with an energy $e_{\mathbf{q}n\sigma}$ and group velocity $\mathbf{v}_{\mathbf{q}n\sigma}$ is usually defined as the distance covered by an electron in a time equal to the lifetime of the state $\tau_{\mathbf{q}n\sigma}$, i.e., $\lambda_{\mathbf{q}n\sigma} \equiv \mathbf{v}_{\mathbf{q}n\sigma}\tau_{\mathbf{q}n\sigma}$. The group velocity is here defined as $\mathbf{v}_{\mathbf{q}n\sigma} = \partial e_{\mathbf{q}n\sigma}/\partial \mathbf{q}$ [114]. In this case, it is assumed that the electron velocity does not change during the lifetime of the state, i.e., the electron motion is ballistic. After calculating the electron velocity and the inelastic lifetime from first principles, it is possible to find the *inelastic* mean free path.

In virtually all experimental works, it is assumed that the motion of an electron with the excess energy approximately equal to 1 eV (typical of the SVTs and MTTs) is ballistic, i.e., that the probability of an electron penetrating a film with a thickness d is given by $p(d) = \exp(-d/\lambda_\mathrm{b})$, where λ_b is the ballistic mean free path, which, however, is determined not only by inelastic scattering of the excited electron but also by a number of other processes described by Eqn (26). Omitting the terms connected with spin waves and including the electron–phonon interaction in the term that describes elastic scattering, we obtain

$$\frac{1}{\lambda_\mathrm{b}} = \frac{1}{\lambda_\mathrm{inel}} + \frac{1}{\lambda_\mathrm{el}} \qquad (97)$$

for paramagnetic materials. The quantity λ_b can be determined from experiments on electron transmission through films of different thicknesses (see Section 2.3). But the values of λ_inel and λ_el cannot be experimentally obtained separately, and here first-principle calculations can be useful.

However, the question arises under what conditions the motion can be considered ballistic, i.e., under what conditions Eqn (97) is valid. It was shown in Ref. [171] that with the elastic scattering by defects and impurities taken into account using the theory of Markov processes, a diffusion term appears in the expression for $p(d)$, and it becomes

$$p(d) = \exp\left(-\frac{d}{\lambda_\mathrm{b}}\right) + \left(1 - \exp\left(-\frac{d}{\lambda_\mathrm{el}}\right)\right)\exp\left(-\frac{n\lambda_\mathrm{el}}{\lambda_\mathrm{inel}}\right). \qquad (98)$$

At small d, of the order of 10 Å, $\ln p$ tends to $-1/\lambda_\mathrm{inel}$, i.e., the electron motion is determined only by inelastic scattering, while at large d, more than 50 Å, $\ln p$ tends to $-1/\lambda_\mathrm{b}$, i.e., the motion is ballistic, but it depends on both elastic and inelastic scattering. At intermediate d, the electron motion is a combination of these two types of motion.

The majority of experiments concerning the determination of the mean free path have been conducted on thick films, for which Eqn (97) is correct. Such experiments with excess energies of excited electrons of approximately 1 eV were carried out for Al, Ag, Au, Pd [172, 173], again for Au [174], for permalloy $Ni_{80}Fe_{20}$ [94, 95], and for iron [93]. These experimental data are compared in Table 1 with the results of first-principle calculations of the inelastic mean free path that was calculated using lifetimes obtained from GW and GW+T calculations. The table also gives the values of the elastic mean free path λ_el calculated from the experimental λ_b and the first-principle λ_inel according to Eqn (97). It is seen that they are comparable in all the cases; i.e., both the processes of inelastic scattering, connected with the finiteness of the lifetime of an excited state, and the processes of elastic scattering, i.e., the randomization of the directions of motion of the excited electron because of the elastic scattering by defects and impurities, are of great importance. But any theoretical approaches to the calculations of the elastic scattering length, either semiempirical or first-principle ones, are absent at present. For aluminum and noble metals, there exist only first-principle data on the dependence of the inelastic mean free path on the electron energy; in Fig. 18, these are given for gold, as an example. The estimations of elastic and inelastic mean free paths according to the existing

Table 1. Experimental values of the mean free path λ_b and the calculated values of the inelastic (λ_inel) and elastic (λ_el) mean free paths at the energy of an excited electron $E - E_\mathrm{F} = 1$ eV.

Metal	λ_b, Å	References	λ_inel, λ_el, Å GW method	λ_inel, λ_el, Å GW+T method	References
Al	100	[173]	670, 117	270, 159	[48]
Ag	265	[173]	797, 397	414, 736	[127]
Au	220	[173]	1300, 283	470, 460	[48]
	220–230	[172]			
	230–280	[174]			
Pd	31	[171]	89, 47	—	[127]
	87	[173]			
Fe(↑)	16	[93]	60	—	[48]
Fe(↓)	4	[93]	1	—	
Ni(↑)	78.43	[95, 94]	95	—	[48]
Ni(↑)	12.10	[95, 94]	12	—	

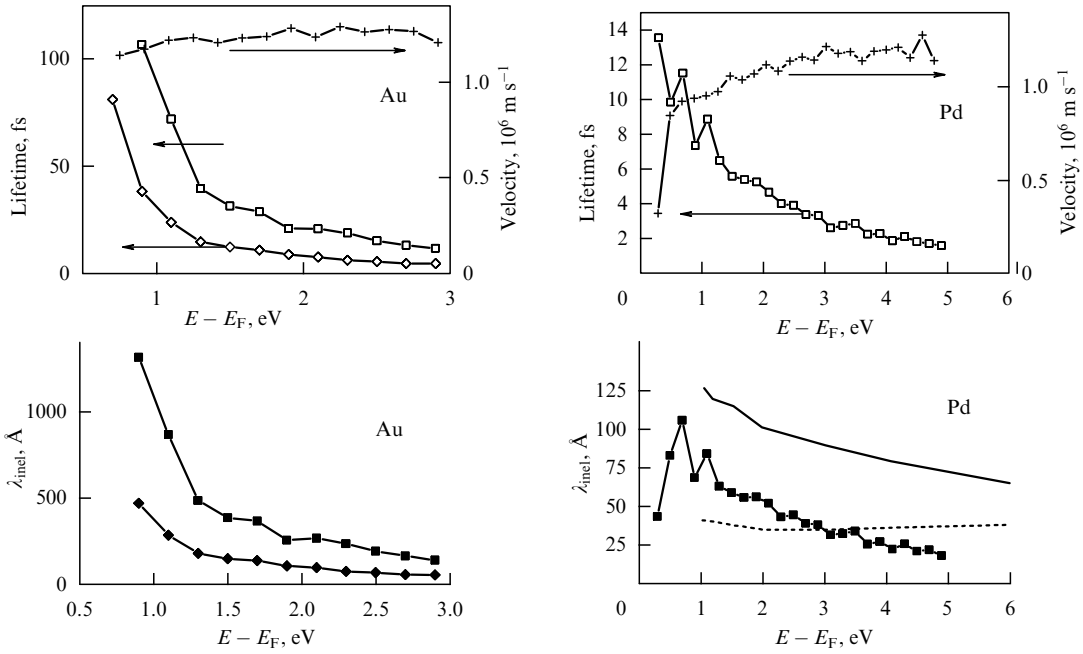

Figure 18. Velocities, lifetimes, and mean free paths for excited electrons in gold and palladium. For gold, the crosses show the electron velocities; open squares, lifetimes in the GW approximation; open rhombi, lifetimes in the GW+T approximation; solid squares, the inelastic mean free paths with lifetimes in the GW approximation; solid rhombi, the inelastic mean free paths with lifetimes in the GW+T approximation. For palladium, the crosses show the electron velocities; open squares, lifetimes in the GW approximation; solid squares, the inelastic mean free paths with lifetimes in the GW approximation [127]; the solid line, the experimental inelastic mean free path; and the dashed line, the experimental elastic mean free path [171].

experimental data were made only for palladium [171]. Together with the appropriate first-principle data, they are shown in Fig. 18.

The 'experimental' values of λ_{inel} and λ_{el} for palladium [171] were obtained by fitting the current passing through the film, calculated via Eqn (98) at varying λ_{inel} and λ_{el}, to the experimental data. The value of λ_{el} is almost independent of the energy of the excited electron, whereas the experimentally found reduction in the value of λ_{inel} with increasing the electron energy agrees with the results of first-principle calculations. For palladium, states with energies $E - E_F > 0.3$ eV are almost free-electron states. Their velocity increases slowly with the energy, whereas the lifetime decreases much more rapidly, as $\tau \sim (E - E_F)^{-2}$, which explains the reduction in λ_{inel} with increasing the electron energy. The variation of λ_{inel} for gold is explained similarly.

Figure 19 displays the theoretical and experimental characteristics of the dynamics of electrons in iron and nickel. In both cases, the inelastic mean free path of spin-up electrons is 5–7 times greater than that for spin-down electrons. But the reasons for this difference in Fe and Ni are different. In iron, spin-up electrons are nearly free, while spin-down electrons are d-like. Therefore, the velocity of spin-up electrons is considerably greater, and at comparable lifetimes, the difference in the mean free paths is determined by the difference in the velocities. In nickel, on the contrary, electrons of both types are nearly free (at $E - E_F > 0.3$ eV) and the difference in the velocities of electrons with spin up and down is considerably less than the difference in the lifetimes. Therefore, the main reason for the spin dependence of the inelastic mean free path is the difference in the lifetimes. This is discussed in more detail in Ref. [48].

The role of the effect of generation of spin waves in the relaxation of excited states with spin down can be determined from a comparison of the inelastic mean free path calculated for iron using the lifetimes estimated from GW and GW+T calculations. It is seen that for iron, the inclusion of the T-matrix terms, which account for the generation of spin waves, sharply reduces the mean free path at the energies of the excited state $E - E_F < 1$ eV, but this effect is insignificant at higher energies. An analogous effect of the reduction in the mean free path upon the inclusion of T-matrix terms (insignificant at the energies above 1 eV) exists in nickel.

The relaxation lengths of electrons in iron were investigated experimentally in Ref. [93]. It was shown that the measured spin asymmetry of the relaxation length, $\lambda_\uparrow/\lambda_\downarrow$, is much less than the theoretical value ($\sim 5-7$), mainly because of the shorter theoretical mean free path for spin-up electrons. The authors of [93], using their results and the data of first-principle calculations [48], estimated the elastic mean free path as barely depending on the energy and equal to 20 Å. As for Al, Ag, Au, and Pd, the mean free path of electrons in iron is thus determined by the processes of both inelastic and elastic scattering.

Experimental data on the attenuation length for electrons in pure nickel are absent; therefore, in Fig. 19 the first-principle results are compared with the experimental data for permalloy $Ni_{80}Fe_{20}$ taken from Refs [94, 95]. It is seen that the correspondence between the calculation and the experiment is better for $Ni_{80}Fe_{20}$ than for iron. However, we are inclined to consider this agreement accidental, because analogous experiments conducted in [94] give the much smaller value $\lambda_{ex} = 43 \pm 0{,}3$ Å for spin up at $E - E_F = 0.9$ eV. Furthermore, the experiments in [95, 94] were carried out on films with a thickness less than 100 Å. According to Eqn (98), electron diffusion may be an important factor at these thicknesses, whereas the experimental data in [95, 94] were fitted to the function $\exp(-d/\lambda_{ex})$, which corresponds only to ballistic motion.

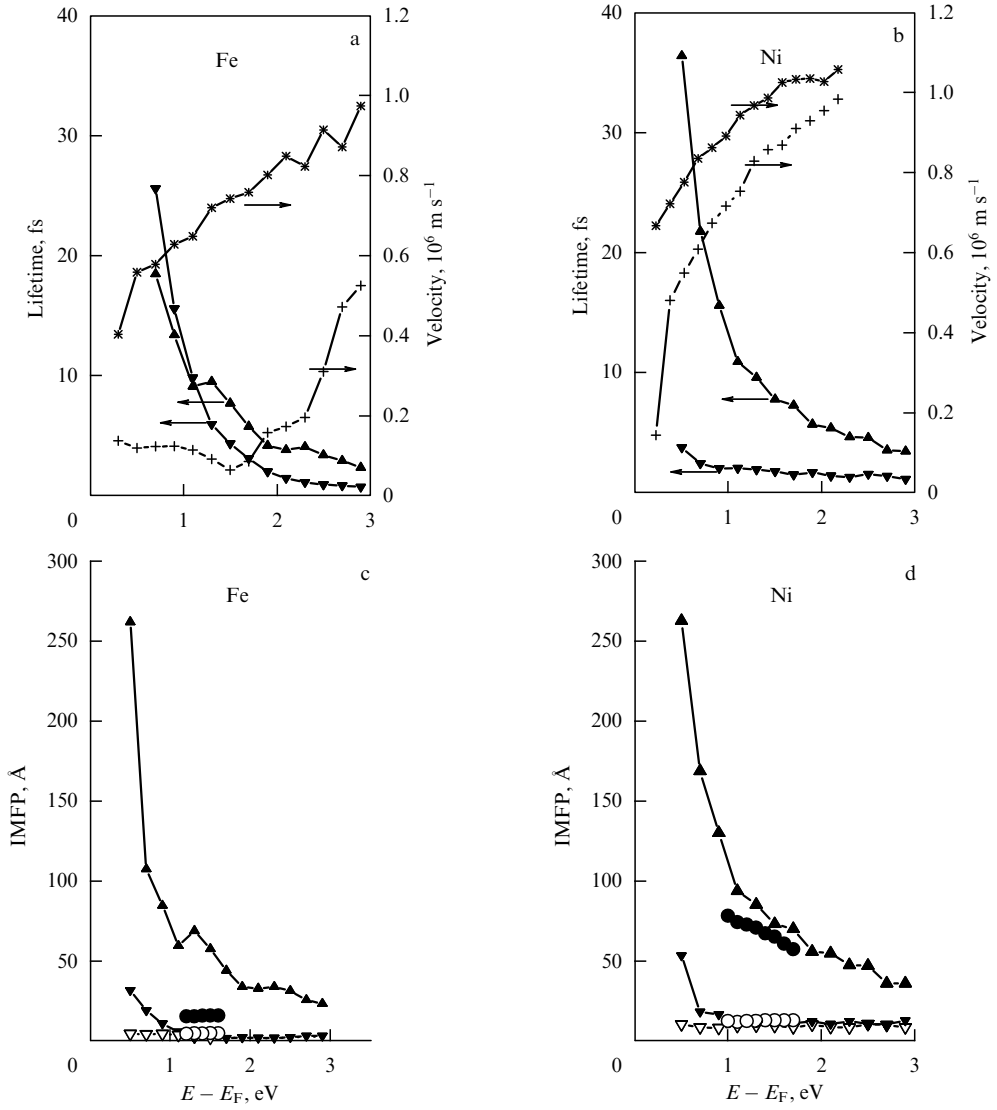

Figure 19. Characteristics of the electron dynamics in iron and nickel. (a, b) Asterisks show the velocities of spin-up electrons; crosses, the velocities of spin-down electrons; triangles with apices directed upward, GW lifetimes for spin-up electrons; triangles with downward apices, GW lifetimes for spin-down electrons. (c, d) Solid triangles with upward apices show the inelastic mean free paths (IMFPs) for spin-up electrons calculated using GW lifetimes; solid triangles with downward apices, analogous data for spin-down electrons; open downward triangles, lifetimes for spin-down electrons calculated using the GW+T lifetimes. Experimental mean free paths for spin-up (solid circles) and spin-down (open circles) electrons are also given. These are the data for pure iron [93] and permalloy [95].

5. Conclusion

The studies on the dynamics of electrons in metals described in this review have led to a number of achievements, but have simultaneously highlighted some difficult problems.

From the standpoint of experiment, the most important result is probably the fact that a sufficiently complex nature of the relaxation of excited states was revealed, which includes a set of processes that affect the population of the excited level, such as the electron–electron and electron–phonon scattering, processes of electron transport, the generation of Auger electrons, and elastic scattering by impurities and defects. Several methods for controlling these processes have been suggested, such as variation of the energy of the pumping photons, experiments with films of different thicknesses on insulating substrates with anneals of different durations, etc. Various methods for extracting characteristics of electron relaxation (relaxation times and mean free paths) from the experimental data have been developed. Based on the scattering theory and the Boltzmann equation, semiempirical models of the most important relaxation processes were developed. In spite of their simplicity, these models describe experimental data qualitatively correctly. But the accuracy of such calculations is often low, and significant divergences between the experimental data and the results of calculations are frequently observed.

From the theoretical standpoint, the most important achievement appears to be the fact that a concretization of the first-principle GW method was carried out and reliable computer programs were created that allow calculating the characteristics of electron dynamics. First-principle calculations performed for a sufficiently large number of objects suggest that in the cases where the inelastic electron–electron scattering that predominates all possible mechanisms of relaxation, the GW method (if necessary, augmented by the

T-matrix method) can lead to good results. Examples are tantalum, molybdenum, rhodium, and ytterbium.

However, in a number of cases with nearly free electrons (aluminum, noble metals, spin-up states in ferromagnetic metals), there are noticeable deviations of the first-principle lifetimes from the experimental data. The reasons for the deviations are thus far obscure. They may be both the influence of relaxation processes that occur in experiment but are not taken into account in the GW approach, and errors inherent in the first-principle approach itself. In this respect, it would be useful to design new experiments that would allow separating processes of electron–electron scattering from the observed relaxation phenomena and obtaining their time characteristics. Because the GW method found a wide application for calculating the energy band structure of real objects beyond the limits of the theory of the electron-density functional, it is very important to continue studies directed toward an increase in the accuracy and speed of the method. Calculations of the lifetime can serve as a good test of the accuracy of new versions of the method. Because the lifetime of nearly free excited electrons in metals obtained with the GW method is reproduced well by GW calculations for an interacting free electron gas with an optimized r_s (DFEG), further studies of the dynamics of electrons in the DFEG model are also of great interest.

Thus far, even the very reason for the relative success of the GW approach in research on electron dynamics is unclear, because, being based on the formalism of a *single-particle* Green's function, it does not entirely correspond to the experimental TR-2PPE method, in which the pumping photon generates electron–hole pairs. A qualitative explanation of the success of the GW approach is based on the assumption that the electron–hole interaction is screened quite rapidly, in several femtoseconds, and subsequently the electron and the hole behave like independent particles. However, the dynamics of electron–hole pairs is a sphere of research in which the introduction of first-principle approaches is just starting.

We also note that no first-principle approaches have yet been developed for the processes that are characterized in this review as 'additional.' These are, for example, processes of the elastic scattering of electrons in experiments with spintronic devices or the cascade, transport, and Auger processes in TR-2PPE experiments.

Acknowledgments

We are grateful to our colleagues at the Donostia International Physical Center (San Sebastian, Spain) who participated in the theoretical studies of femtosecond dynamics, in particular, to P M Echenique and I A Nechaev. We are also grateful to the experimentalists of the University of Kaiserslautern (Germany), namely, M Aeschlimann, A Marienfeld, and M Chinchetti, for the fruitful collaboration. We thank R Jansen and T Banerjee from the University of Twente (the Netherlands) for the fruitful discussions.

References

1. Bonn M et al. *Science* **285** 1042 (1999)
2. Dai H-L, Ho W (Eds) *Laser Spectroscopy and Photochemistry on Metal Surfaces* (Singapore: World Scientific, 1995)
3. Ho W *J. Phys. Chem.* **100** 13050 (1996)
4. Nienhaus H *Surf. Sci. Rep.* **45** 1 (2002)
5. Lindstrom C D, Zhu X-Y *Chem. Rev.* **106** 4281 (2006)
6. Gadzuk J W *Surf. Sci.* **342** 345 (1995)
7. Güdde J, Berthold W, Höfer U *Chem. Rev.* **106** 4261 (2006)
8. Hüfner S *Photoelectron Spectroscopy: Principles and Applications* (Springer Series in Solid-State Sciences, Vol. 82) (Berlin: Springer-Verlag, 1995)
9. Kevan S D (Ed.) *Angle-Resolved Photoemission: Theory and Current Applications* (Studies in Surface Science and Catalyses, Vol. 74) (Amsterdam: Elsevier, 1992)
10. Jablonski A, Powell C J *Surf. Sci. Rep.* **47** 33 (2002)
11. Žutić I, Fabian J, Das Sarma S *Rev. Mod. Phys.* **76** 323 (2004)
12. Jansen R *J. Phys. D: Appl. Phys.* **36** R289 (2003)
13. Bobo J F, Gabillet L, Bibes M *J. Phys.: Condens. Matter* **16** S471 (2004)
14. Inglesfield J E, Plummer E W, in *Angle-Resolved Photoemission: Theory and Current Applications* (Ed. S D Kevan) (Amsterdam: Elsevier, 1992)
15. Matzdorf R *Surf. Sci. Rep.* **30** 153 (1998)
16. Petek H, Ogawa S *Prog. Surf. Sci.* **56** 239 (1997)
17. Bennemann K H *J. Phys.: Condens. Matter* **16** R995 (2004)
18. Knoesel E et al. *Chem. Phys. Lett.* **240** 409 (1995)
19. Hertel T et al. *Phys. Rev. Lett.* **76** 535 (1996)
20. Bauer M, Pawlik S, Aeschlimann M *Phys. Rev. B* **60** 5016 (1999)
21. Zarate E, Apell P, Echenique P M *Phys. Rev. B* **60** 2326 (1999)
22. Knorren R et al. *Phys. Rev. B* **61** 9427 (2000)
23. Drouhin H-J *Phys. Rev. B* **56** 14886 (1997)
24. Drouhin H-J *Phys. Rev. B* **62** 556 (2000)
25. Quinn J J, Ferrell R A *Phys. Rev.* **112** 812 (1958)
26. Schmuttenmaer C A et al. *Phys. Rev. B* **50** 8957 (1994)
27. Aeschlimann M, Bauer M, Pawlik S *Chem. Phys.* **205** 127 (1996)
28. Cao J et al. *Phys. Rev. B* **56** 1099 (1997)
29. McDougall B A, Balasubramanian T, Jensen E *Phys. Rev. B* **51** 13891 (1995)
30. Matzdorf R et al. *Solid State Commun.* **92** 839 (1994)
31. Matzdorf R et al. *Appl. Phys. B* **68** 393 (1999)
32. Knoesel E, Hotzel A, Wolf M *Phys. Rev. B* **57** 12812 (1998)
33. Petek H, Nagano H, Ogawa S *Phys. Rev. Lett.* **83** 832 (1999)
34. Kliewer J et al. *Science* **288** 1399 (2000)
35. Abrikosov A A, Gor'kov L P, Dzyaloshinskii I E *Metody Kvantovoi Teorii Polya v Statistichskoi Fizike* (Quantum Field Theoretical Methods in Statistical Physics) (Moscow: Fizmatgiz, 1962) [Translated into English (Oxford: Pergamon Press, 1965)]
36. Hedin L, Lundqvist S, in *Solid State Physics* Vol. 23 (Eds H Ehrenreich, F Seitz, D Turnbull) (New York: Academic Press, 1969)
37. Aryasetiawan F, Gunnarsson O *Rep. Prog. Phys.* **61** 237 (1998)
38. Aulbur W G, Jönsson L, Wilkins J W *Solid State Phys.* **54** 1 (1999)
39. Aryasetiawan F, in *Strong Coulomb Correlations in Electronic Structure Calculations* (Ed. V I Anisimov) (Amsterdam: Gordon and Breach, 2000)
40. Echenique P M et al. *Chem. Phys.* **251** 1 (2000)
41. Pitarke J M et al. *ChemPhysChem* **5** 1284 (2004)
42. Chulkov E V et al. *Chem. Rev.* **106** 4160 (2006)
43. Echenique P M et al. *Surf. Sci. Rep.* **52** 219 (2004)
44. Chulkov E V, Silkin V M, Machado M *Surf. Sci.* **482–485** 693 (2001)
45. Springer M, Aryasetiawan F, Karlsson K *Phys. Rev. Lett.* **80** 2389 (1998)
46. Zhukov V P, Chulkov E V, Echenique P M *Phys. Rev. Lett* **93** 096401 (2004)
47. Zhukov V P, Chulkov E V, Echenique P M *Phys. Rev. B* **72** 155109 (2005)
48. Zhukov V P, Chulkov E V, Echenique P M *Phys. Rev. B* **73** 125105 (2006)
49. Zhukov V P et al. *Phys. Rev. B* **70** 233106 (2004)
50. Zhukov V P et al. *Phys. Rev. B* **76** 193107 (2007)
51. Fleszar A, Hanke W *Phys. Rev. B* **62** 2466 (2000)
52. Kidd T E et al. *Phys. Rev. Lett.* **94** 107003 (2005)
53. Murzyn P et al. *Phys. Rev. B* **67** 235202 (2003)
54. Nohara Y et al. *Phys. Rev. B* **74** 064417 (2006)
55. Perfetti L et al. *Phys. Rev. B* **64** 115102 (2001)
56. Tanaka A, Watkins N J, Gao Y *Phys. Rev. B* **67** 113315 (2003)
57. Ahn K H et al. *Phys. Rev. B* **69** 045114 (2004)
58. Demsar J, Sarrao J L, Taylor A J *J. Phys.: Condens. Matter* **18** R281 (2006)

59. Bansil A et al. *Phys. Rev. B* **71** 012503 (2005)
60. Dahm T et al. *Phys. Rev. B* **72** 214512 (2005)
61. Koitzsch A et al. *Phys. Rev. B* **69** 140507 (2004)
62. Kordyuk A et al. *Phys. Rev. Lett.* **92** 257006 (2004)
63. Kordyuk A A et al. *Phys. Rev. B* **71** 214513 (2005)
64. Zhang Y et al. *Phys. Rev. Lett.* **86** 890 (2001)
65. Zamkov M et al. *Phys. Rev. Lett.* **94** 056803 (2005)
66. Marienfeld A et al. *J. Phys.*: *Condens. Matter* **19** 496213 (2007)
67. Bauer M, Aeschlimann M *J. Electron. Spectrosc. Relat. Phenom.* **124** 225 (2002)
68. Mönnich A et al. *Phys. Rev. B* **74** 035102 (2006)
69. Timm C, Bennemann K H *J. Phys.*: *Condens. Matter* **16** 661 (2004)
70. Vernes A, Weinberger P *Phys. Rev. B* **71** 165108 (2005)
71. Loudon R *The Quantum Theory of Light* 2nd ed. (New York: Oxford Univ. Press, 1983)
72. Landau L D, Lifshitz E M *Kvantovaya Mekhanika. Nerelyativistskaya Teoriya* (Quantum Mechanics: Non-Relativistic Theory) (Moscow: Nauka, 1969) [Translated into English (Oxford: Pergamon Press, 1977)]; Schiff L I *Quantim Mechanics* 3rd ed. (New York: McGraw-Hill, 1968) [Translated into Russian (Moscow: IL, 1959)]
73. Bauer M "Real-time investigations of the lifetime of electronic excitations at clean and adsorbate-covered metal surfaces", Dissertation ... Doctor Natural Sciences (Zurich: ETH, 1998)
74. Petek H et al. *Chem. Phys.* **251** 71 (2000)
75. Ogawa S *J. Electron. Spectrosc. Relat. Phenom.* **124** 245 (2002)
76. Ogawa S et al. *Phys. Rev. Lett.* **78** 1339 (1997)
77. Quinn J J *Phys. Rev.* **126** 1453 (1962)
78. Ritchie R H *Phys. Rev.* **114** 644 (1959)
79. Ashcroft N W, Mermin N D *Solid State Physics* (New York: Holt, Rinehart and Winston, 1976) [Translated into Russian (Moscow: Mir, 1979)]
80. Aeschlimann M et al. *Appl. Phys. A* **71** 485 (2000)
81. Mönnich A "Hot electron lifetimes in metals probed by time-resolved two-photon photoemission", Dissertation (Keiserslautern: Technische Univ. Keiserslautern, 2007)
82. Petek H, Nagano H, Ogawa S *Appl. Phys. B* **68** 369 (1999)
83. Sklyadneva I Yu et al. *Phys. Rev. B* **71** 174302 (2005)
84. Sklyadneva I Yu et al. *J. Phys.*: *Condens. Matter* **18** 7923 (2006)
85. Smith N V, Thiry P, Petroff Y *Phys. Rev. B* **47** 15476 (1993)
86. Goldmann A, Altmann W, Dose V *Solid State Commun.* **79** 511 (1991)
87. Berge K et al. *Surf. Sci.* **498** 1 (2002)
88. Gerlach A et al. *Phys. Rev. B* **64** 085423 (2001)
89. Gerlach A et al. *Surf. Sci.* **497** 311 (2002)
90. Matzdorf R *Chem. Phys.* **251** 151 (2000)
91. Theilmann F et al. *Phys. Rev. B* **56** 3632 (1997)
92. Grimvall G *The Electron–Phonon Interaction in Metals* (Amsterdam: North-Holland, 1981)
93. Banerjee T, Lodder J C, Jansen R *Phys. Rev. B* **76** 140407(R) (2007)
94. Vlutters R et al. *Phys. Rev. Lett.* **88** 027202 (2001)
95. van Dijken S, Jiang X, Parkin S P *Phys. Rev. B* **66** 094417 (2002)
96. van 't Erve O M J et al. *Appl. Phys. Lett.* **80** 3787 (2002)
97. Vlutters R et al. *Phys. Rev. B* **65** 024416 (2001)
98. Hong J, Mills D L *Phys. Rev. B* **59** 13840 (1999)
99. Rendell R W, Penn D R *Phys. Rev. Lett.* **45** 2057 (1980)
100. Penn D R, Apell S P *Phys. Rev. Lett.* **55** 518 (1985)
101. Valet T, Fert A *Phys. Rev. B* **48** 7099 (1993)
102. Drouhin H-J *J. Appl. Phys.* **89** 6805 (2001)
103. Knorren R, Bouzerar G, Bennemann K H *J. Phys.*: *Condens. Matter* **14** R739 (2002)
104. Nozières P *Theory of Interacting Fermi Systems* (Reading, Mass.: Addison-Wesley, 1997)
105. Mahan G D *Many-Particle Physics* 2nd ed. (New York: Plenum Press, 1990)
106. Penn D R, Apell S P, Girvin S M *Phys. Rev. B* **32** 7753 (1985)
107. Berglund C N, Spicer W E *Phys. Rev.* **136** A1030 (1964)
108. Kane E O *Phys. Rev.* **159** 624 (1967)
109. Aeschlimann M et al. *Phys. Rev. Lett.* **79** 5158 (1997)
110. Zhukov V P, Chulkov E V *J. Phys.*: *Condens. Matter* **14** 1937 (2002)
111. Zhukov V P et al. *Phys. Rev. B* **65** 115116 (2002)
112. Knorren R, Bouzerar G, Bennemann K H *Phys. Rev. B* **63** 125122 (2001)
113. Knorren R, Bouzerar G, Bennemann K H *Phys. Rev. B* **63** 094306 (2001)
114. Ziman J M *Principles of the Theory of Solids* 2nd ed. (Cambridge: Univ. Press, 1972) [Translated into Russian (Moscow: Mir, 1974)]
115. Ritchie R H, Ashley J C *J. Phys. Chem. Solids* **26** 1689 (1965)
116. Pines D *Elementary Excitations in Solids* (New York: W.A. Benjamin, 1963) [Translated into Russian (Moscow: Mir, 1965)]
117. Campillo I et al. *Phys. Rev. Lett.* **83** 2230 (1999)
118. Keyling R, Schöne W-D, Ekardt W *Phys. Rev. B* **61** 1670 (2000)
119. Hedin L *Phys. Rev.* **139** A796 (1965)
120. Lundqvist B I *Phys. Status Solidi B* **32** 273 (1969)
121. Fetter A L, Walecka J D *Quantum Theory of Many-Particle Systems* (San Francisco: McGraw-Hill, 1971)
122. Inkson J C *Many-Body Theory of Solids*: *An Introduction* (New York: Plenum Press, 1984)
123. Dreizler R M, Gross E K U *Density Functional Theory* (Berlin: Springer-Verlag, 1990)
124. Campillo I et al. *Phys. Rev. Lett.* **85** 3241 (2000)
125. Campillo I et al. *Phys. Rev. B* **61** 13484 (2000)
126. Aryasetiawan F, Karlsson K *Phys. Rev. B* **60** 7419 (1999)
127. Zhukov V P, Chulkov E V, Echenique P M *Phys. Status Solidi A* **205** 1296 (2008)
128. Northrup J E, Hybertsen M S, Louie S G *Phys. Rev. Lett.* **59** 819 (1987); *Phys. Rev. B* **39** 8198 (1989)
129. Hybertsen M S, Louie S G *Phys. Rev. B* **34** 5390 (1986)
130. Mahan G D, Sernelius B E *Phys. Rev. Lett.* **62** 2718 (1989)
131. Gurtubay I G, Pitarke J M, Echenique P M *Phys. Rev. B* **69** 245106 (2004)
132. Zhukov V P, Silkin V M, Chulkov E V, Echenique P M *Phys. Rev. B* **64** 180507 (2001)
133. Palik E D (Ed.) *Handbook of Optical Constants of Solids* (Orlando: Academic Press, 1985)
134. Kanamori J *Prog. Theor. Phys.* **30** 275 (1963)
135. Baym G, Kadanoff L P *Phys. Rev.* **124** 287 (1961)
136. Kadanoff L P, Baym G *Quantum Statistical Mechanics* (Redwood City, Calif.: Addison-Wesley, 1989)
137. Hertz J A, Edwards D M *J. Phys. F*: *Met. Phys.* **3** 2174 (1973); **3** 2191 (1973); *Phys. Rev. Lett.* **28** 1334 (1972)
138. Plihal M, Mills D L *Phys. Rev. B* **58** 14407 (1998)
139. Liebsch A *Phys. Rev. B* **23** 5203 (1981)
140. Karlsson K, Aryasetiawan F *Phys. Rev. B* **62** 3006 (2000)
141. Mahan G D *Comm. Condens. Matter Phys.* **16** 333 (1994)
142. Campillo I et al. *Phys. Rev. B* **62** 1500 (2000)
143. Schöne W-D et al. *Phys. Rev. B* **60** 8616 (1999)
144. Andersen O K *Phys. Rev. B* **12** 3060 (1975)
145. Andersen O K, Jepsen O, Sob M *Lecture Notes Phys.* **283** 1 (1987)
146. Aryasetiawan F, Gunnarsson O *Phys. Rev. B* **49** 16214 (1994)
147. Zhukov V P et al. *Phys. Rev. B* **64** 195122 (2001)
148. Zhukov V P, Chulkov E V, Echenique P M *J. Magn. Magn. Mater.* **272–276** 466 (2004)
149. Nechaev I A, Zhukov V P, Chulkov E V *Fiz. Tverd. Tela* **49** 1729 (2007) [*Phys. Solid State* **49** 1811 (2007)]
150. van Schilfgaarde M, Kotani T, Faleev S *Phys. Rev. Lett.* **96** 226402 (2006)
151. van Schilfgaarde M, Kotani T, Faleev S V *Phys. Rev. B* **74** 245125 (2006)
152. Zhukov V P, Chulkov E V, Echenique P M *Phys. Rev. B* **68** 045102 (2003)
153. Zhukov V P, Usuda M, Chulkov E V, Echenique P M *J. Electron. Spectrosc. Relat. Phenom.* **129** 127 (2003)
154. Ladstädter F et al. *Phys. Rev. B* **70** 235125 (2004)
155. Moruzzi V L, Janak J F, Williams A R *Calculated Electronic Properties of Metals* (New York: Pergamon Press, 1978)
156. Bauer M, Pawlik S, Aeschlimann M *Proc. SPIE* **3272** 201 (1998)
157. Ekardt W, Schöne W-D, Keyling R *Appl. Phys. A* **71** 529 (2000)
158. Nechaev I A, Chulkov E V *Phys. Rev. B* **71** 115104 (2005)
159. Nechaev I A, Chulkov E V *Phys. Rev. B* **73** 165112 (2006)
160. Pawlik S, Bauer M, Aeschlimann M *Surf. Sci.* **377–379** 206 (1997)
161. Ogawa S, Nagano H, Petek H *Phys. Rev. B* **55** 10869 (1997)
162. Wolf M, Aeschlimann M *Phys. Blätter* **54** 145 (1998)
163. Knoesel E et al. *Surf. Sci.* **368** 76 (1996)

164. Merschdorf M, Kennerknecht C, Pfeiffer W *Phys. Rev. B* **70** 193401 (2004)
165. Knapp J A, Himpsel F J, Eastman D E *Phys. Rev. B* **19** 4952 (1979)
166. Purdie D et al. *Surf. Sci.* **407** L671 (1998)
167. Bacelar M R et al. *Phys. Rev. B* **66** 153101 (2002)
168. Tang H, Plihal M, Mills D L *J. Magn. Magn. Mater.* **187** 23 (1998)
169. Plihal M, Mills D L, Kirschner J *Phys. Rev. Lett.* **82** 2579 (1999)
170. Costa A T (Jr.), Muniz R B, Mills D L *Phys. Rev. B* **69** 064413 (2004)
171. Ludeke R, Bauer A *Phys. Rev. Lett.* **71** 1760 (1993)
172. Crowell C R, Sze S M *Phys. Rev. Lett.* **15** 659 (1965)
173. Sze S M et al. *J. Appl. Phys.* **37** 2690 (1966)
174. Weilmeier M K, Rippard W H, Buhrman R A *Phys. Rev. B* **59** R2521 (1999)
175. Jedema F J et al. *Phys. Rev. B* **67** 085319 (2003)
176. Johnson M *Appl. Phys. Lett.* **65** 1460 (1994)
177. Jedema F J et al. *Nature* **416** 713 (2002)
178. Elezzabi A Y, Freeman M R, Johnson M *Phys. Rev. Lett.* **77** 3220 (1996)